

COMPUTER MODELING FOR WAVE OSCILLATION PROBLEMS IN HARBORS
AND COASTAL REGIONS

by

Xiuying Xing

A Dissertation Presented to the
FACULTY OF THE GRADUATE SCHOOL
UNIVERSITY OF SOUTHERN CALIFORNIA
In Partial Fulfillment of the
Requirements for the Degree
DOCTOR OF PHILOSOPHY
(CIVIL ENGINEERING)

May 2009

Copyright 2009

Xiuying Xing

DEDICATION

I would like to dedicate this dissertation work to my beloved family.

ACKNOWLEDGMENTS

Many people have provided their help and encouragement during this dissertation study. This work would not have been done without them.

I like to specially thank my advisor, Professor Jiin-Jen Lee, who not only gave me the great opportunity to pursue a Ph.D. degree at the University of Southern California, but also provided invaluable advice, assistance, and encouragement throughout the whole study.

I highly appreciate the advice and guidance provided by Professor Fredric Raichlen at California Institute of Technology in this study. I also like to thank other members of the dissertation committee, Professors Carter Wellford, Vincent Lee, Sami Masri in the Department of Civil and Environmental Engineering and Professor Julian Domaradzki in the Department of Aerospace and Mechanical Engineering at USC, for their guidance and help.

I would like to thank all of the group members, Mehrdad Bozorgnia, Jen Chang, Chanin Chaun-Im, Hyoung-Jin Kim, Zhiqing Kou, Hyuk-Jae Kwan, Yuan-Hung Tan, Ben Willardson (following the alphabetic sequence of the last names, no special order) for their incessant help and the warm atmosphere they provided since I came to USC.

I like to thank our visiting scholars Dr Li-Hung Tsai and Dr Moonsu Kwak for the valuable field data and suggestions they provided in the study of Hualien Harbor and Pohang Harbor.

I also like to thank my family for their continuous support and belief.

TABLE OF CONTENTS

DEDICATION.....	ii
ACKNOWLEDGEMENTS	iii
LIST OF TABLES.....	vii
LIST OF FIGURES.....	viii
ABSTRACT.....	xvi
CHAPTER 1 INTRODUCTION	1
1.1 Background and Objective of the Study.....	1
1.2 Scope of the Study.....	4
CHAPTER 2 LITERATURE SURVEY	6
2.1 Field Observations and Causation Investigations on Harbor Resonance Phenomena.....	6
2.2 Prior Theoretical, Experimental and Numerical Studies of Harbor Resonance	9
2.3 General Comments on Computer Modeling Techniques.....	17
2.3.1 Finite Difference Method	18
2.3.2 Boundary Element Method	19
2.3.3 Finite Element Method.....	19
CHAPTER 3 MODEL CONSTRUCTION AND VERIFICATION	21
3.1 FEM Computer Model	22
3.1.1 Governing Equation	22
3.1.2 Boundary Conditions and Hybrid Functional Construction	22
3.1.3 FEM Scheme	32
3.2 FEM Model Verification	36
3.3 Spectrum Analysis.....	41
CHAPTER 4 WAVE OSCILALTION MECHANISM STUDY IN HARBORS AND BAYS.....	44
4.1 Modeling of Crescent City Harbor, California.....	44
4.2 Modeling of San Pedro Bay, California	58
4.3 Wave Oscillation Comparison between Crescent City Harbor and San Pedro Bay	70
4.4 Discussion on Local Response	75
4.5 Modeling of Bay of Fundy, Canada	86
4.6 Summary	96
CHAPTER 5 APPLICATION FOR HARBOR IMPROVEMENTS.....	98
5.1 Modeling of Pohang Harbor, Korea	98
5.1.1 Introduction	98
5.1.2 Study of the Previous Condition of Pohang Harbor	100
5.1.3 Study of the Presend Condition at Pohang Harbor.....	103
5.1.4 Modeling of Additional Modification Strategy for Pohang Harbor	110
5.2 Modeling of Hualien Harbor, Taiwan.....	123
5.2.1 Introduction	123
5.2.2 Simulation of Present Condition at Hualien Harbor.....	124

5.2.3	Modification Strategy 1: A Second Opening	127
5.2.4	Modification Strategy 2: An Interior Gate.....	131
5.2.5	Modification Strategy 3: Energy Dissipaters.....	134
5.2.6	Modification Strategy 4: Energy Dissipaters with A Jetty Added	137
5.2.7	Modification Strategy 5: Combination of Energy Dissipaters.....	140
5.3	Summary	144
CHAPTER 6 CONCLUSION.....		146
REFERENCES.....		148

LIST OF TABLES

Table 4.1	Dominant waves in Crescent City Harbor and Los Angeles harbor during recent earthquake events	71
Table 4.2	Comparison between the observed and simulated amplification factor	95

LIST OF FIGURES

Figure 3.1	Calculation domain for the hybrid FEM model	23
Figure 3.2	The FEM mesh used for the rectangular harbor	38
Figure 3.3	Result comparisons for the rectangular harbor	39
Figure 3.4	Pumping mode in the rectangular harbor ($kl=1.32$)	40
Figure 3.5	Sloshing mode in the rectangular harbor ($kl=4.25$)	41
Figure 4.1	Location of Crescent City Harbor	45
Figure 4.2	Air photo of the small inner harbor in Crescent City Harbor with the broken docks during the tsunami event on November 15, 2006 noted	45
Figure 4.3	Simulation domain for Crescent City Harbor (left) and locations of special interest as A, B, C, D, E and the tide gauge (right)	46
Figure 4.4	Response curves at tide gauge location for different incoming wave directions	47
Figure 4.5	Response curves at locations noted by A-E and tide gauge station with incident wave from direction 2	48
Figure 4.6	The mode shape at 22.0 min for incoming wave direction 1	49
Figure 4.7	Oscillation mode at 10.3 min for incoming wave direction 2	50
Figure 4.8	(a) Tide gauge record in Crescent City Harbor for event on June 15, 2005	51
Figure 4.8	(b) Tide gauge record in Crescent City Harbor for event on November 15, 2006	51
Figure 4.8	(c) Tide gauge record in Crescent City Harbor for event on January 13, 2007	52
Figure 4.8	(d) Tide gauge record in Crescent City Harbor for event on August 15, 2007	52
Figure 4.9	(a) Corresponding spectral density of the tide gauge record at the Crescent City Harbor on June 15, 2005	53
Figure 4.9	(b) Corresponding spectral density of the tide gauge record at the Crescent City Harbor on November 15-16, 2006	54
Figure 4.9	(c) Corresponding spectral density of the tide gauge record at the Crescent City Harbor on January 13, 2007	54

Figure 4.9	(d) Corresponding spectral density of the tide gauge record at the Crescent City Harbor August 16-17, 2007	55
Figure 4.10	(a) Simulated response curve with the field observed dominant wave superimposed at Crescent City Harbor for event on June 15, 2005	56
Figure 4.10	(b) Simulated response curve with the field observed dominant wave superimposed at Crescent City Harbor for event on November 15, 2006	56
Figure 4.10	(c) Simulated response curve with the field observed dominant wave superimposed at Crescent City Harbor for event on January 13, 2007	57
Figure 4.10	(d) Simulated response curve with the field observed dominant wave superimposed at Crescent City Harbor for event on August 15, 2007	57
Figure 4.11	Illustration of changing of wave period due to water depth variation for certain wave length	58
Figure 4.12	Air photos of San Pedro Bay with simulation domain imposed (a) and LA/LB port (b)	59
Figure 4.13	Response curve at LA Berth60 for different incoming wave directions	60
Figure 4.14	(a) Historical records at the LA Berth60 for event on June 15, 2005	62
Figure 4.14	(b) Historical records at the LA Berth60 for event on November 15, 2006	62
Figure 4.14	(c) Historical records at the LA Berth60 for event on January 13, 2007	63
Figure 4.14	(d) Historical records at the LA Berth60 for event on April 01, 2007	63
Figure 4.14	(e) Historical records at the LA Berth60 for event on August 15, 2007	64
Figure 4.15	(a) Corresponding spectral density of the tide gauge record at LA Berth60 on June 15, 2005	64
Figure 4.15	(b) Corresponding spectral density of the tide gauge record at LA Berth60 on November 15, 2006	65
Figure 4.15	(c) Corresponding spectral density of the tide gauge record at LA Berth60 on January 13, 2007	65
Figure 4.15	(d) Corresponding spectral density of the tide gauge record at LA Berth60 on April 01, 2007	66
Figure 4.15	(e) Corresponding spectral density of the tide gauge record at LA Berth60 on August 15, 2007	66
Figure 4.16	(a) Simulated response curve with field observed dominant waves superimposed at LA Berth60 for event on June 15, 2005	67

Figure 4.16	(b) Simulated response curve with field observed dominant waves superimposed at LA Berth60 for event on November 15, 2006	68
Figure 4.16	(c) Simulated response curve with field observed dominant waves superimposed at LA Berth60 for event on January 13, 2007	68
Figure 4.16	(d) Simulated response curve with field observed dominant waves superimposed at LA Berth60 for event on April 01, 2007	69
Figure 4.16	(e) Simulated response curve with field observed dominant waves superimposed at LA Berth60 for event on August 15, 2007	69
Figure 4.17	Wave Spectrum at the tide gauge station in Crescent City Harbor during May, June and July, 2008	72
Figure 4.18	Wave Spectrum at the tide gauge station in Los Angeles harbor during May, June and July, 2008	72
Figure 4.19	(a) Water level time series at the tide gauge station in Crescent City Harbor on July 21, 2008	73
Figure 4.19	(b) Wave spectrum at the tide gauge station in Crescent City Harbor on July 21, 2008	74
Figure 4.20	(a) Water level time series at the tide gauge station LA Berth60 on July 21, 2008	74
Figure 4.20	(b) Wave spectrum at the tide gauge station LA Berth60 on July 21, 2008	75
Figure 4.21	Air photo of Los Angeles/Long Beach harbor with location ABCD noted	76
Figure 4.22	(a) Simulated response curves at location A for real bathymetry and uniform depth conditions	77
Figure 4.22	(b) Simulated response curves at location B for real bathymetry and uniform depth conditions	77
Figure 4.22	(c) Simulated response curves at location C for real bathymetry and uniform depth conditions	78
Figure 4.22	(d) Simulated response curves at location D for real bathymetry and uniform depth conditions	78
Figure 4.23	(a) Simulated response curves at location A for conditions of real bathymetry and uniform depth for the outside breakwater region	80
Figure 4.23	(b) Simulated response curves at location B for conditions of real bathymetry and uniform depth for the outside breakwater region	80
Figure 4.23	(c) Simulated response curves at location C for conditions of real bathymetry and uniform depth for the outside breakwater region	81

Figure 4.23	(d) Simulated response curves at location D for conditions of real bathymetry and uniform depth for the outside breakwater region	81
Figure 4.24	Bathymetry map of San Pedro Bay	82
Figure 4.25	Three simulation domains noted by small, medium and large	83
Figure 4.26	(a) Simulated response curves from three simulation domains at location A noted in Figure 4.21	84
Figure 4.26	(b) Simulated response curves from three simulation domains at location B noted in Figure 4.21	84
Figure 4.26	(c) Simulated response curves from three simulation domains at location C noted in Figure 4.21	85
Figure 4.26	(d) Simulated response curves from three simulation domains at location D noted in Figure 4.21	85
Figure 4.27	Map of Bay of Fundy and Gulf of Maine	87
Figure 4.28	Simulation domain for Bay of Fundy with mesh and incoming wave direction superimposed	89
Figure 4.29	Locations of gauge 1 to 10 selected for the result demonstration	90
Figure 4.30	Response curves at gauge 1,2,3,4,5 and 6	90
Figure 4.31	Response curves at gauge 1,2,3,7,8,9 and 10	91
Figure 4.32	Distribution of amplification factor in the simulation domain	92
Figure 4.33	Distribution of tidal range in the simulation domain (assuming that the tidal range outside of Gulf of Maine to be 7.5 ft)	93
Figure 4.34	Locations of 13 tide stations in Bay of Fundy	94
Figure 5.1	Location of Yongil Bay (left) and the layout of simulation domain with mesh and incoming wave directions superimposed (right)	99
Figure 5.2	Layouts of Pohang Harbor before and after the modifications	100
Figure 5.3	Results of numerical simulation (a) and field data (b) at Station T1	102
Figure 5.4	Results of numerical simulation (a) and field data (b) at Station T2	103
Figure 5.5	(a) Comparison between the simulated response curve for NE wave direction and the wave spectrum obtained from field data (1999) at Location P1	106

Figure 5.5	(b) Comparison between the simulated response curve for NE wave direction and the wave spectrum obtained from field data (1999) at Location P2	106
Figure 5.5	(c) Comparison between the simulated response curve for NE wave direction and the wave spectrum obtained from field data (1999) at Location P3	104
Figure 5.5	(d) Comparison between the simulated response curve for NE wave direction and the wave spectrum obtained from field data (1999) at Location P4	107
Figure 5.6	Response curves before and after the modification at Station T1 in Pohang Harbor	108
Figure 5.7	Response curves before and after the modification at Station T2 in Pohang Harbor	109
Figure 5.8	Response curves before and after the modification at Station T9 in Pohang Harbor	109
Figure 5.9	Layout of Pohang new harbor with the modification Case A	110
Figure 5.10	(a) Response curves at location P1 for present condition and after proposed Case A	111
Figure 5.10	(b) Response curves at location P2 for present condition and after proposed Case A	112
Figure 5.10	(c) Response curves at location P3 for present condition and after proposed Case A	112
Figure 5.10	(d) Response curves at location P4 for present condition and after proposed Case A	113
Figure 5.11	Layouts of Pohang new harbor with the modification Case B (left) and C (right)	113
Figure 5.12	(a) Response curves at location P1 for present condition and after proposed Case B and C	114
Figure 5.12	(b) Response curves at location P2 for present condition and after proposed Case B and C	115
Figure 5.12	(c) Response curves at location P3 for present condition and after proposed Case B and C	115
Figure 5.12	(d) Response curves at location P4 for present condition and after proposed Case B and C	116
Figure 5.13	Layouts of Pohang new harbor with the modification Case D	117

Figure 5.14	(a) Response curve at location P1 for present condition and after proposed Case A and D	117
Figure 5.14	(b) Response curve at location P2 for present condition and after proposed Case A and D	118
Figure 5.14	(c) Response curve at location P3 for present condition and after proposed Case A and D	118
Figure 5.14	(d) Response curves at location P4 for present condition and after proposed Case A and D	119
Figure 5.15	Layouts of Pohang new harbor with the modification Case E	120
Figure 5.16	(a) Response curves at location P1 for present condition and after proposed Case D and E	120
Figure 5.16	(b) Response curves at location P2 for present condition and after proposed Case D and E	121
Figure 5.16	(c) Response curves at location P3 for present condition and after proposed Case D and E	121
Figure 5.16	(d) Response curves at location P4 for present condition and after proposed Case D and E	122
Figure 5.17	Location of Hualien Harbor, Taiwan	123
Figure 5.18	Air photos of Hualien Harbor, Taiwan with simulation domain imposed (left) and stations #8, #10, #17 and #22 indicated (right)	124
Figure 5.19	(a) Simulated response curve and the observed field data at stations #22	125
Figure 5.19	(b) Simulated response curve and the observed field data at stations #17	126
Figure 5.19	(c) Simulated response curve and the observed field data at stations #08	126
Figure 5.19	(d) Simulated response curve and the observed field data at stations #10	127
Figure 5.20	Layout of the second opening modification strategy with reflection coefficients indicated	128
Figure 5.21	(a) Simulated response curves for the second opening modification strategy at stations #22	129
Figure 5.21	(b) Simulated response curves for the second opening modification strategy at stations #17	130
Figure 5.21	(c) Simulated response curves for the second opening modification strategy at stations #08	130

Figure 5.21	(d) Simulated response curves for the second opening modification strategy at stations #10	131
Figure 5.22	Layout of the interior gate modification strategy with reflection coefficients indicated	132
Figure 5.23	(a) Simulated response curves for the interior gate modification strategy at stations #22	133
Figure 5.23	(b) Simulated response curves for the interior gate modification strategy at stations #17	133
Figure 5.24	Layout of the energy dissipater modification strategy with reflection coefficients indicated	134
Figure 5.25	(a) Simulated response curves for energy dissipater modification strategy at station #22	135
Figure 5.25	(b) Simulated response curves for energy dissipater modification strategy at station #17	135
Figure 5.25	(c) Simulated response curves for energy dissipater modification strategy at station #08	136
Figure 5.25	(d) Simulated response curves for energy dissipater modification strategy at station #10	136
Figure 5.26	Layout of the added jetty modification strategy with reflection coefficients indicated	138
Figure 5.27	(a) Simulated response curves for the added jetty modification strategy at station #22	138
Figure 5.27	(b) Simulated response curves for the added jetty modification strategy at station #17	139
Figure 5.27	(c) Simulated response curves for the added jetty modification strategy at station #08	139
Figure 5.27	(d) Simulated response curves for the added jetty modification strategy at station #10	140
Figure 5.28	Layout of the combined energy dissipater modification strategy with reflection coefficients indicated	142
Figure 5.29	(a) Simulated response curves for the combined energy dissipater modification strategy at station #22	142
Figure 5.29	(b) Simulated response curves for the combined energy dissipater modification strategy at station #17	143

Figure 5.29	(c) Simulated response curves for the combined energy dissipater modification strategy at station #08	143
Figure 5.29	(d) Simulated response curves for the combined energy dissipater modification strategy at station #10	144

ABSTRACT

Harbors are built to provide a sheltered environment for the mooring of ships and vessels. For some wave periods the semi-enclosed harbor basin acts as a resonator to amplify the wave motions in the harbor due to the combined effects of wave diffractions, refractions and multiple reflections from the boundaries. This undesirable wave motion could induce significant ship motions, damage ships and dock facilities, and delay loading and unloading activities if the resonant wave periods are close to that of the ship mooring system. Harbor planners and engineers need to study the wave induced oscillations as new harbor layouts are contemplated.

This dissertation study presents a finite element model which could be used for predicting the response characteristics of harbors and bays of arbitrary shape and variable depth. The model incorporates the effects of wave reflection, refraction, diffraction and dissipation losses due to boundary absorption, bottom friction and energy losses due to the flow separation at the entrances. The model has been applied to three harbors (Crescent City Harbor in northern California, Pohang Harbor in Korea, and Hualien Harbor in Taiwan) and two bays (San Pedro Bay in southern California and Bay of Fundy in the east coast of Canada and US). The results from the finite element model have been shown to agree surprisingly well with the field data obtained from events such as earthquake generated tsunamis and hurricane induced wave oscillations, as well as normal day observations. The results reveal the fact that the wave oscillation condition inside a harbor or bay is determined by the local layout and bathymetry. The harbor or

bay responds to the incident wave in a predictable manner irrespective to the sources of driving forces such as typhoon, tsunami, winter storms, etc. The study also explains the tremendous tide phenomena at Bay of Fundy.

Modification strategy studies for reducing the seiche problems in Pohang Harbor and Hualien Harbor have also been presented. The model is shown to be an effective engineering tool for harbor planning and design to derive ways of eliminating or altering the harbor response so that the harbor may indeed provide a sheltered environment for moored ships and vessels.

CHAPTER 1 INTRODUCTION

1.1 Background and Objective of the Study

Long waves, whose periods range from tens of seconds to several hours, are always considered as a serious problem to coastal regions. They can be generated by winds, large structure collapses, landslides, earthquakes, and atmospheric pressure anomalies, etc. When they approach the coastline, they could cause severe damages to ships, vessels, and coastal structures and facilities.

To escape from those waves, harbors are built for providing a sheltered environment for the mooring of ships and vessels. In order to accomplish this goal, marine structures such as breakwaters and jetties are constructed (either attached or detached to the shore) to reduce the wave energy incident from the open sea.

The effectiveness of the breakwaters and jetties in reducing the incident wave energy must be ascertained in the planning and design of harbors. Normally, the breakwaters and jetties are effective in reducing the incident wave amplitude for waves with shorter wave periods (in the order of sixteen seconds or less). As the wave period increases, the effectiveness of the breakwaters or jetties in reducing the incident wave amplitude is progressively decreased. For waves of shorter wave period the effect of wave reflection from the harbor boundaries is quite small, thus only wave refraction due to changing

water depth and wave diffraction around the breakwaters and jetties need to be considered.

When the wave period increases (thus the wave length increases), the combined effect of wave diffraction, wave refraction and wave reflection from the harbor boundaries is very significant. In fact, it is possible that for certain semi-enclosed harbor the combined effect of wave diffraction, refraction and multiple reflections from the boundaries can cause significant increase in the wave amplitude compared with the incident wave amplitude. This is commonly referred to as “harbor resonance” due to long waves (see Raichlen, 1965; Raichlen and Lee, 1992).

Resonances or oscillations due to long period waves in bays and harbors have often been observed. For example, the seiche problem induced by typhoon generated waves in Hualien Harbor, Taiwan and the wave oscillation problem caused by winter storms in Pohang Harbor, Korea. In response to the daily flooding and ebbing tide, the Bay of Fundy (at the border of eastern Canada and north east of United States) has produced the largest tidal range in the world (approximately 50 ft). At the Crescent City Harbor region in northern California, larger than usual water surface elevations have been observed in response to a tsunami-genic event whether it is distant tsunami or local tsunami. The records at the tide gauge station located in Crescent City Harbor will be discussed in later chapters.

The resonance in a harbor could result in large fluctuation of water level in certain areas and produce strong currents throughout the harbor. In addition, it may also induce large ship motions for moored ships, especially if the fundamental resonant period of the harbor is close to that of the ship mooring system. Such oscillations could last as long as several days, delaying the cargo loading and unloading activities, breaking the mooring lines, and even damaging the moored boats and dock facilities. As a result, some ships or boats may have to move out to the open sea to avoid those large oscillations within the harbor, resulting in significant economic loss.

It is important for harbor planners and engineers to have the answers to the important questions such as:

1. What are the important wave periods that the harbor would respond to?
2. Are these wave periods close to the resonant periods of the ship mooring system?
3. What amplification of wave and current can be expected?
4. How will the harbor respond to different forcing functions such as tsunamis or hurricanes (called typhoons in the Pacific region) as opposed to long period swells?

Is this study useful for disaster warning system?

5. What are the essential factors that determine the oscillation wave periods?

6. Will the response characteristics change when the harbor layout is changed or modified?

This study has attempted to show that the numerical model can be used to arrive at the answers to those questions listed above. Even though no one can completely eliminate the need for physical models, the use of computer models can be shown to provide fast and reliable answers to the questions in such a way that the physical models, if absolutely needed, can be performed more efficiently and effectively to save time and money.

1.2 Scope of the Study

The second chapter includes the literature review. The field observations and the causation investigations of the wave oscillations in harbors and bays will be discussed first. Then a brief history of harbor resonance study will be summarized. The computer modeling techniques will also be outlined.

A hybrid finite element model using the mild slope equation will be derived in Chapter 3. Both the governing equation and boundary conditions will be discussed in detail. The model is verified with rectangular harbor experiments done by Ippen and Goda (1963) and Lee (1969). Spectral analysis is often used in the study to analyze the field observations and will be discussed at the end of Chapter 3.

In Chapter 4, the present model was used in the tsunami vulnerability study for Crescent City Harbor in northern California and the wave oscillation study for San Pedro Bay in southern California. The tide records in the two harbors during five recent earthquake generated tsunami events were used for the comparison with simulation results. Interesting observation was obtained and will be presented. Then the effects of harbor layout and bathymetry will be discussed based on the study of San Pedro Bay. The study for Bay of Fundy in the east coast of Canada and the United States is also included in Chapter 4.

The study in Chapter 5 focuses on harbor improvement. The modeling for Pohang Harbor in Korea and Hualien Harbor in Taiwan are included in this chapter. Each of the numerical simulation result was compared with the available field data. Different modification strategies to lessen the harbor resonance effect were proposed for each harbor and discussed in detail.

Significant conclusions drawn from this study are presented in Chapter 6.

CHAPTER 2 LITERATURE SURVEY

2.1 Field Observations and Causation Investigations on Harbor Resonance Phenomena

Resonances or oscillations due to long waves in bays and harbors have often been observed and the reasons were found to be varied in different cases. Direct observations have provided essential information for the harbor resonance study and thus future disaster prevention.

Observed sea-surface oscillations with periods of about 2.5 hours in New Zealand east coast harbors have been regarded as a response to edge waves generated by atmospheric forcing and occasionally by tsunamis (Heath, 1982). The large sea level oscillations in the Western Mediterranean were found to be the result of resonant coupling between an atmospheric wave, a coastal trapped edge wave and the normal modes of the harbor (Tintoré, et al., 1988).

The oscillations of long period waves in the vicinity of Onagawa Bay, north-east Japan were found to be induced by remarkable atmospheric pressure waves (Aida et al., 1972; Aida, 1974; Aida et al., 1975). The air pressure variances were also found to be the reason of the seiches in the Baltic Sea (Metzner, 2000). The significant correlation between the sea level oscillations and the atmospheric pressure disturbances was found in the inlets of the Balearic Islands (Gomis, et al., 1993). Later on the seiche motions were

explained as a result of “a resonant coupling between offshore surface waves generated by atmospheric disturbances and the fundamental mode of that inlet” (Garcies, et al., 1996).

The coastal seiches observed at Palawan Island, the Philippines and Magueyes Island, Puerto Rico were explained to be generated by tide-generated internal waves propagated from far-field (Giese, et al., 1987; Giese, et al., 1982; Giese, et al., 1990). However it was pointed by Huang, et al. (2000) that the waves could not propagate several days due to the strong dispersion. A local internal wave generation scenario was suggested.

The seiches induced by typhoons in Hualien Harbor, Taiwan have produced significant damages to the vessels moored inside the harbor (Su and Tsay, 2002). The wave oscillation generated by winter storms inside Pohang Harbor, Korea resulted in downtime about 2 months every year (Jeong, et al., 1997). The large amplitude ship motions in the Esperance Harbour, Australia were generated by surge and sway motions due to low frequency water-level oscillations amplified by harbor resonance (Morison and Imberger, 1992).

It was first found by Bowers (1977) that a set-down beneath short period wave groups can also cause long period harbor resonances. Lately Mei and Agnon (1989) and Wu and Liu (1990) discussed separately that locked long wave within the group will not cause the resonance, but the long free wave generated to compensate the discontinuity of the locked long wave will. The experiment on harbor resonance induced by incident regular waves

and irregular short waves studied on a long and narrow bay by Girolamo (1996) showed that the bay responded equally to the long waves generated nonlinearly by incoming short waves and the incident linear free long waves.

The Wellington Harbor, New Zealand was reported of experiencing oscillations during both 1960 Chilean and 1964 Alaskan earthquake-generated tsunamis, the results were used to define the three longest periods of the characteristic oscillation modes (Gilmour, 1990). The wave oscillation on November 3, 1994, in Skagway, Alaska was generated by an underwater landslide formed during the collapse of a cruise ship wharf undergoing construction at the head of Taiya Inlet. Persistent wave motion with an amplitude of 1 m and a period of 3 min recorded by a tide gauge in Skagway Harbor following the landslide was linked to the formation of a cross-inlet seiche and quarter-wave resonance within the harbor (Kulikov and Rabinovich, 1996). Seiche motions in three small harbors were discussed by Okihiro and Guza (1996). It was observed that the amplification of seiche energy varied with the seiche frequency, with the largest at the lowest resonant mode of each harbor. The seiche motions observed in the Heda Bay, Japan were compared with the theoretical results by Tada, et al. (1992). It was found that the largest inundation height of a tsunami incident into a bay occurs near the anti-node of the theoretically expected fundamental mode of the bay. It was also mentioned that the mode analysis for different bays would offer effective material for tsunami disaster prevention research.

The oscillations of water level were observed in numerous harbors and bays and the causations were addressed to many reasons. However, it's seen that many were found to be the coupling of harbor resonant modes with other driving forces. This mechanism will be discussed in the later chapters.

2.2 Prior Theoretical, Experimental and Numerical Studies of Harbor Resonance

Since the resonance in harbors could cause tremendous economic and property loss, many experimental, theoretical, and numerical approaches have been done on this topic. As early as in 1950s, both theoretical and experimental studies were started on the oscillations in simple-shaped harbor such as circular and rectangular harbors (McNown, 1952; Kravtchenko and McNown, 1955). For steady, irrotational, incompressible flow, the governing equation is the Laplace's Equation:

$$\frac{\partial^2 \phi}{\partial x^2} + \frac{\partial^2 \phi}{\partial y^2} + \frac{\partial^2 \phi}{\partial z^2} = 0 \quad (2.1)$$

Where ϕ is the velocity potential function. In those studies the wave condition at the harbor entrance was assumed to be the crest of a standing wave, which was proved to be invalid in the later research.

The classic Laplace's equation or Helmholtz equation was used by many later on to solve for the velocity potential (e.g. Lee, 1971; Grilli et al., 1989; Lee et al., 1992).

It was pointed out by Wiegel (1964) and Wilson (1972) that the resonant (eigen) periods of a particular harbor are determined by the basin geometry and depth. The study herein will have a more concrete proof and a more precise discussion on this point.

The study by Raichlen (1966) on a non-rotating rectangular harbor described the resonant (eigen) periods of a enclosed rectangular harbor with length L and uniform depth H by the “Merian’s formula”:

$$T_n = \frac{2L}{n\sqrt{gH}}, \text{ for mode } n = 1, 2, 3, \dots \quad (2.2)$$

Where g is the gravitational acceleration. A similar expression for an open-mouth basin is

$$T_n = \frac{4L}{(2n+1)\sqrt{gH}}, \text{ for mode } n = 1, 2, 3, \dots \quad (2.3)$$

These formulas can be roughly used to estimate the oscillation periods of a harbor basin.

Miles and Munk (1961) studied wave oscillation in a harbor connected to the open sea condition by including the effect of wave radiation from the harbor mouth to the open sea.

It was shown that a Green’s function $g(x, y, \xi)$ satisfies the Helmholtz equation inside the harbor if the water depth can be treated as a constant.

$$\frac{\partial^2 g}{\partial x^2} + \frac{\partial^2 g}{\partial y^2} + k^2 g = 0 \quad (2.4)$$

However, Green’s function for an arbitrary shape harbor layout could not be easily obtained. Ippen and Goda (1963) studied the rectangular harbor connected to the open sea

condition with both theoretical and experimental methods. The Fourier transformation method was used to simulate the wave radiation from the harbor entrance to the open sea. Good agreement between the theoretical results and experiments made the study a good reference example for the validation of later numerical models.

The study was improved by Lee (1969, 1971) by including the theoretical and experimental studies conducted for an arbitrary shape harbor. The experimental results by Lee (1969) had a better agreement with the theoretical approaches than those of Ippen and Goda (1963) because the more effective absorption (or damper) boundary have made the simulation of open sea condition more realistic in the laboratory basin. The so-called 'boundary element method' were first used by Lee (1969). The solution of the Helmholtz equation (2.4) is formulated as an integral equation, an approximation is employed to solve the integral equation for an arbitrary shape harbor of constant depth by converting it to a matrix equation. The final solution is obtained by matching solutions for the inside and outside regions at the harbor entrance. This method has been proven to be powerful for arbitrary shape harbors with relatively uniform water depth and reflective interior boundaries.

Several other investigators, such as Hwang and Tuck (1970) using boundary element method; Chen and Mei (1974) and Houston (1980) using finite element method, have continuously studied the harbor resonance problem for arbitrary shape harbors. These

studies have also been restricted to cases without considering entrance loss, bottom friction and effect of boundary absorption.

The dissipative effects on harbor resonance have gradually been considered in the later studies. Ito (1970) and Horikawa and Nishimura (1970) both considered a quadratic law of head loss. Ito (1970) investigated numerically the effect of a narrow passage between two breakwaters in reducing the response of Ofunato Bay in Japan to tsunamis. The quadratic law was employed to formulate the entrance head loss

$$\Delta\eta = \frac{1}{2} \frac{f_e}{g} u |u| \quad (2.5)$$

where u is the velocity at the entrance and f_e is the separation loss coefficient which was assumed to be equal to 1.5. This quadratic head loss law was widely used in the future studies (Miles and Lee, 1975; Ünlüata and Mei, 1975). The quadratic law was also used to simulate the bottom friction (Lee et al., 1998; Terra et al., 2005), in which u is the velocity at the bottom instead of at the entrance. Chen (1986) gave another approach in which he assumed the bottom friction is proportional to flow velocity with a phase difference.

Lepelletier (1980) investigated harbor oscillation problem due to nonlinear transient long waves under the effect of various sources of energy dissipation, including the separation loss, bottom and wall friction, surface and dry friction. The higher order Boussinesq type

of equations for velocity potential have been successfully applied to harbor modeling (e.g. Lepelletier and Raichlen, 1987; Zelt and Raichlen, 1990).

With the rapid development of computers, many later numerical models dealing with large domain simulation were developed including the effect of separation losses and dissipative boundary conditions, such as Demirbilek and Panchang (1998) and Lee et al. (1998).

Time domain modeling tools are usually used for tsunami propagation through the ocean and consequent inundation at coast (Titov, et al., 2005; Synolakis and Bernard, 2006). Compared with unsteady state (or time domain) solutions, steady state (frequency domain) approaches are widely selected to solve harbor resonance problems for long waves. An effective and convenient model equation which has been found to be well suited for combining the effects of wave refraction and diffraction in the coastal region is the two-dimensional elliptic mild slope wave equation first derived by Berkholf (1972).

The mild slope equation can be written in the form as

$$\nabla \cdot CC_g \nabla \phi + k^2 CC_g \phi = 0 \quad (2.6)$$

Where ϕ is the horizontal variation in velocity potential Φ ,

$$\Phi = R \left\{ \phi(x, y) \frac{\cosh k(z+h)}{\cosh kh} \exp(-i\omega t) \right\} \quad (2.7)$$

in which ω and k are wave frequency and wave number. $C = \omega/k$ is the wave celerity, and $C_g = \partial\omega/\partial k$ is group velocity. The equations were derived using a

vertical-averaging procedure, by which the three-dimensional equations were reduced to the depth-integrated equations in horizontal plane. This approach made an important achievement that it considered the combined refraction and diffraction phenomenon.

The theory is restricted to irrotational and inviscid linear harmonic waves, and a slowly varying bathymetry condition. The work by Ehrenmark and Williams (2001) examined the limitation of the mild slope equation and attempted to highlight the possibility of a more liberal use than was previously assumed possible. It was found that specifying phase and group velocity which are consistent with linear wave beach theory can lead to improvements in solving the mild slope equation over steep beaches.

It has been found that the results of regular mild slope equation tend to overestimate the amplification factor of the harbor resonance because of ignoring the separation and dissipation loss (Okehiro et al., 1993). The effects of bottom friction and boundary absorption on wave scattering were examined by Chen (1986). The regular mild slope equation (2.6) was modified by including a parameter λ :

$$\frac{\partial}{\partial x_j} \lambda C C_g \frac{\partial \phi}{\partial x_j} + k^2 C C_g \phi = 0 \quad (2.8)$$

Similar approaches were developed by Lejeune et al. (1989) and Yu (1996) that the regular mild slope equation was modified by a parameter to account for the bottom friction. Shoaling and breaking effects were included in many works such as by Balas

and Inan (2002) and Massel (1995). The nonlinear effects of high order were investigated by Mei (1999).

The regular mild slope equation was found to fail to give adequate approximation for certain types of topography such as rippled beds. O'Hare and Davies (1992) achieved a successful result for ripple beds by dividing the smoothly varying bed profile into a series of horizontal steps and relating the wave fields on either side of each step by a transfer matrix.

Various extended and modified approaches (so called extended mild slope equation and modified mild slope equation) were generated to improve the performance of the regular mild slope equation for abrupt and undulating topography. Terms of bottom curvature and slope were included into the regular mild slope equation by groups of researchers (Massel 1993; Chamberlain and Porter, 1995; Chandrasekera and Cheung, 1997). Although different approaches were used to derive the equations, they all obtained equivalent formulas as:

$$\nabla \cdot CC_g \nabla \phi + \left(k^2 CC_g + f_1 \nabla^2 h g + f_2 (\nabla h)^2 g k \right) \phi = 0 \quad (2.9)$$

in which f_1 and f_2 are functions of kh , and h is the water depth.

The effects of curvature and slope terms were examined by Chandrasekera and Cheung (1997) and Lee and Yoon (2004). More efforts were expended by Chandrasekera and Cheung (2001) to involve two coupled governing equations in the refraction-diffraction modeling. The two equations were derived from the exact seabed boundary condition and

the Laplace equation. Two terms were used to approximate the velocity potential. It was found that the two coupled equations can predict more accurate vertical fluid velocities than the extended mild slope equation.

A so-called complementary mild slope equation was developed by Kim and Bai (2004). The equation was derived from Hamilton's principle in terms of stream function. A sloping-bottom mode was added to the local mode series expansions and improved the performance of the velocity field simulation.

A consistent coupled-mode model was developed by Athanassoulis and Belibassakis (1999) and continuously studied by Belibassakis et al. (2001). The vertical distribution of the wave potential was represented by local-mode series containing the propagating, evanescent, and additional modes (also called slopping-bottom modes) at each horizontal position. The method improved the pressure and tangential velocity modeling at the bottom. Because of the involvement of more modes, the model has a higher computation cost. The coupled-mode model was further evaluated by comparing with the data from directional wave buoys deployed around the rim and over Scripps Canyon, near San Diego, California, during the Nearshore Canyon Experiment (Magne et al., 2007). It was concluded that the evanescent and slopping-bottom modes may be important for wave propagation over a canyon at small incident angles, but minor important for the energy transformation at large oblique angles, in which condition the standard and modified mild slope equation also yield good results.

Although the mild slope equation was obtained with the assumption of “mild slope”, the work by Booji (1983) showed that the regular mild slope equation is applicable for bottom slope as large as $1/3$. Since the mild slope equation can be conveniently implemented in a finite element model, we will apply it to real harbors in this presentation. The basics of the model will be shown in the next chapter.

2.3 General Comments on Computer Modeling Techniques

As discussed in Raichlen and Lee (1992), there were three numerical methods to be employed for the computer models: (1) finite difference method; (2) boundary element method; (3) finite element method. The model could either be run in time domain with the results expressed as a function of time or in frequency domain with the results expressed as a function of wave frequency. When the time sequence of the dependant parameters (such as wave amplitude and water particle velocity field) is important, time domain simulations will be appropriate. For harbor planning and design purpose, usually the exact incident wave form is not known or not yet occurred, frequency domain computations would appear to be more appropriate. With frequency domain simulation one can explore all possible scenarios in the model more effectively.

We will first discuss the pros and cons of the three numerical method used in the computer models. We must realize at the outset that no one particular computer modeling technique is superior in all applications. Each has its own pros and cons. Selection of a

modeling technique will depend on the experience and background of the individuals, or the scope and objective of the modeling efforts.

2.3.1 Finite Difference Method

Finite difference method discretizes the function on rectangular grids with equal or varying spacing. The function on a node is related to the values on the neighboring nodes which define the grid system. Spatial or time derivatives are approximated by the difference of the values on the neighboring nodes or the successive time steps. The functions on each node of the whole system are calculated by solving a series of difference equations with certain boundary conditions. The finite difference method is not restricted to any governing equations and the approximation is straightforward. But the calculation might not always be stable for time dependent problems and the curved boundary can only be approximated by rectangular grids. The earliest use of the method was conducted by Leendertse (1967). The two-dimensional depth-averaged governing equations containing nonlinear terms were solved to study the long wave propagation mechanism. Other examples can be found in Chiang and Lee (1982) and Titov and Synolakis (1998).

2.3.2 Boundary Element Method

Boundary element method formulates the solution inside a harbor domain by an integral equation along the boundary, and the boundary integral equation is converted into a matrix equation with approximation from each of the boundary elements. The method was first used for harbor resonance study by Lee (1969) and Hwang and Tuck (1970) independently. Physically, this method can be considered as distributing sources, sinks and doublets with proper strength along the boundary to satisfy the governing equation and the boundary conditions. The unique virtue of this method is that it can reduce the domain of calculation by one dimension. A three dimensional problems can be formulated to solve equations on the boundary surface and a two dimensional problem can be reduced to integration along the line boundary. The limitation of this method is that it can only be used for well known differential equations such as the Laplace's equation and the Helmholtz equation with known fundamental solutions. Examples of computer models based on boundary element method can be found in Lee (1971), Lee and Raichlen (1972), Grille et al. (1989) and Lee et al. (1992).

2.3.3 Finite Element Method

Finite element method divides the simulation domain into finite polygons or polyhedrons, called elements. A shape function is needed to approximate the solution inside each element. The boundary value problem is presented by a variational principle with a

functional that contains a bilinear form for the unknown coefficients of the shape function. The functional is then minimized to obtain a series of linear algebraic equations about the unknown coefficients for the shape function, from which the sought unknowns at the nodal points can be obtained. If the functional is not attainable, weak form formulation or Galerkin method can be used. This makes the method applicable to a wide range of physical and engineering problems since almost any governing partial differential equation can be approximated by the Galerkin procedure. Another advantage of the method is that the boundary of the simulation domain can be more precisely approximated and finer grids can be easily applied for special local regions. One of the first applications of this method in this field was conducted by Chen and Mei (1974). Mild slope equation was solved and an eigenfunction expansion was used at a common boundary in the exterior region of the harbor. It is also called hybrid finite element method. Examples of finite element model can be found in Ganaba et al. (1984), Houston (1978), Lepelletier and Raichlen (1987), Lee et al. (1998), Mei et al. (2005) and Lee and Lai (2006).

CHAPTER 3 MODEL CONSTRUCTION AND VERIFICATION

The construction of a physical model would occupy a large amount of space and be costly in both time and money. Numerical modeling is a much more cost-effective approach. A hybrid finite element model using the mild slope equation will be described in detail in this chapter. The present computer model solves the mild slope equation over arbitrary shape harbor of variable water depth. It incorporated the effects of wave reflection, refraction, diffraction and dissipation losses due to boundary absorption, bottom friction and energy losses due to the flow separation at the entrances. An earlier version of the model has been applied successfully for the modeling of harbor responses of Los Angeles and Long Beach harbors by Lee et al. (1998). Similar model has also been used to model a large coastal region for assessing the potential coastal impacts of tsunamis surrounding the island of Taiwan (see Lee and Lai, 2006). The present finite element model performed extremely well in all the case studies with results to be presented in the next chapter. Parts of the present study were published in a chapter in the book “Handbook of Coastal Engineering” (Lee and Xing, 2008) and four conference papers (Xing et al., 2008; Lee et al., 2008; Tsai et al., 2008; Kwak et al., 2008).

3.1 FEM Computer Model

3.1.1 Governing Equation

The governing equation is the mild slope equation first derived by Berkhoff (1972):

$$\nabla \cdot (CC_g \nabla \phi) + \frac{C_g \omega^2}{C} \phi = 0 \quad (3.1)$$

which also can be written in the form of (2.6). In which $\phi = \phi(x, y)$ is the horizontal variation in velocity potential Φ as shown in equation (2.7), $C = \frac{\omega}{k}$ is wave celerity,

$C_g = \frac{C}{2}(1+G) = \frac{C}{2} \left(1 + \frac{2kh}{\sinh 2kh} \right)$ is the group velocity and $G = \frac{2kh}{\sinh 2kh}$. k and ω

are wave number and frequency, h is water depth. This equation can be obtained on the base of energy conservation principle.

3.1.2 Boundary Conditions and Hybrid Functional Construction

The modeling area is divided into two parts, the inner area and the outer area, as shown in Figure 3.1. The inner area includes the harbor and a connected semicircular area ∂A . The half ring-shaped outer area is assumed to have a uniform water depth and a radius of infinity.

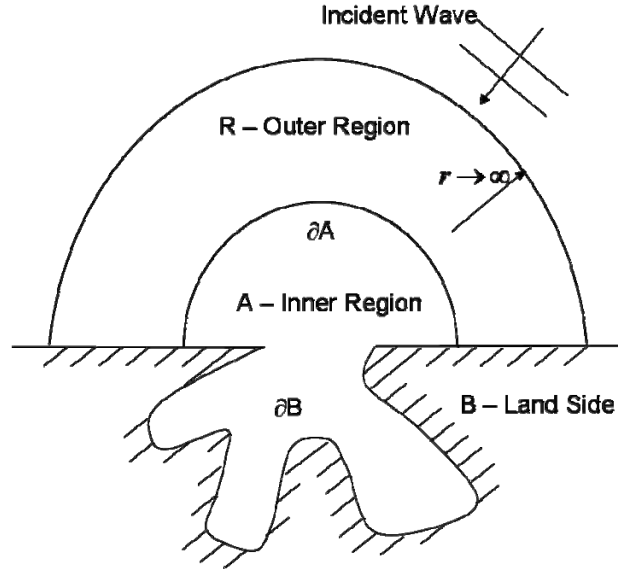


Figure 3.1 Calculation domain for the hybrid FEM model

The conservation of the total complex wave energy in the inner and outer areas can be formulated in two equations as:

$$\frac{\partial}{\partial t} E_A + \int_{\partial A + \partial B} E_F^A ds = 0 \quad (3.2)$$

$$\frac{\partial}{\partial t} E_R + \int_{\partial A + \partial R} E_F^R ds = 0 \quad (3.3)$$

Where A indicates the inner area, R indicates the outer area, B is the landside. E_A and E_R are the total instantaneous complex wave energy in inner area and outer area. E_F^A and E_F^R are the instantaneous complex wave energy flux through the boundaries from inner and outer areas.

The complex potential wave energy per horizontal unit area is

$$E_p = \frac{1}{2} \rho g \eta^2 \quad (3.4)$$

where η is the free surface elevation.

$$\eta = -\frac{1}{g} \left(\frac{\partial \Phi}{\partial t} \right)_{z=0} = -\frac{1}{g} (-i\omega) \phi \exp(-i\omega t) \quad (3.5)$$

Thus,

$$E_p = \frac{1}{2} \rho g \eta^2 = \frac{1}{2} \rho g (-\omega^2) \frac{1}{g^2} \phi^2 \exp(-2i\omega t) = -\frac{\rho}{g} \exp(-2i\omega t) \left(\frac{1}{2} \omega^2 \phi^2 \right) \quad (3.6)$$

The complex kinetic wave energy per horizontal unit area is

$$\begin{aligned} E_k &= \int_{-h}^0 \frac{\rho}{2} (u^2 + v^2 + w^2) dz \\ &= \frac{\rho}{2} \int_{-h}^0 (\nabla \phi)^2 \left(\frac{\cosh k(z+h)}{\cosh kh} \right)^2 \exp(-2i\omega t) dz \\ &\quad + \frac{\rho}{2} \int_{-h}^0 \phi^2 \left(\frac{k \sinh k(z+h)}{\cosh kh} \right)^2 \exp(-2i\omega t) dz \\ &= \frac{\rho}{2} (\nabla \phi)^2 \exp(-2i\omega t) \frac{1}{(\cosh kh)^2} \int_{-h}^0 (\cosh k(z+h))^2 dz \\ &\quad + \frac{\rho}{2} \phi^2 \exp(-2i\omega t) \frac{1}{(\cosh kh)^2} \int_{-h}^0 \left[(k \cos k(z+h))^2 - k^2 \right] dz \\ &= \frac{\rho}{2} (\nabla \phi)^2 \exp(-2i\omega t) \frac{1}{(\cosh kh)^2} \frac{1}{k} \left(\frac{\sinh 2kh}{4} + \frac{kh}{2} \right) \\ &\quad + \frac{\rho}{2} \phi^2 \exp(-2i\omega t) \frac{1}{(\cosh kh)^2} \left[k \left(\frac{\sinh 2kh}{4} + \frac{kh}{2} \right) - k^2 h \right] \\ &= \frac{\rho}{2} (\nabla \phi)^2 \exp(-2i\omega t) \frac{\tanh kh}{\sinh kh \cosh kh} \frac{1}{k} \left(\frac{\sinh 2kh}{4} + \frac{kh}{2} \right) \\ &\quad + \frac{\rho}{2} \phi^2 \exp(-2i\omega t) \frac{\tanh kh}{\sinh kh \cosh kh} \left[k \left(\frac{\sinh 2kh}{4} - \frac{kh}{2} \right) \right] \end{aligned} \quad (3.7)$$

By introducing the dispersion relation $\omega^2 = gk \tanh kh$, the complex kinetic energy can be written as

$$\begin{aligned}
E_k &= \frac{\rho}{2} (\nabla \phi)^2 \exp(-2i\omega t) \frac{\omega^2}{gk \sinh 2kh} \frac{1}{k} \left(\frac{\sinh 2kh}{2} + kh \right) \\
&\quad + \frac{\rho}{2} \phi^2 \exp(-2i\omega t) \frac{\omega^2}{gk \sinh 2kh} \left[k \left(\frac{\sinh 2kh}{2} - kh \right) \right] \\
&= \frac{\rho}{2g} (\nabla \phi)^2 \exp(-2i\omega t) cc_g + \frac{\rho}{2g} \phi^2 \exp(-2i\omega t) \omega^2 \left[\frac{1}{2}(1-G) \right] \\
&= \frac{\rho}{g} \exp(-2i\omega t) \frac{1}{2} \left[cc_g (\nabla \phi)^2 + \frac{1}{2}(1-G) \omega^2 \phi^2 \right] \quad (3.8)
\end{aligned}$$

The total complex wave energy density can be obtained:

$$\begin{aligned}
E &= E_p + E_k \\
&= -\frac{\rho}{g} \exp(-2i\omega t) \left(\frac{1}{2} \omega^2 \phi^2 \right) + \frac{\rho}{g} \exp(-2i\omega t) \frac{1}{2} \left[cc_g (\nabla \phi)^2 + \frac{1}{2}(1-G) \omega^2 \phi^2 \right] \\
&= \frac{\rho}{g} \exp(-2i\omega t) \frac{1}{2} \left[cc_g (\nabla \phi)^2 - \frac{c_g \omega^2}{c} \phi^2 \right] \quad (3.9)
\end{aligned}$$

The instantaneous complex energy flux, E_f , in any specified n direction through a section of unit width can be expressed as

$$E_f = -\int_{-h}^0 p_d u_n dz \quad (3.10)$$

where p_d is the dynamic pressure, and u_n is the water velocity along the n direction.

$$p_d = \rho \frac{\partial \Phi}{\partial t} = (-i\omega) \phi \frac{\cosh k(z+h)}{\cosh kh} \exp(-i\omega t) \quad (3.11)$$

Thus

$$\begin{aligned}
E_f &= -\rho \int_{-h}^0 \frac{\partial \Phi}{\partial t} \frac{\partial \Phi}{\partial n} dz \\
&= -\rho \int_{-h}^0 (-i\omega) \exp(-2i\omega t) \left(\frac{\cosh k(z+h)}{\cosh kh} \right)^2 \phi \frac{\partial \phi}{\partial n} dz \\
&= \rho(i\omega) \exp(-2i\omega t) \phi \frac{\partial \phi}{\partial n} \frac{1}{(\cosh kh)^2} \frac{1}{k} \left(\frac{\sinh 2kh}{4} + \frac{kh}{2} \right) \\
&= \rho(i\omega) \exp(-2i\omega t) \phi \frac{\partial \phi}{\partial n} \frac{\tanh kh}{2 \cosh kh \sinh kh} \frac{1}{k} \left(\frac{\sinh 2kh}{2} + kh \right) \\
&= \rho(i\omega) \exp(-2i\omega t) \phi \frac{\partial \phi}{\partial n} \frac{\omega^2}{gk} \frac{1}{k} \frac{1}{2} (1+G) \\
&= \frac{\rho}{g} (i\omega) \exp(-2i\omega t) c c_g \phi \frac{\partial \phi}{\partial n}
\end{aligned} \tag{3.12}$$

A hybrid finite element scheme can be obtained from the above equations considering the different boundary conditions.

(I). Partial Absorption Boundary

The solid boundary such as a vertical wall or a natural beach and the energy releasing boundary such as a river outlet can be treated as that energy is partially absorbed and partially reflected. The energy flux out through the boundary is formulated using a second-order scheme as

$$\frac{\partial \phi}{\partial n} = -i\alpha k \phi - \frac{i\alpha}{2k} \frac{\partial^2 \phi}{\partial s^2} \tag{3.13}$$

where α is the absorption coefficient with a range of $0 \leq \alpha \leq 1$. It should be mentioned

that for partially absorbing boundaries, the changing of absorption coefficient α may represent different boundary conditions. When $\alpha = 0$, it represents fully reflecting condition, i.e. $\frac{\partial \phi}{\partial n} = 0$. When $\alpha = 1$, it represents fully absorbing condition. The relation between absorption coefficient and reflection coefficient R for an incident wave angel θ^i is

$$R = -\frac{(\alpha \cos \theta^i)^2 - 2\alpha \cos \theta^i + \alpha^2}{(\alpha \cos \theta^i)^2 + 2\alpha \cos \theta^i + \alpha^2} \quad (3.14)$$

In the functional, the absorption boundary can be included by a term as

$$\begin{aligned} \iint_{\partial B} E_f dt ds &= \frac{\rho}{g} \frac{1}{-2i\omega} \exp(-2i\omega t) \int_{\partial B} i\omega C C_g \phi \frac{\partial \phi}{\partial n} ds \\ &= -\frac{\rho}{g} \exp(-2i\omega) \frac{1}{2} \int_{\partial B} C C_g \phi (-i\alpha k \phi) ds \\ &= \frac{\rho}{g} \exp(-2i\omega) \int_{\partial B} \frac{1}{2} i\omega C_g \alpha \phi^2 ds \end{aligned} \quad (3.15)$$

Only first-order scheme, the first term in (3.13), is considered in (3.15).

(II). Bottom Friction Boundary

The energy dissipation due to bottom friction is described as an instantaneous energy flux throughout the bottom:

$$E_f = \tau_b U_b \quad (3.16)$$

where τ_b is the instantaneous complex shear stress at the bottom, which can be formulated by the water particle velocity near the bed as

$$\tau_b = \frac{1}{2} \rho K_b |U_b| U_b \quad (3.17)$$

where K_b is a dimensionless friction coefficient. The particle velocity near the bed is

$$U_b = \left. \frac{\partial \phi}{\partial s} \right|_b = \nabla \phi \left(\frac{1}{\cosh kh} \right) \exp(-2i\omega t) \quad (3.18)$$

With introducing a bottom friction coefficient, $f_\omega = \frac{1}{2} g K_b |U_b|$, the energy flux through bottom becomes

$$E_f = \frac{\rho}{g} f_\omega \left(\frac{1}{\cosh kh} \right)^2 (\nabla \phi)^2 \exp(-2i\omega t) \quad (3.19)$$

In order to get the frequency domain formulation, the energy flux is integrated over time and space, the result of the bottom friction energy flux is

$$\iint_A E_f dt dA = \frac{\rho}{g} \exp(-2i\omega t) \int_A \frac{i}{2\omega} f_\omega \left(\frac{1}{\cosh kh} \right)^2 (\nabla \phi)^2 dA \quad (3.20)$$

The bottom friction coefficient can be obtained based on the bottom roughness study by Jonsson (1976) and Jonsson and Carlsen (1976). The resulted formula is

$$\begin{aligned}
f_\omega &= 0.2g\omega C_{bf}^{0.75} \alpha_b^{0.25} & \text{for } 1.6 < \frac{\alpha_b}{C_{bf}} < 100 \\
f_\omega &= 0.15g\omega\alpha_b & \text{for } \frac{\alpha_b}{C_{bf}} < 1.6
\end{aligned} \tag{3.21}$$

where $\alpha_b = \frac{a}{\sinh kh}$, C_{bf} is the Nikuradse roughness height, a is wave amplitude.

(III). Entrance Loss

The quadratic entrance head loss at the harbor entrance is applied in the present model,

$$\Delta H = f_e \frac{U^2}{2g} = f_e |U_0| \frac{U}{2g} = K_e U \tag{3.22}$$

In which $K_e = \frac{f_e}{2g} |U_0|$. f_e is the dimensionless entrance loss coefficient. $|U_0|$ is the averaged velocity at the harbor entrance computed considering no entrance loss, U is the new entrance velocity to be computed considering the entrance loss in the model. Thus the relationship of the complex velocity potentials at the entrance can be written as

$$\phi_1 = \phi_2 + \Delta\phi = \phi_2 + \frac{g}{i\omega} f_e |U_0| \frac{U}{2g} \tag{3.23}$$

The weighted residual method is used to find the functional for the harbor entrance,

$$\delta F_e = \int_{\partial E} \delta\phi^* C C_g \left(\phi_1 - \phi_2 - \frac{g}{i\omega} f_e |U_0| \frac{U}{2g} \right) ds \tag{3.24}$$

where ϕ_1 and ϕ_2 are the velocity potential before and after the harbor entrance.

(IV). Wave Transmission through Porous Breakwater

Wave energy is considered as partially transmitted and partially absorbed when a wave passes through a porous breakwater. The transmitted wave potential ϕ_T is assumed to be proportional to the incoming wave potential ϕ_i

$$\frac{\partial \phi_T}{\partial n} = K_T \frac{\partial \phi_i}{\partial n} = ikK_T \phi_i \quad (3.25)$$

where K_T is the transmission coefficient through the breakwater.

The integrated wave energy transmission can be written as

$$\begin{aligned} \int_{\partial T} \int E_f dt ds &= -\frac{\rho}{g} \exp(-2i\omega t) \int \frac{1}{2} CC_g \phi_T \frac{\partial \phi_T}{\partial n} ds \\ &= -\frac{\rho}{g} \exp(-2i\omega t) \int \frac{1}{2} CC_g (K_T \phi_i) (ikK_T \phi_i) ds \\ &= -\frac{\rho}{g} \exp(-2i\omega t) \int \frac{1}{2} C_g i\omega K_T^2 \phi_i^2 ds \end{aligned} \quad (3.26)$$

(V). Far Field Boundary

For the far field boundary, the Sommerfeld radiation condition is applied

$$\lim_{r \rightarrow \infty} \sqrt{r} \left(\frac{\partial}{\partial r} - ik \right) \phi_s = 0 \quad (3.27)$$

where $\phi_S = \phi_R - \phi_I$. ϕ_I , ϕ_R , and ϕ_S are incident wave potential, outer region wave potential, and scattered wave potential respectively. The scattered potential satisfying the Helmholtz equation and the radiation condition can be expressed as

$$\phi_S = \sum_{n=0}^{\infty} \alpha_n H_n(kr) \cos n\theta \quad (3.28)$$

where α_n is unknown coefficients and H_n is the Hankel function.

Integration of equation (3.2) and (3.3) can be written as:

$$E_A + \int_{\partial A + \partial B} E_f^A dt ds = const \quad (3.29)$$

$$E_R + \int_{\partial A + \partial R} E_f^R dt ds = const \quad (3.30)$$

Based on the equations previously derived, the Hybrid functional can be obtained by adding equation (3.29) and (3.30)

$$\begin{aligned} F(\phi) = & \frac{\rho}{g} \exp(-2i\omega t) \left\{ \iint_A \frac{1}{2} \left[CC_g (\nabla \phi)^2 - \frac{C_g \omega^2}{C} \phi^2 \right] dx dy \right. \\ & + \int_{\partial A} CC_g \left[\frac{1}{2} \phi_S - (\phi_A - \phi_I) \right] \frac{\partial \phi_R}{\partial n_A} ds \\ & \left. - \int_{\partial A} \frac{1}{2} CC_g \phi_S \frac{\partial \phi_I}{\partial n_A} ds \right\} \end{aligned}$$

$$\begin{aligned}
& -\int_A \frac{i}{2\omega} f_\omega \left(\frac{1}{\cosh kh} \right)^2 (\nabla \phi)^2 dx dy \\
& -\int_{\partial B} \frac{1}{2} i \omega C_g \alpha \phi^2 ds \\
& +\int_{\partial T} \frac{1}{2} C_g i \omega K_T^2 \phi_i^2 ds \\
& -\int_{\partial E} \delta \phi^* i \omega C C_g \left(\phi_1 - \phi_2 - \frac{g}{i\omega} f_e |U_0| \frac{U}{2g} \right) ds \Big\} \\
& = const
\end{aligned} \tag{3.31}$$

Where $\frac{\rho}{g} \exp(-2i\omega t)$ can be deleted in the above equation. The terms in the functional considering boundary ∂A can be reorganized as

$$\begin{aligned}
& \int_{\partial A} C C_g \left[\frac{1}{2} \phi_s - (\phi_A - \phi_l) \right] \frac{\partial \phi_R}{\partial n_A} ds - \int_{\partial A} \frac{1}{2} C C_g \phi_s \frac{\partial \phi_l}{\partial n_A} ds \\
& = \int_{\partial A} C C_g \left[\frac{1}{2} \phi_s - (\phi_A - \phi_l) \right] \frac{(\partial \phi_s + \partial \phi_l)}{\partial n_A} ds - \int_{\partial A} \frac{1}{2} C C_g \phi_s \frac{\partial \phi_l}{\partial n_A} ds \\
& = \int_{\partial A} C C_g \left(\frac{1}{2} \phi_s \frac{\partial \phi_s}{\partial n_A} - \phi_A \frac{\partial \phi_s}{\partial n_A} - \phi_A \frac{\partial \phi_l}{\partial n_A} + \phi_l \frac{\partial \phi_s}{\partial n_A} + \phi_l \frac{\partial \phi_l}{\partial n_A} \right) ds
\end{aligned} \tag{3.32}$$

3.1.3 FEM Scheme

The variational principle method and the shape function are used to derive the FEM matrix. With the shape functions, the velocity potential and its variation can be transformed as

$$\phi = N^i \phi^i \quad (3.33)$$

$$\nabla \phi = \nabla N^i \phi^i = B^i \phi^i \quad (3.34)$$

$$\phi_S = N_S^i \phi_S^i \quad (3.35)$$

$$\frac{\partial \phi_S}{\partial r} = \frac{\partial N_S^i}{\partial r} \phi_S^i = P_S^i \phi_S^i \quad (3.36)$$

The first term in the Functional can be presented as

$$\iint_A \frac{1}{2} \left[CC_g (\nabla \phi)^2 - \frac{C_g \omega^2}{C} \phi^2 \right] dx dy = \phi^T \left(\iint_A CC_g B^T B - \frac{C_g \omega^2}{C} N^T N dx dy \right) \phi \quad (3.37)$$

The term on boundary ∂A can be written as

$$\begin{aligned} & \int_{\partial A} CC_g \left(\frac{1}{2} \phi_S \frac{\partial \phi_S}{\partial n_A} - \phi_A \frac{\partial \phi_S}{\partial n_A} - \phi_A \frac{\partial \phi_I}{\partial n_A} + \phi_I \frac{\partial \phi_S}{\partial n_A} + \phi_I \frac{\partial \phi_I}{\partial n_A} \right) ds \\ &= \phi_S^T \left(\int_{\partial A} \frac{1}{2} CC_g P_S^T N_S ds \right) \phi_S - \phi^T \left(\int_{\partial A} CC_g N^T P_S ds \right) \phi_S - \phi^T \left(\int_{\partial A} CC_g N^T \frac{\partial \phi_I}{\partial n_A} \right) \\ &+ \phi_S^T \left(\int_{\partial A} CC_g P_S^T \phi_I ds \right) + \int_{\partial A} CC_g \phi_I \frac{\partial \phi_I}{\partial n_A} ds \end{aligned} \quad (3.38)$$

The last term in (3.38) is a constant.

The bottom friction loss term is

$$-\int_A \frac{i}{2\omega} f_\omega \left(\frac{1}{\cosh kh} \right)^2 (\nabla \phi)^2 dx dy = -\phi^T \left[\int_A \frac{i}{2\omega} f_\omega \left(\frac{1}{\cosh kh} \right)^2 B^T B dx dy \right] \phi \quad (3.39)$$

The boundary absorption term is

$$-\int_{\partial B} \frac{1}{2} i \omega C_g \alpha \phi^2 ds = -\phi^T \left(\int_{\partial B} \frac{1}{2} i \omega C_g \alpha N^T N ds \right) \phi \quad (3.40)$$

The transmission loss term is

$$\int_{\partial T} \frac{1}{2} C_g i \omega K_T^2 \phi_i^2 ds = \phi^T \left(\int_{\partial T} \frac{1}{2} i \omega C_g K_T^2 N^T N ds \right) \phi \quad (3.41)$$

The entrance loss term is

$$\begin{aligned} & -\int_{\partial E} \delta \phi^* i \omega C C_g \left(\phi_1 - \phi_2 - \frac{g}{i\omega} f_e |U_0| \frac{U}{2g} \right) ds \Big\} \\ & = -\int_{\partial E} \nabla \phi i \omega C C_g \left((1 - k_j) \phi - \frac{g}{i\omega} K_e U \right) ds \\ & = -\phi^T \left\{ \int_{\partial E} i \omega C C_g \left[(1 - k_j) N^T B - \frac{g}{i\omega} K_e B^T B \right] ds \right\} \phi \end{aligned} \quad (3.42)$$

where $\phi_1 - \phi_2 = (1 - K_j) \phi$ and $K_e = \frac{f_e U_o}{2g}$.

Based on the variational principle, the first variation of the functional is equal to zero,

that is

$$\delta F(\phi) = 0 \quad (3.43)$$

The matrix equations can be written as

$$[K][\Psi] + [Q] = 0 \quad (3.44)$$

Where $[\Psi]$ is the unknown matrix, and

$$K = \begin{bmatrix} [M] & [M_2] \\ [M_2]^T & [M_1] \end{bmatrix} \quad (3.45)$$

In which,

$$\begin{aligned} M = & \int_A \left(CC_g B^T B - \frac{C_g \omega^2}{C} N^T N \right) dx dy \\ & - \int_{\partial B} i\omega C_g \alpha N^T N ds \\ & + \int_{\partial T} i\omega C_g K_t^2 N^T N ds \\ & - \int_A \frac{i}{\omega} f_\omega \left(\frac{1}{\cosh kh} \right)^2 B^T B dx dy \\ & - \int_{\partial E} i\omega CC_g \left[(1 - K_j) N^T B - \frac{g}{i\omega} K_c B^T B \right] ds \end{aligned} \quad (3.46)$$

$$M_1 = \int_{\partial A} CC_g P_s^T N_s ds \quad (3.47)$$

$$M_2 = - \int_{\partial A} CC_g N^T P_s ds \quad (3.48)$$

$$Q_1 = - \int_{\partial A} CC_g N^T \frac{\partial \phi_I}{\partial n_A} ds \quad (3.49)$$

$$Q_2 = \int_{\partial A} CC_g P_S^T \phi_I ds \quad (3.50)$$

The quadratic Lagrange elements are used for the region shoreward of the imaginary common boundary ∂A . For the open sea region an eigen function expansion is used to represent its solution. Solutions for the two regions are matched at the common boundary ∂A .

A substructure technique is used in the model for which the whole calculation domain is divided into several small domains. The matrix equations are generated in each sub domain. The solutions in each sub domain are solved separately based on their own boundary values. The solution for the entire domain is obtained by matching the results at the imaginary boundaries between those sub domains. This technique largely decreases the matrix size, thus effectively accelerating the calculation efforts.

3.2 FEM Model Verification

The FEM model is tested with the widely used experimental and theoretical results of resonance in a rectangular harbor conducted by Ippen and Goda (1963) and Lee (1969). The fully opened rectangular harbor, 12.25 in. long and 2.38 in. wide, was installed in a basin of 11 ft long and 9 ft wide by Ippen and Goda (1963). The constant water depth is

0.844 ft in both the inner harbor and open-sea area. Energy dissipators were installed around the basin to simulate the open-sea condition. The experiment performed by Lee (1969) used a larger wave basin and more efficient dissipators to more adequately simulate the open sea condition. In order to compare the numerical result by the present FEM model with their experiments, a mesh was generated in which the rectangular harbor has the same size as the experiments, as shown in Figure 3.2. The right plot shows the whole calculation domain, the left plot shows the part that contains the harbor.

Total reflection boundary condition is used for the vertical walls, the entrance loss coefficient used here is $f_e = 0.8$.

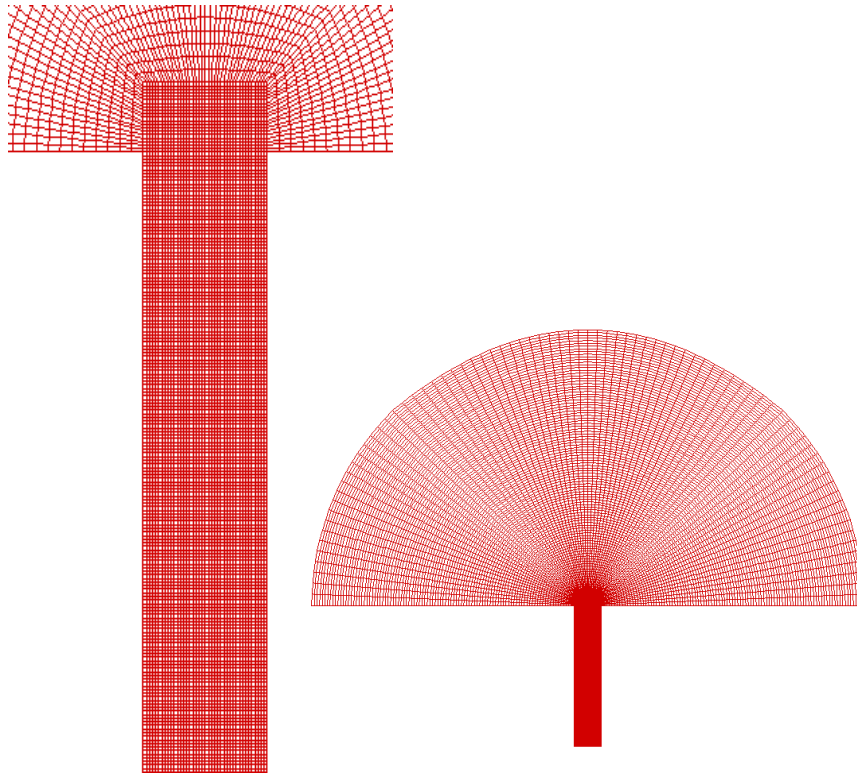


Figure 3.2 The FEM mesh used for the rectangular harbor

The amplification factor R at the middle point of the back wall as a function of kl were plotted and compared with those experimental and theoretical results by Ippen and Goda (1963) and Lee (1969), shown in Figure 3.3. Where $R = \frac{a_R}{a_I}$, a_R and a_I are response and incident wave amplitude. $k = \frac{2\pi}{L}$ is the wave number, and $l = 12.25$ in. is the length scale. h is the water depth, C_{bf} is the Nikuradse roughness height which was discussed previously in the bottom friction boundary section.

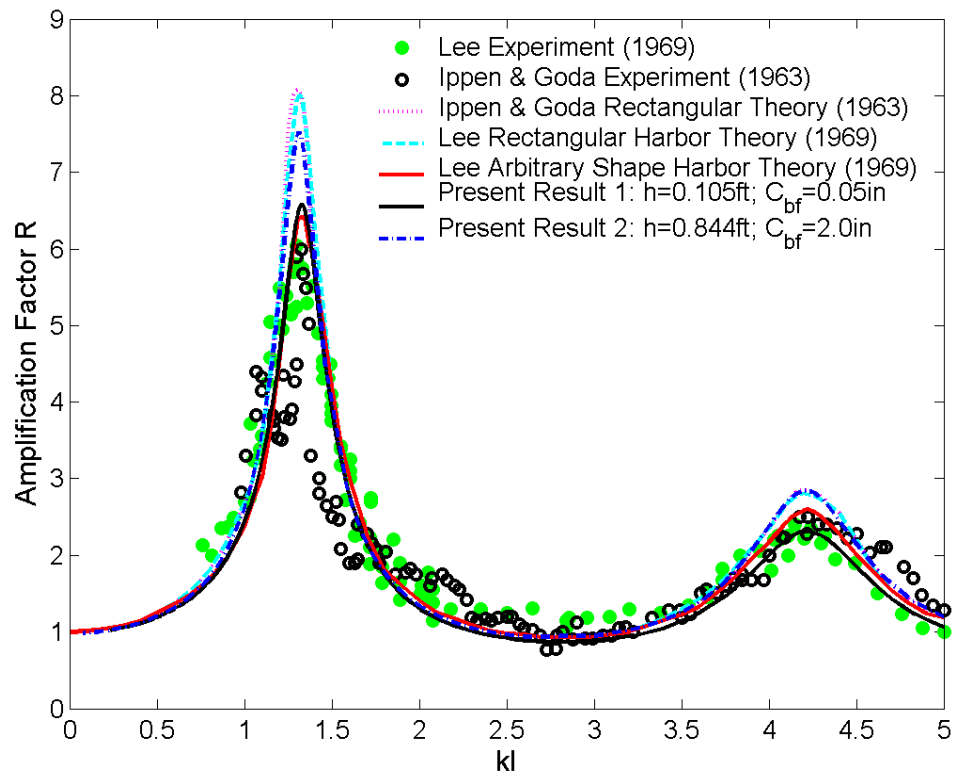


Figure 3.3 Result comparisons for the rectangular harbor

In order to test the friction effect at the bottom, a shallower water depth $h = 0.105$ ft is also selected. The black solid line shows the simulation result with a water depth of 0.105 ft instead of 0.844 ft which is shown in the blue curve, and the Nikuradse roughness height 0.05 in. is much smaller than the one used for the deeper water depth. The result with a shallower water depth performs better than the one with a deeper depth, meaning that the bottom friction is more significant when the water depth is lower.

The present simulation results using the present FEM model are totally comparable with

the previous experimental and theoretical studies, which confirmed the applicability of the present model. The result with a depth of 0.105 ft agrees better with the experiments than all other approaches for the second resonance peak.

In Figure 3.3, the first peak shows the ‘pumping mode’, for which the water level in the entire harbor either fluctuates up or fluctuates down together. The mode is plotted in figure 3.4, in which the incident wave period is $T = 26.4$ sec. The negative sign for the amplification factor shown in figure 3.4 means the response wave has a latter phase (within π) than the incident wave, while the positive sign means the response wave has a former phase (within π). It can be seen that the amplification factors shown in the entire inner harbor are all positive in the pumping mode.

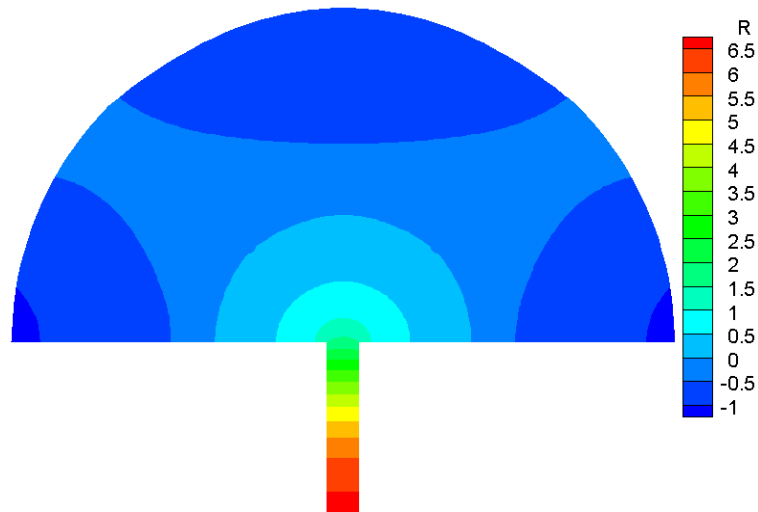


Figure 3.4 Pumping mode in the rectangular harbor ($kl=1.32$)

The second peak in Figure 3.3 shows the ‘sloshing mode’, for which the water surface

oscillated in the harbor with opposite phase. The mode is shown in figure 3.5, with a period of 0.85 sec. The amplification factors are somewhere positive while somewhere negative in this case.

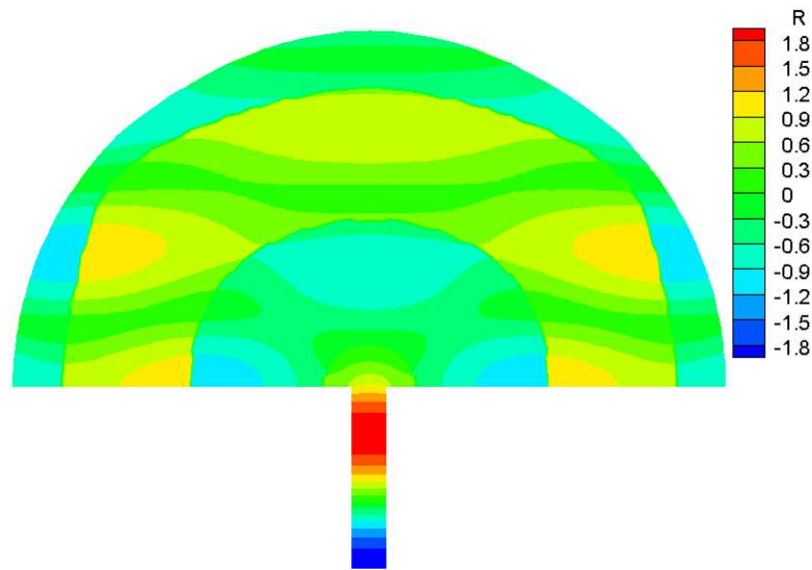


Figure 3.5 Sloshing mode in the rectangular harbor ($kl=4.25$)

As shown in Figure 3.3 the resonance of the sloshing mode is much less severe than the pumping mode, the largest amplification factor in Figure 3.5 is much lower than the one in Figure 3.4. The present FEM model has generated results that explained clearly the physics of resonant wave motion and have compared well with the available experimental data.

3.3 Spectrum Analysis

Spectrum analysis is widely used in the frequency domain studies in various academic

fields. In the present research, wave spectrum analysis will be performed for the incident and response waves in real case studies. A wave spectrum is the distribution of wave energy as a function of frequency. It describes the total energy transmitted by a wave-field at a given time.

Spectrum is also called spectral density function, which can be defined in three different equivalent ways: (1) via correlation functions; (2) via finite Fourier transforms; (3) via filtering-squaring-averaging operations (Bendat and Piersol, 2000). The spectral density function is denoted as $S(f)$, where f is wave frequency. The derivation through correlation functions can be written as

$$S_{xx}(f) = \int_{-\infty}^{+\infty} R_{xx}(\tau) \exp(-j2\pi f\tau) d\tau \quad (3.51)$$

$R_{xx}(\tau)$ is the auto-correlation function, which is formulated as

$$R_{xx}(\tau) = E[x_k(t)x_k(t+\tau)] \quad (3.52)$$

Where $x_k(t)$ is a random variable such as an incoming wave time series outside a harbor or the response wave time series inside a harbor.

Wave spectrum is proportional to the square of wave amplitude and the length of the time series, but not related to wave phase. As waves oscillated in harbors or rivers, the energy (or spectrum) will be amplified in some areas for certain frequencies while depressed in

other frequencies. The spectrum analysis can directly illustrate the dominant frequencies in the incident wave and the resonance mode frequency for the response wave.

CHAPTER 4 WAVE OSCILLATION MECHANISM STUDY IN HARBORS AND BAYS

As mentioned before, many harbors or bays have encountered extreme oscillations due to long waves. For some harbors, the problem was mainly induced by the earthquake generated tsunamis, such as the Crescent City Harbor. Some of them were caused by the typhoons and winter storms, such as the Hualien Harbor in Taiwan and the Pohang Harbor in Korea. The oscillation modeling in the Crescent City Harbor and San Pedro Bay, which respectively located in northern and southern California, and the Bay of Fundy located in eastern Canada and north east of United States were examined by the numerical model discussed in the previous Chapter. The results will be presented in this chapter. Conclusions will be drawn at the end of this chapter.

4.1 Modeling of Crescent City Harbor, California

Crescent City Harbor, located in northern California, is one of the oldest harbors in California. The surrounding area is well known for its tsunami vulnerability. Due to its location and topography along the Pacific coast as shown in Figure 4.1, many have described it as a “sitting duck” for tsunami waves originated from the Pacific Ocean. It was severely damaged by tsunamis in the past such as the one generated by Alaskan earthquake in 1964, in which 11 people were killed and the property loss was estimated

to be in the tens of million US Dollars (Magoon, 1965; Powers, 2005). Most recently, another heavy loss in the harbor was caused by the tsunami produced by the Kuril Islands earthquake on November 15, 2006. Three docks close to the entrance of the small inner harbor were broken during the event, as shown in the circled region in Figure 4.2.



Figure 4.1 Location of Crescent City Harbor



Figure 4.2 Air photo of the small inner harbor in Crescent City Harbor with the broken docks during the tsunami event on November 15, 2006 noted

The model region for the computer model is shown in Figure 4.3 (left). Only the major grid blocks are plotted, the model contains 9,709 finite elements and 39,688 nodes with eight incident wave directions (indicated as 1 to 8). The Crescent City Harbor is shown in Figure 4.3 (right) with five chosen locations of special interest and they are noted as A, B, C, D, and E. The location where the tide gauge was placed has also been noted in Figure 4.3 (right).

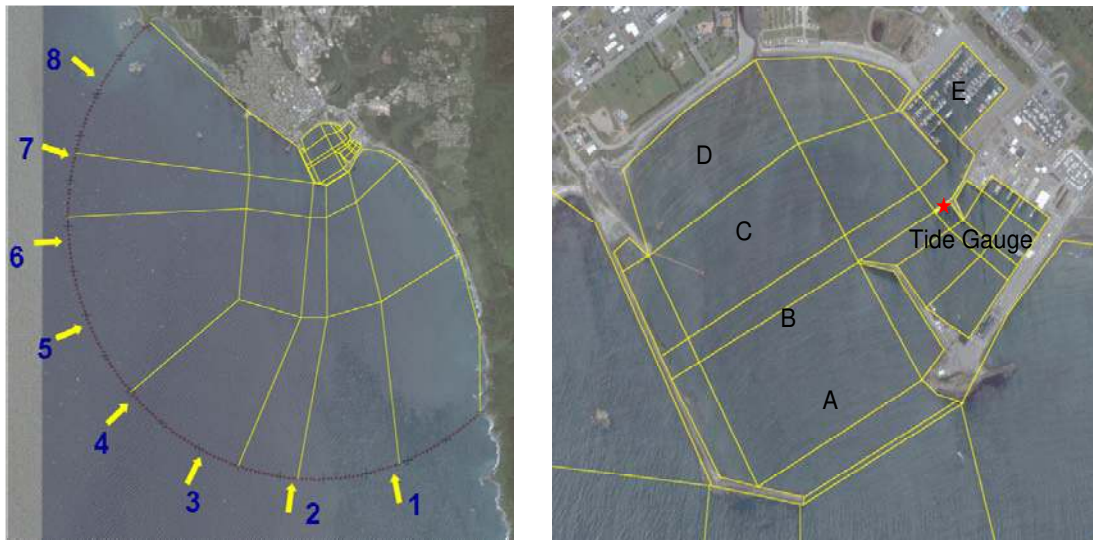


Figure 4.3 Simulation domain for Crescent City Harbor (left) and locations of special interest as A, B, C, D, E and the tide gauge (right)

Figure 4.4 presents the computer simulation response curves with the two distinct resonant periods at the tide gauge station of Crescent City Harbor under different scenarios of wave directions. The ordinate is the amplification factor defined as the wave height at the tide gauge station divided by the incident wave height. The abscissa is the dimensionless wave number kl (where k is the wave number which is defined as 2π divided by the wave length L , and l is the characteristic length of the harbor which is

the length from the outer harbor entrance to the facing coastal line about 4,363 feet in the present model). The first two resonant modes at the tide gauge station have the wave periods of 22.0 min and 10.3 min as indicated.

The difference in amplification factor caused by different incoming wave directions can also be seen in Figure 4.4. For the first mode at 22.0 min, the amplification factor for direction 1 is the largest and the one for direction 8 is the least, which means that the oscillation becomes more severe when waves come from south to north than from west to east. This can be explained that when waves come from south to north, they actually propagate directly into the harbor. While waves come from west to east, the reflection and diffraction due to the outside jetty and beach reduce the energy and thus reduce the amplification factor.

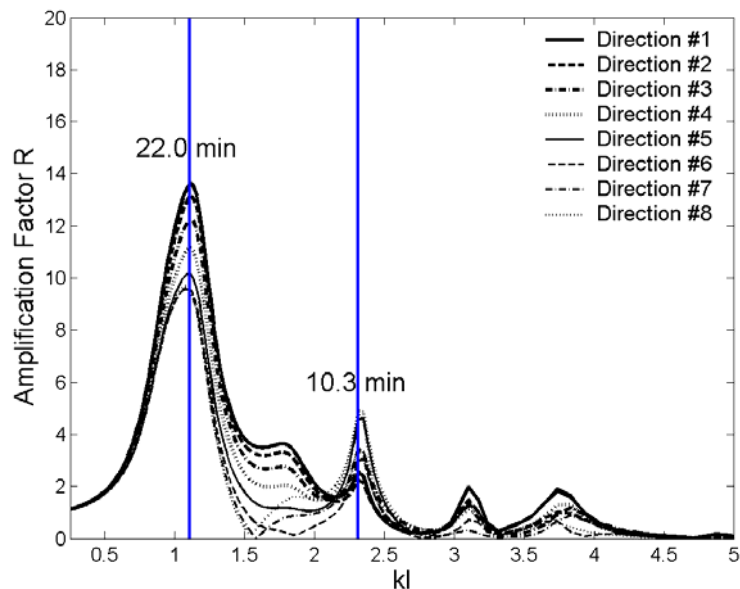


Figure 4.4 Response curves at tide gauge location for different incoming wave directions

Figure 4.5 shows the response curves at locations A-E and tide gauge station with incident wave coming from direction 2 (oriented toward north). It provides a clear indication that the waves are amplified as the inner harbor region is approached for both the 22.0 min and 10.3 min resonant wave periods. Thus, it appears that the more inner the location is, the more vulnerable for tsunami hazards. This can also be seen in Figure 4.6, in which the mode shape at resonant wave period of 22.0 min is plotted. The color contours show how the amplification factor varies with location. It explained the damage occurred in the small inner harbor on November 15, 2006 during which strong currents were invoked by the large oscillations. This large oscillation pushed the boats against the berth facilities and colliding with other neighboring boats.

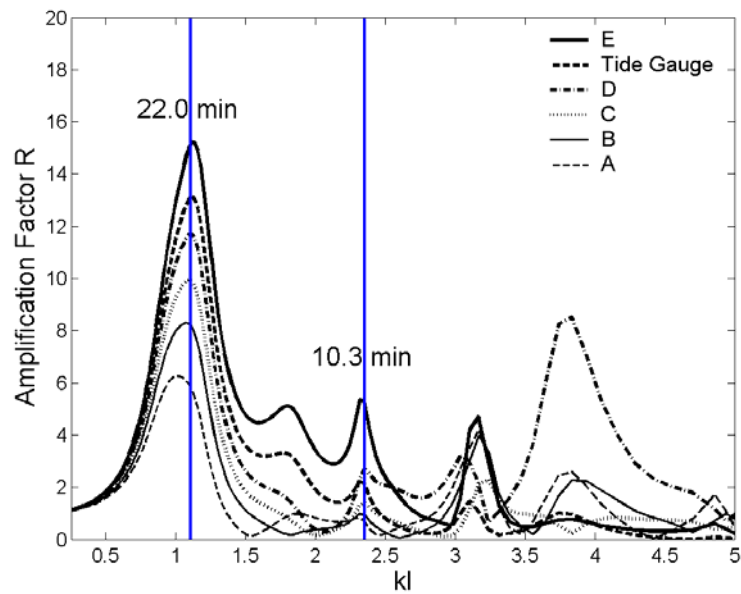


Figure 4.5 Response curves at locations noted by A-E and tide gauge station with incident wave from direction 2

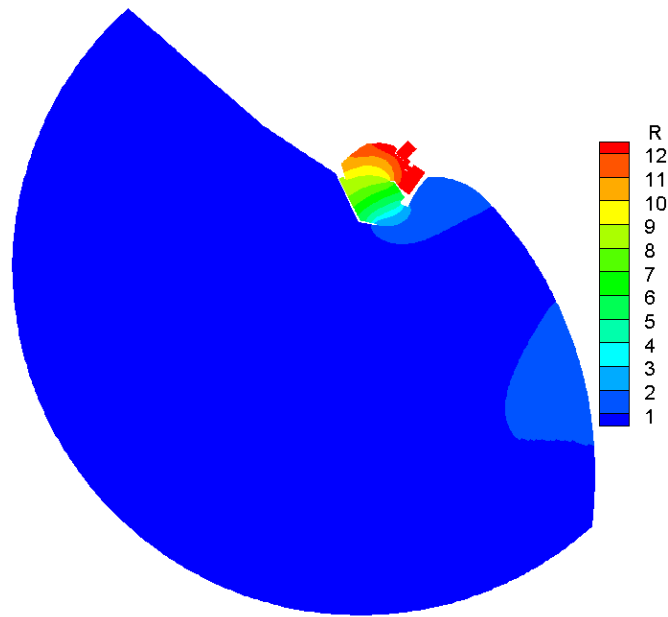


Figure 4.6 The mode shape at 22.0 min for incoming wave direction 1

For the second resonant mode (with wave period of 10.3 min) shown in Figure 4.4, the wave direction effects are not the same as the one for the first resonant mode. For the first mode, the whole simulation domain has the same phase. The water surface of the whole region will be moving up and down together. But for the second mode, there exist a local oscillation inside the harbor, and the area near the entrance of the small inner harbor acts like a nodal line, as shown in Figure 4.7. The tide gauge location is within the nodal line region. Thus the amplification factor for the second mode at the tide gauge location is not very large and the trend changing with direction is not very obvious.

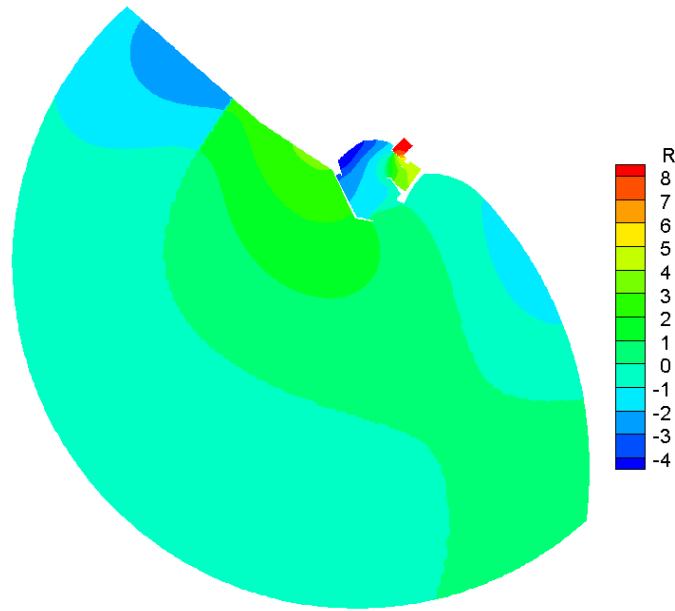


Figure 4.7 Oscillation mode at 10.3 min for incoming wave direction 2

An examination of the tide record associated with several different tsunami events indicates that water levels at the recording station at Crescent City Harbor have been amplified from waves originated from near-field as well as that from far-field. Figure 4.8 (a), (b), (c) and (d) show tide gauge records of water surface elevations during the near-field earthquake generated in offshore of northern California (June 15, 2005, Magnitude 7.2), and the three far-field earthquakes. Two generated in Kuril Islands, Japan (November 15, 2006 and January 13, 2007, with Magnitude 8.3 and 8.1), and one generated in offshore of Peru (August 15, 2007, Magnitude 7.9). Tides were filtered out in these records. It can be seen that the wave heights are as high as 30-40 cm during the events on January 13, 2007 and August 15, 2007. The most serious one occurred on November 15, 2006, with the wave height reaching 1.5 m on top of the tidal variation!

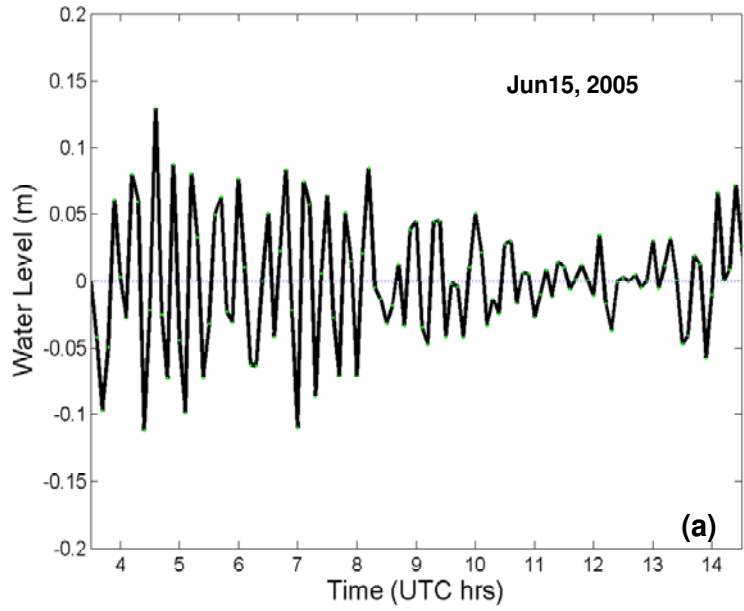


Figure 4.8 (a) Tide gauge record in Crescent City Harbor for event on June 15, 2005

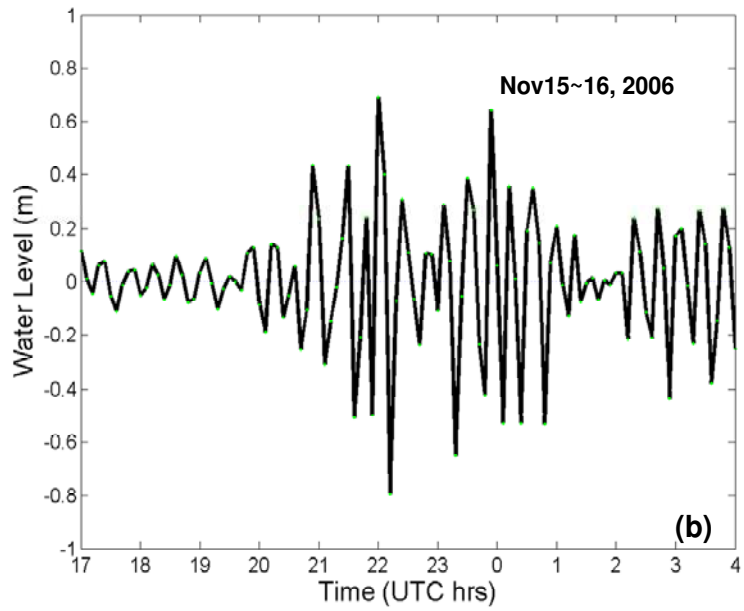


Figure 4.8 (b) Tide gauge record in Crescent City Harbor for event on November 15, 2006

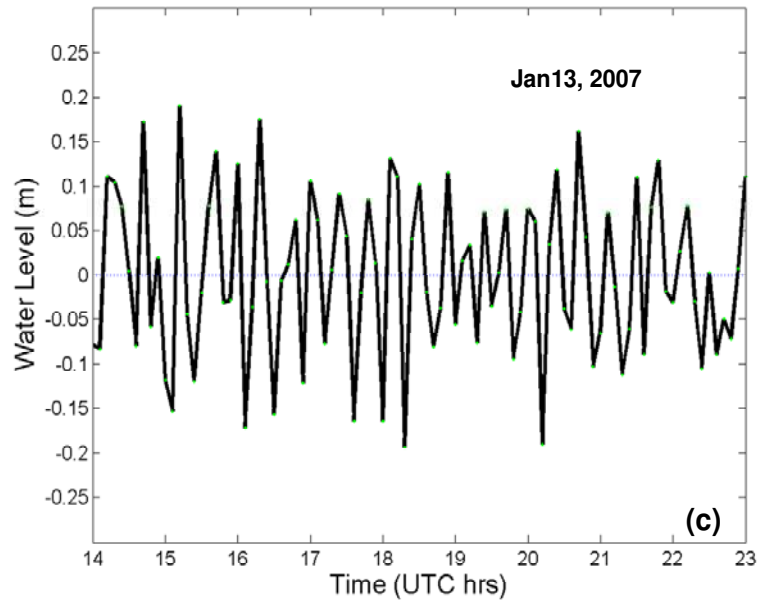


Figure 4.8 (c) Tide gauge record in Crescent City Harbor for event on January 13, 2007

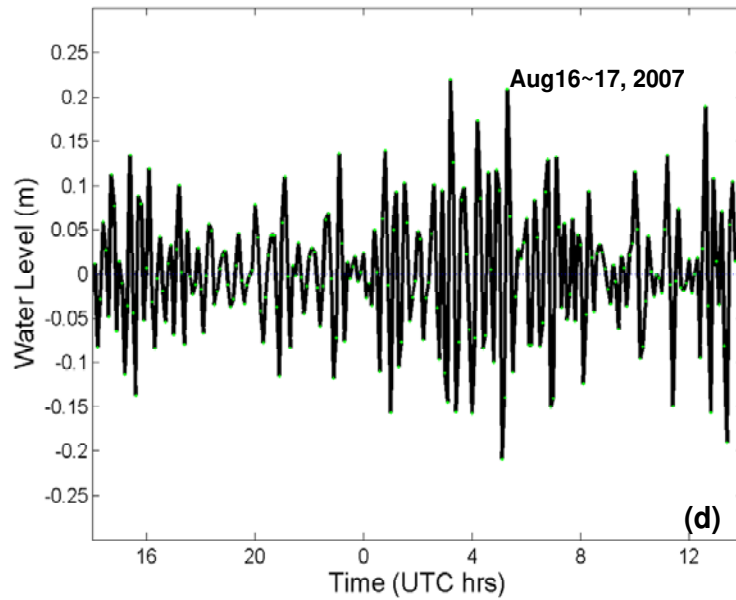


Figure 4.8 (d) Tide gauge record in Crescent City Harbor for event on August 15, 2007

The spectral analysis of the records shown in Figure 4.8 has been performed, and the spectral density distributions are correspondingly shown in Figure 4.9. It can be seen that the

dominant waves in those events, which have the highest energy density, are all around 21 to 22 minutes.

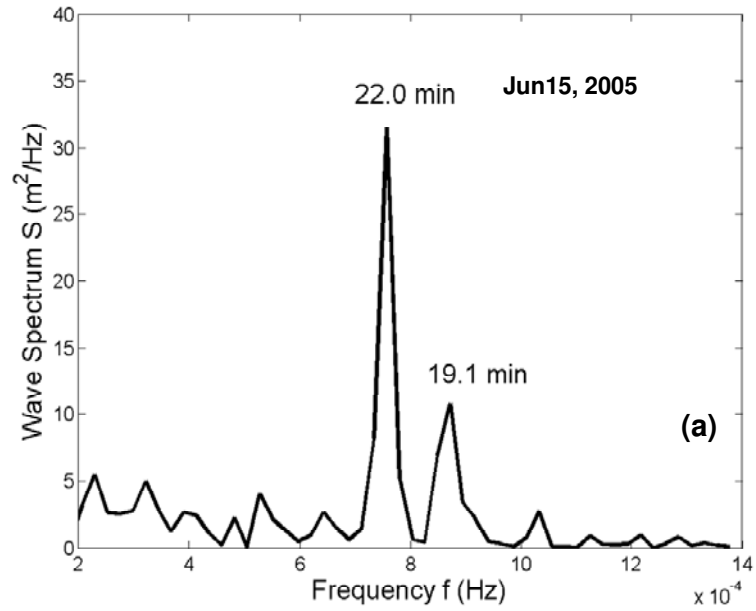


Figure 4.9 (a) Corresponding spectral density of the tide gauge record at the Crescent City Harbor on June 15, 2005

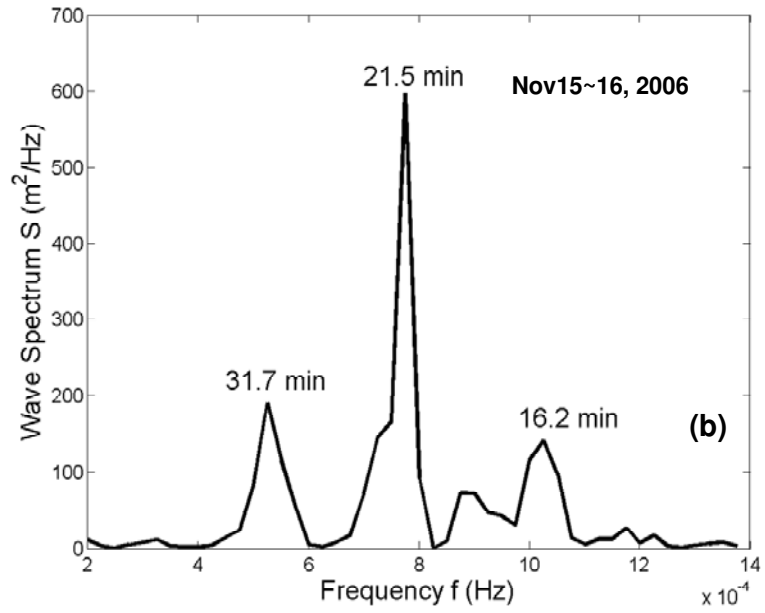


Figure 4.9 (b) Corresponding spectral density of the tide gauge record at the Crescent City Harbor on November 15-16, 2006

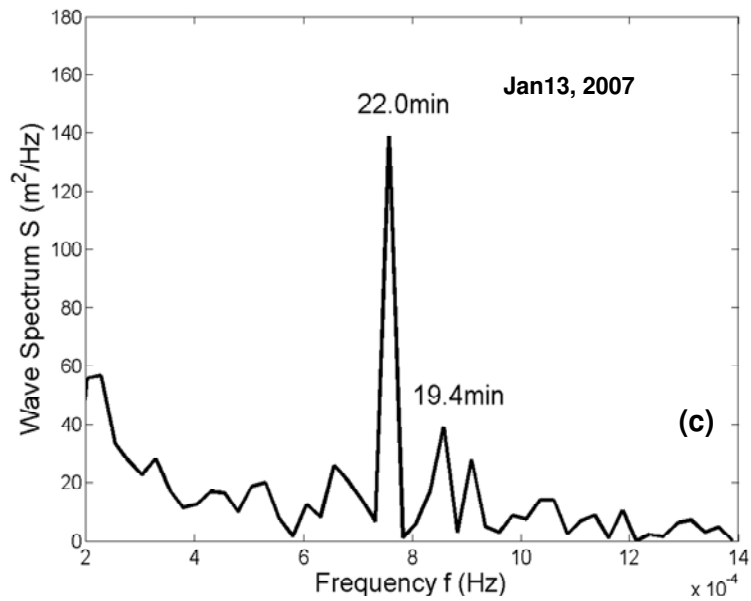


Figure 4.9 (c) Corresponding spectral density of the tide gauge record at the Crescent City Harbor on January 13, 2007

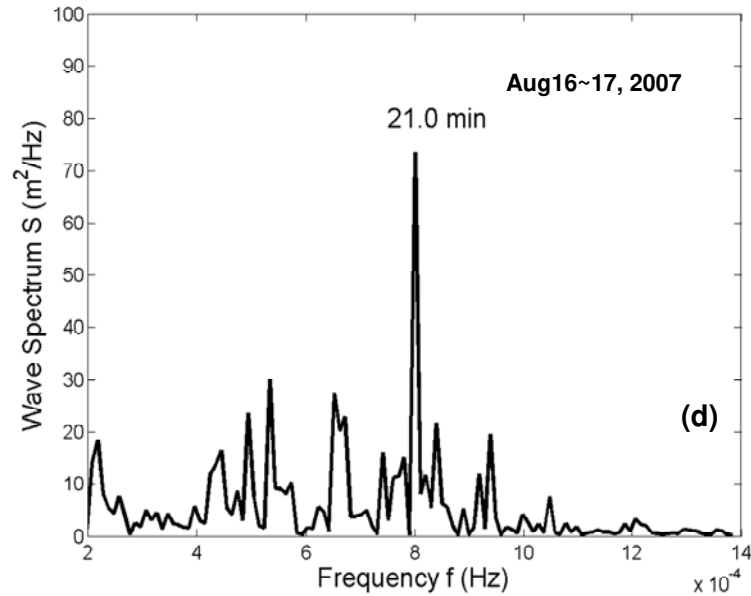


Figure 4.9 (d) Corresponding spectral density of the tide gauge record at the Crescent City Harbor August 16-17, 2007

The incoming wave directions in the four events are roughly from south-west for the northern California earthquake (June 15, 2008), from west for the two Kuril Islands earthquakes (November 15-16, 2006 and January 13, 2007), and from south for the Peru earthquake (August 16-17, 2007). The simulated response curves for these incoming wave directions superimposed with the observed resonant waves corresponding to those events are plotted in Figure 4.10. The results indicate that the actual resonant periods are very close to those computed, especially the fundamental mode at 22 min.

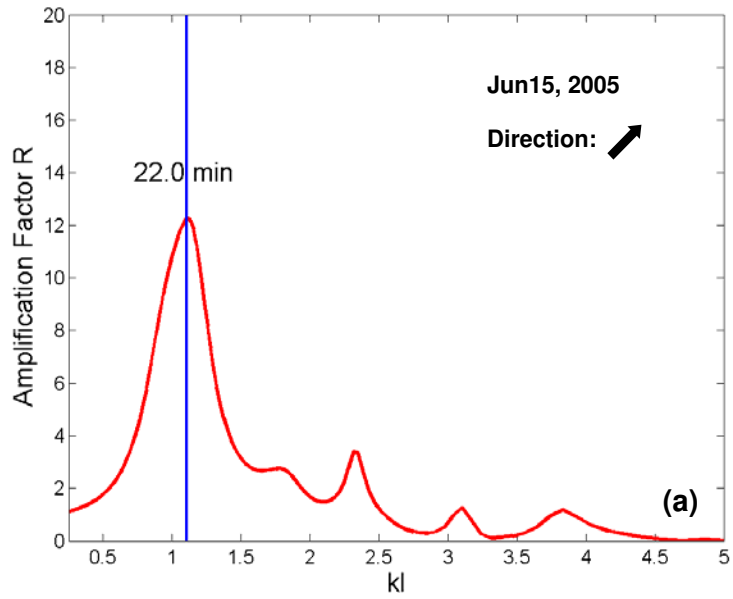


Figure 4.10 (a) Simulated response curve with the field observed dominant wave superimposed at Crescent City Harbor for event on June 15, 2005

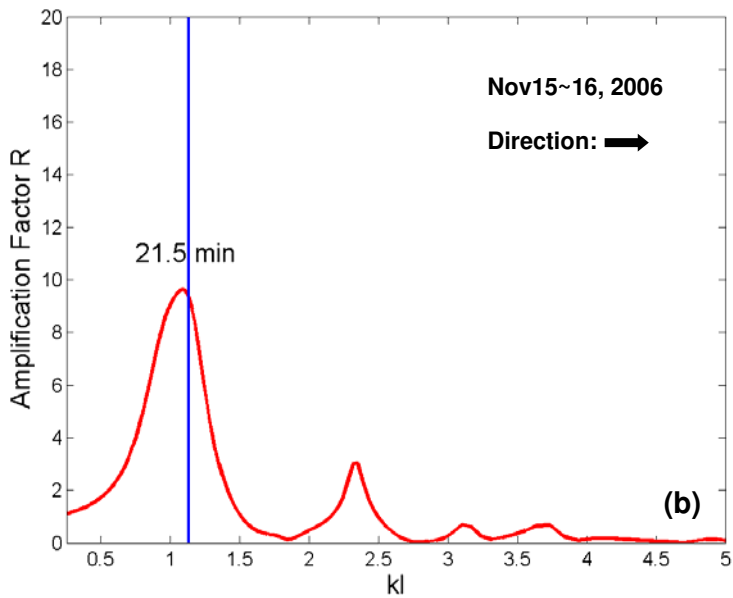


Figure 4.10 (b) Simulated response curve with the field observed dominant wave superimposed at Crescent City Harbor for event on November 15, 2006

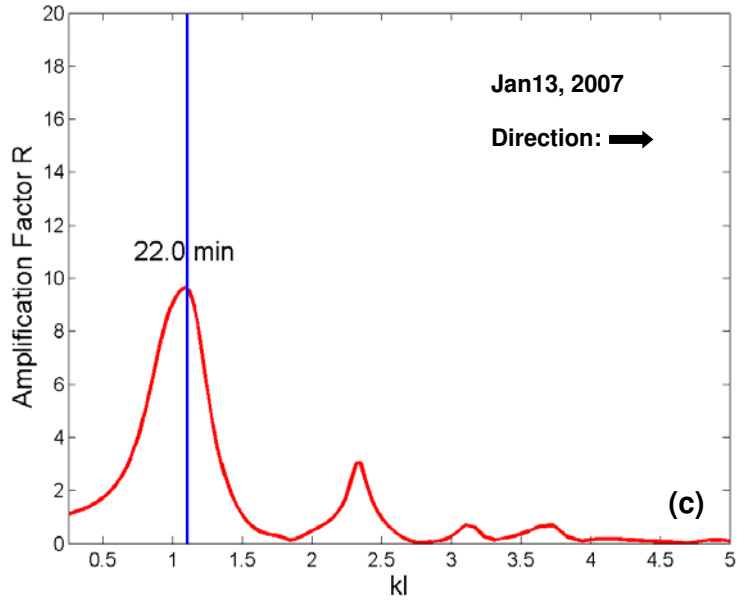


Figure 4.10 (c) Simulated response curve with the field observed dominant wave superimposed at Crescent City Harbor for event on January 13, 2007

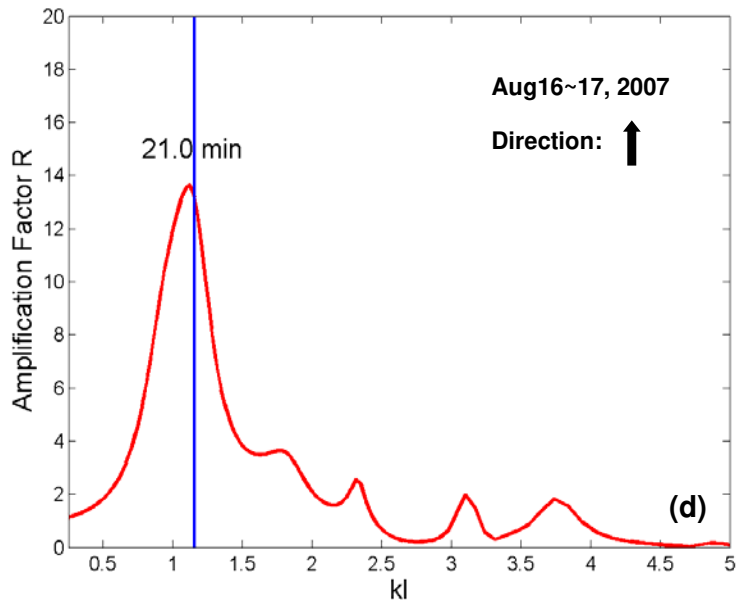


Figure 4.10 (d) Simulated response curve with the field observed dominant wave superimposed at Crescent City Harbor for event on August 15, 2007

Water depth affects the value of wave length for a certain wave period. And wave length is the key factor for wave resonance. Figure 4.11 shows for the same wave length (20,000

ft assumed), how the wave period changes (200 sec difference) with the variation of water depths (10 ft and 15 ft assumed). Since the actual water depth may be varied due to the tide condition, the wave period may change for a certain wave length in different events. The slight variation of the resonant wave period is reasonable. The results presented clearly indicate the effect of local topography in amplifying the incident tsunami waves whether they are near-field or far-field tsunamis.

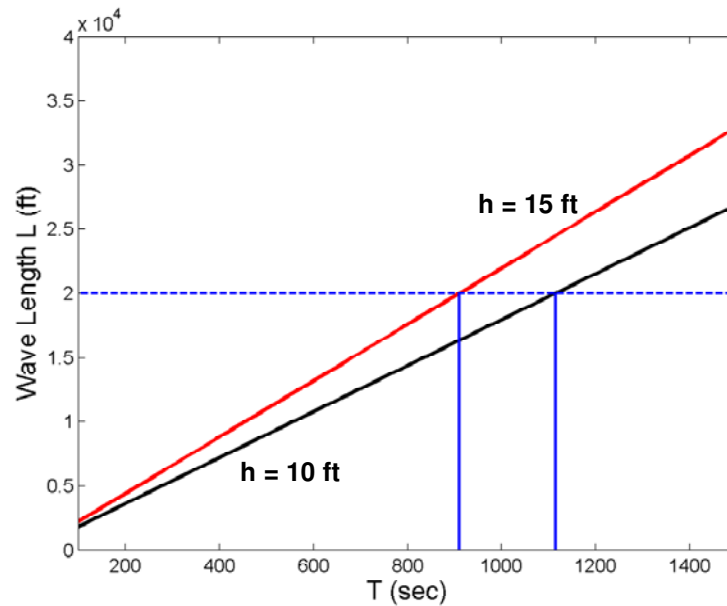


Figure 4.11 Illustration of changing of wave period due to water depth variation for certain wave length

4.2 Modeling of San Pedro Bay, California

San Pedro Bay in southern California is one of the most important economic zones in United States. It includes the ports of Los Angeles and Long Beach (LA/LB harbor),

which are one of the largest and busiest ports in the world. The simulation for San Pedro Bay covers a very large area including the LA/LB harbor to capture the basin resonance characteristics. An air photo of the San Pedro Bay is shown in Figure 4.12 with the simulated region indicated in Figure 4.12 (a). The radius of the semi-circle of the simulation domain is about 12 miles. The model grids contain 13,263 elements and 56,134 nodes. The location of tide gauge station Los Angeles Berth60 (LA Berth60) is also shown.

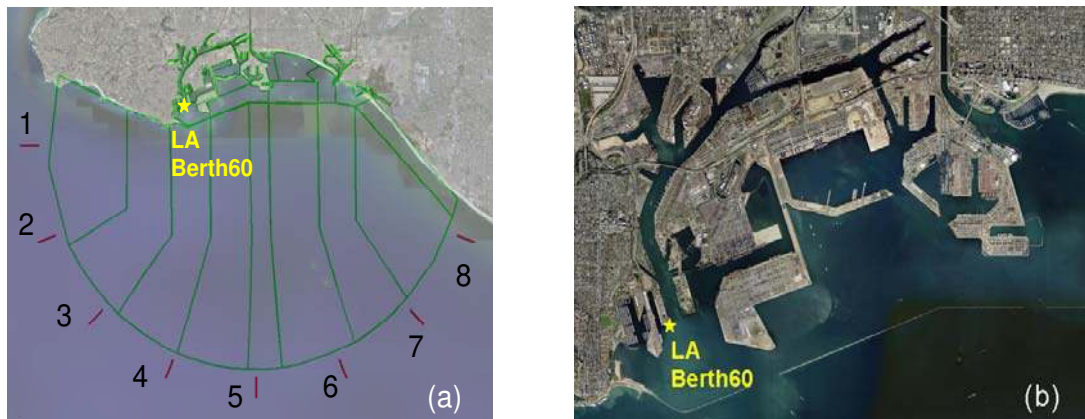


Figure 4.12 Air photos of San Pedro Bay with simulation domain imposed (a) and LA/LB port (b). The computed response curves at the tide gauge LA Berth60 for different incoming wave directions are plotted in Figure 4.13. It can be seen that the indicated first resonant wave period is about 59.0 min, the second resonant mode is at 16.3 min and the third resonant mode is at 18.0 min. Generally, the amplification factor increases for incident waves coming from the south. Since waves coming from the south can go inside the harbor

directly otherwise the reflection and diffraction due to the coast and breakwaters will have weakened the wave field.

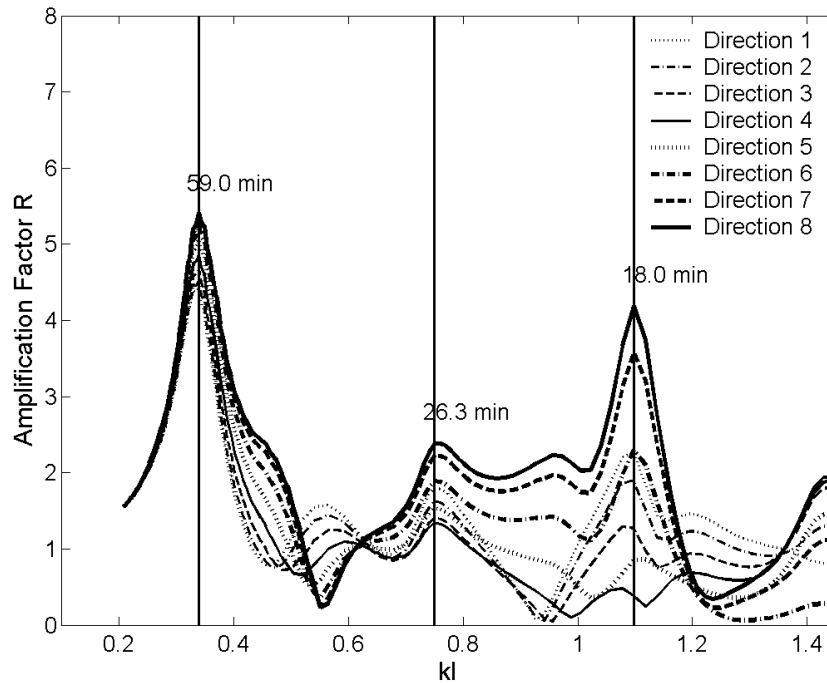


Figure 4.13 Response curve at LA Berth60 for different incoming wave directions

Similar to the modeling for Crescent City Harbor, the simulation results were compared with the tide gauge (LA Berth60) records. The ports of Los Angeles and Long Beach have experienced modifications and expansion over the years. The harbor layout is now different from which existed several decades ago. Thus we focused on the recorded data for recent tsunamis generated by: the earthquake in offshore of northern California on June 15, 2005; two major earthquakes near the Kuril Islands, Japan on November 15, 2006 and January 13, 2007; the Solomon Islands earthquake on April 01, 2007, with a magnitude of 8.1; the Peru offshore earthquake on August 15, 2007, with a magnitude of

7.9. Both local and distant tsunamis generated by those earthquakes reached San Pedro Bay, causing water level oscillations. The tide records at station LA Berth60 were analyzed to obtain the periods of the dominant modes of oscillation at that location during those events. The tide gauge records and the corresponding spectral density distributions at LA Berth60 are shown in Figure 4.14 and 4.15. One or two dominant waves occurred during those events, all of them are around 60 min. Wave amplitude at tide gauge LA Berth60 during these events are not as high as those at the tide gauge inside the Crescent City Harbor. The extreme oscillation amplitude is about 10-15 cm. This is expected since the simulated amplification factor at the tide gauge in Crescent City Harbor is much higher than those at LA Berth60. The shifting from the peak wave period (59 min) will also reduce the amplification factor, thus the oscillation wave amplitude.

The recorded data on April 01, 2007 was not used in the modeling examination for Crescent City Harbor because the tide record was not available during that period for Crescent City Harbor (tide gauge failed).

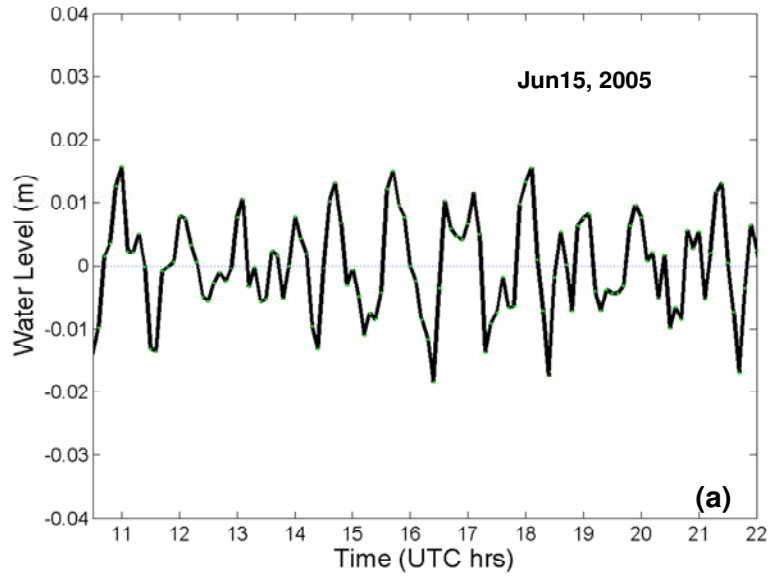


Figure 4.14 (a) Historical records at the LA Berth60 for event on June 15, 2005

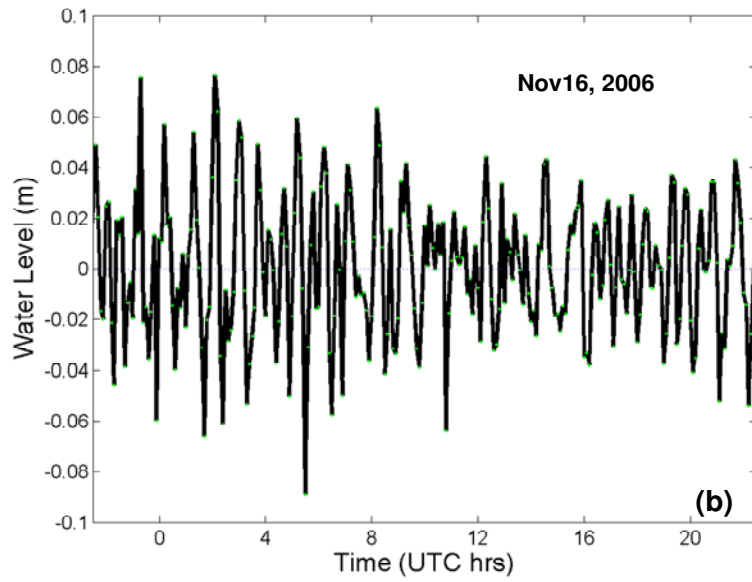


Figure 4.14 (b) Historical records at the LA Berth60 for event on November 15, 2006

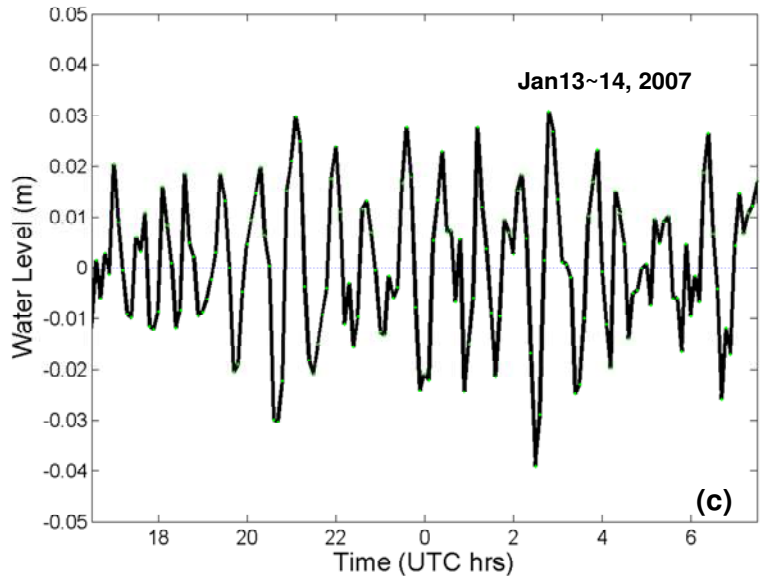


Figure 4.14 (c) Historical records at the LA Berth60 for event on January 13, 2007

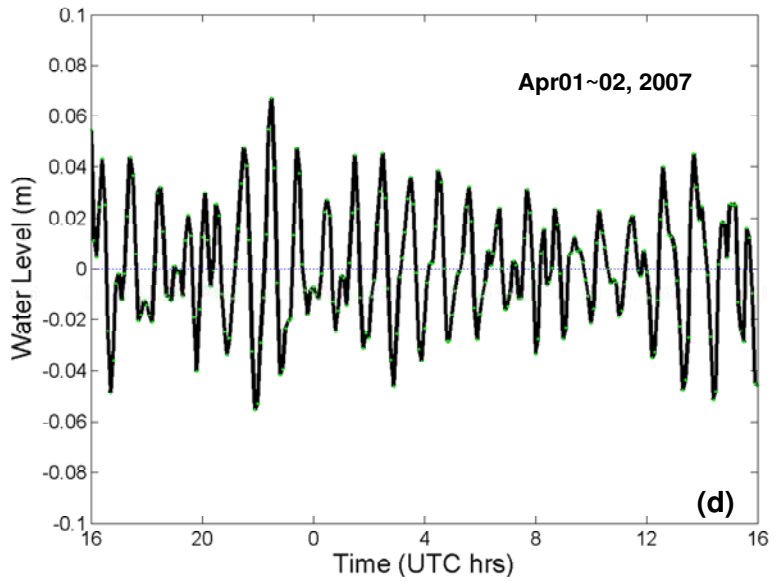


Figure 4.14 (d) Historical records at the LA Berth60 for event on April 01, 2007

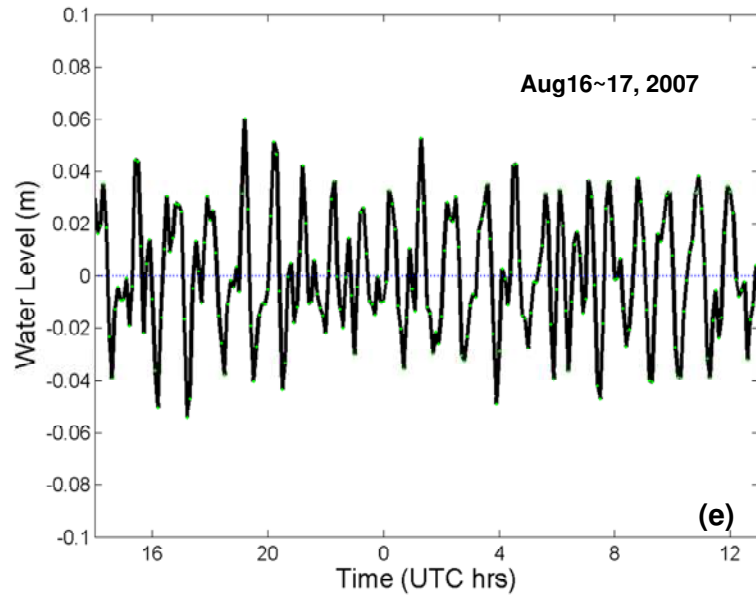


Figure 4.14 (e) Historical records at the LA Berth60 for event on August 15, 2007

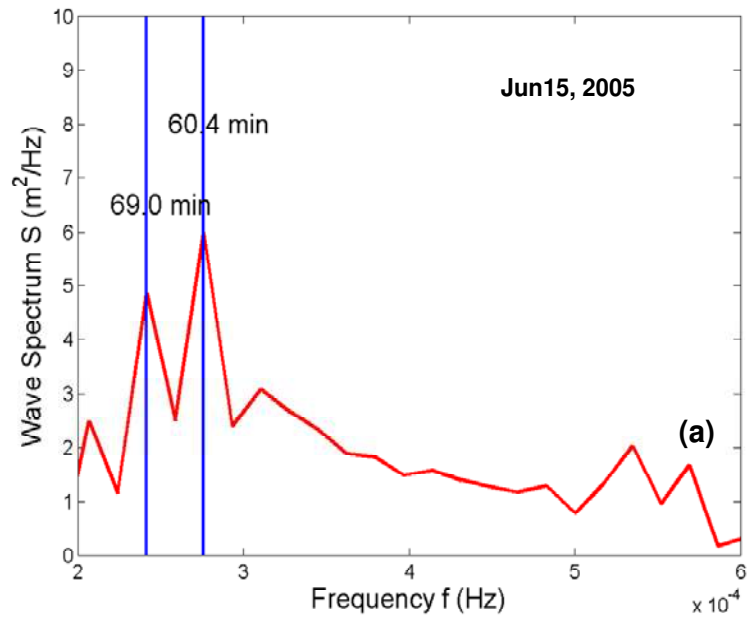


Figure 4.15 (a) Corresponding spectral density of the tide gauge record at LA Berth60 on June 15, 2005

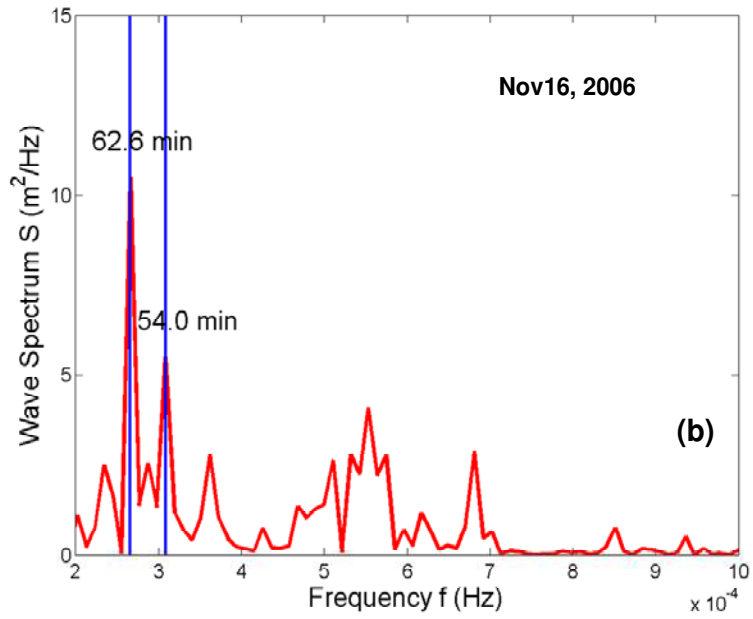


Figure 4.15 (b) Corresponding spectral density of the tide gauge record at LA Berth60 on November 15, 2006

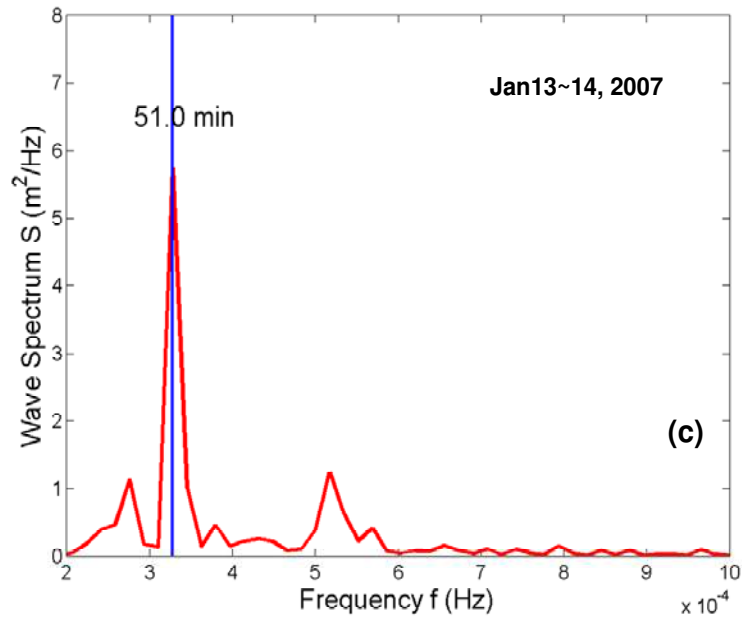


Figure 4.15 (c) Corresponding spectral density of the tide gauge record at LA Berth60 on January 13, 2007

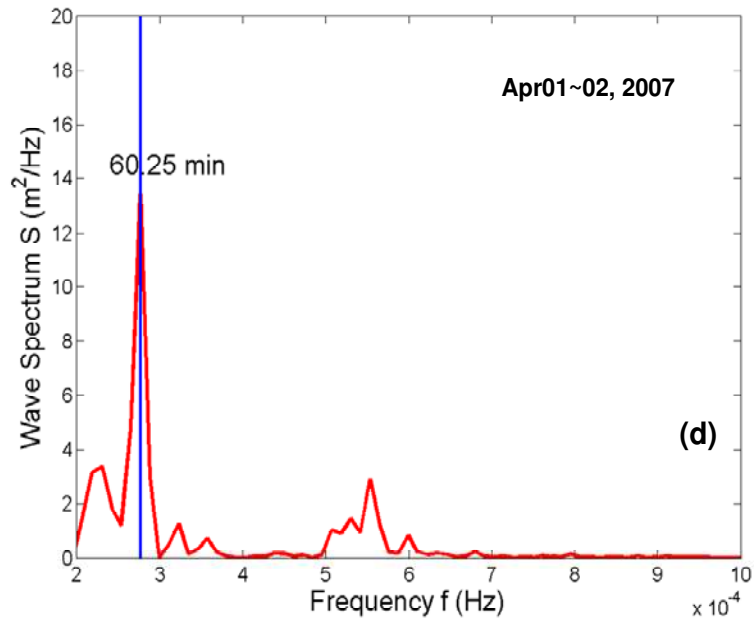


Figure 4.15 (d) Corresponding spectral density of the tide gauge record at LA Berth60 on April 01, 2007

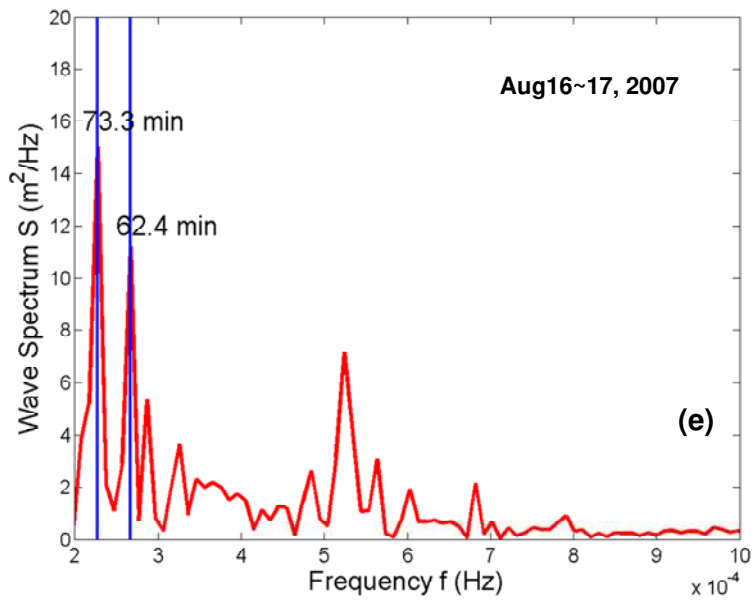


Figure 4.15 (e) Corresponding spectral density of the tide gauge record at LA Berth60 on August 15, 2007

For further comparison, the observed dominant waves are superimposed on the response curves simulated with the corresponding incoming wave direction for each event. This is shown in Figure 4.16. Roughly, the incident wave came from the north-west direction for the northern California offshore earthquake, from west for the Kuril Islands earthquakes, and from south-west for the Solomon Islands earthquake. Apparently, all the observed dominant waves have all been found to correspond to the first mode of the response curves, indicating that the computer model catches the resonance characteristics of the basin quite well.

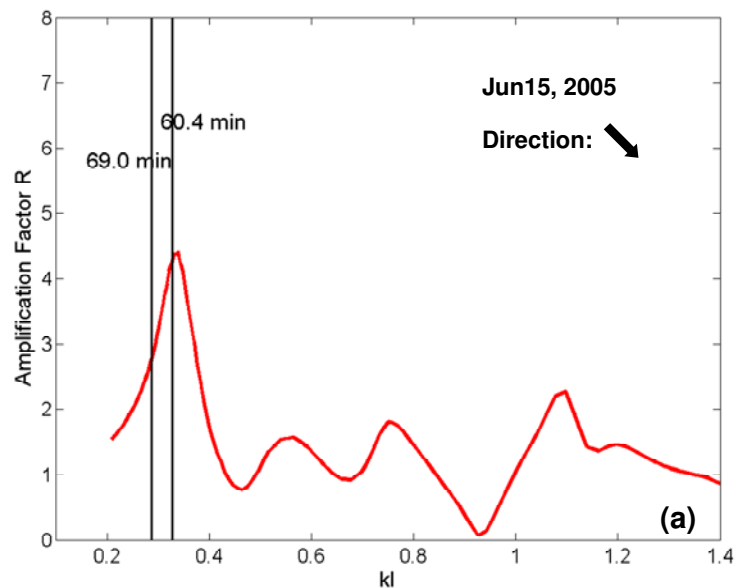


Figure 4.16 (a) Simulated response curve with field observed dominant waves superimposed at LA Berth60 for event on June 15, 2005

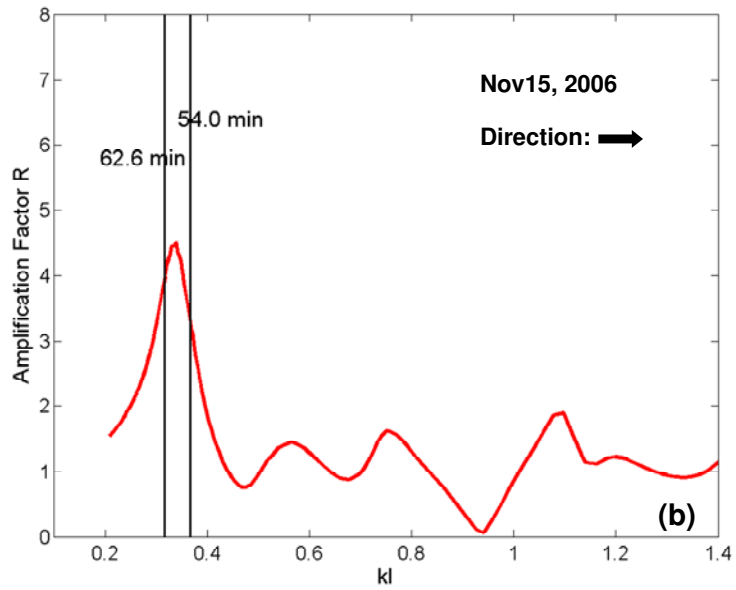


Figure 4.16 (b) Simulated response curve with field observed dominant waves superimposed at LA Berth60 for event on November 15, 2006

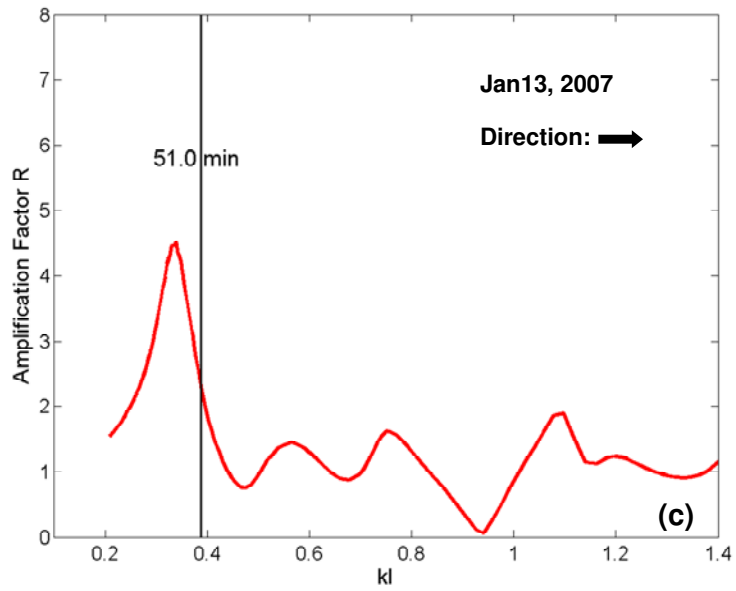


Figure 4.16 (c) Simulated response curve with field observed dominant waves superimposed at LA Berth60 for event on January 13, 2007

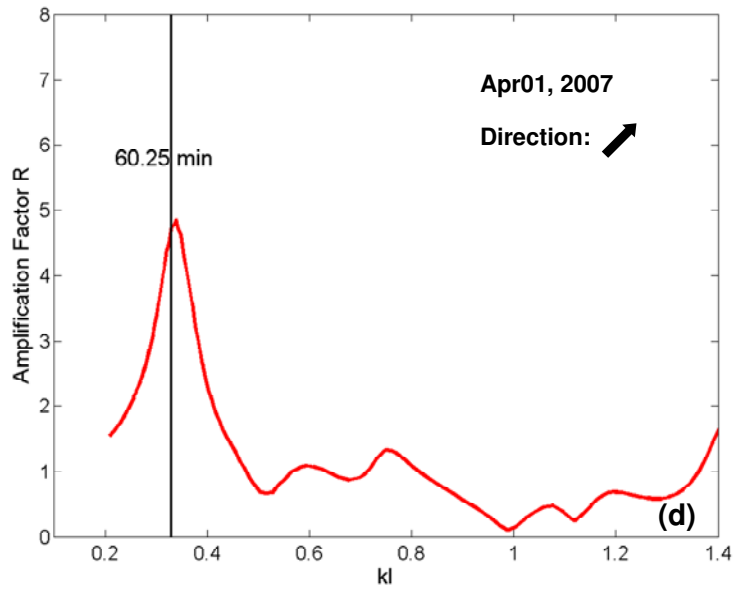


Figure 4.16 (d) Simulated response curve with field observed dominant waves superimposed at LA Berth60 for event on April 01, 2007

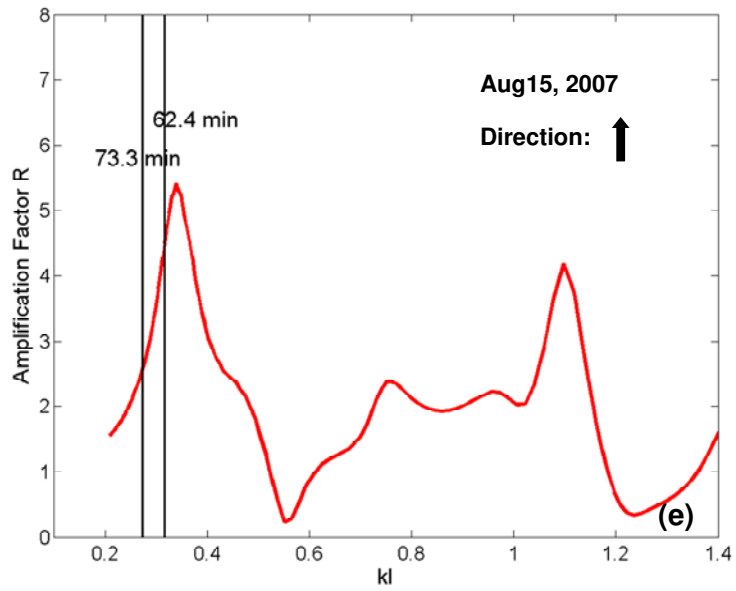


Figure 4.16 (e) Simulated response curve with field observed dominant waves superimposed at LA Berth60 for event on August 15, 2007

4.3 Wave Oscillation Comparison between Crescent City Harbor and San Pedro Bay

It is interesting to note that the four tide records for Crescent City Harbor shown in Figure 4.8 and 4.9 had the dominant wave period at 22 minutes which was predicted by the computed response curves. However, the same tide records at San Pedro Bay (or LA/LB harbor) presented in Figure 4.14 and 4.15 showed that the dominant resonant modes are all close to 60 minutes. The dominant waves in Crescent City Harbor and Los Angeles harbor during those events are listed in Table 4.1. This implies that the local topography and the plan form strongly affect the resonant response. This discovery strongly suggests that whenever a harbor layout is changed, the resonant response of the basin will also change. Thus, for harbor planners or harbor engineers there is a need for performing the computer modeling of the harbor basin whenever modifications of harbor layouts are planned.

As shown in Table 4.1, the oscillation waves inside the each of the two harbors during recent tsunami events are quite consistent. Now, let us examine the wave conditions on normal days as revealed from the tide gauge records on both the Crescent City Harbor and the LA/LB harbor. The wave oscillation condition in the three month period from May to July of 2008 at the two tide gauges are analyzed, and the wave spectrum in Crescent City Harbor is plotted in Figure 4.17 and the one in LA/LB harbor is plotted in Figure 4.18. In each figure the colored contours demonstrate the distribution of wave

energy contained in different frequencies during the 3 months. The red bands at the bottom of the two figures indicate the high energy contained in tides (12+ hour wave period). Beside the tide, the 22 minute and 60 minute waves are clearly shown in the spectrums respectively. It's very apparent that the 22 minute wave always oscillates inside Crescent City Harbor and the 60 minute wave always exists inside LA/LB harbor as well. The two spectrums further prove that the oscillation waves inside a harbor are local response and determined by the harbor itself.

Table 4.1 Dominant waves in Crescent City Harbor and Los Angeles harbor during recent earthquake events

	Crescent City Harbor	LA/LB Harbor
North California Offshore 06-15-2005	22.0 min	60.4 min 69.0 min
Kuril Islands 11-15-2006	22.0 min	50.4 min 62.6 min
Kuril Islands 01-13-2007	21.5 min	51.0 min
Solomon Islands 04-01-2007	N/A	60.2 min
Peru 08-15-2007	21.0 min	62.4 min 73.3 min

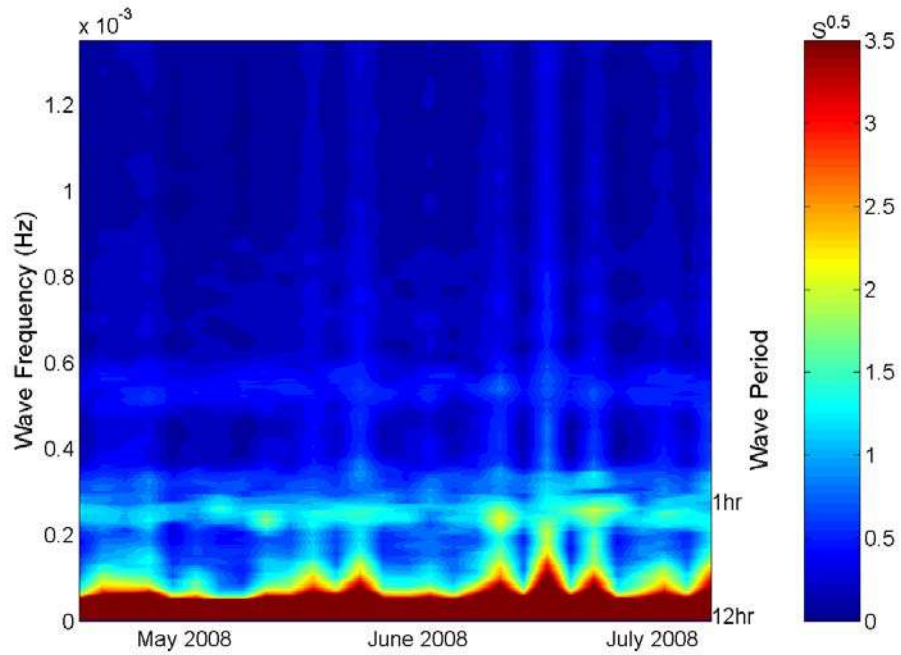


Figure 4.17 Wave Spectrum at the tide gauge station in Crescent City Harbor during May, June and July, 2008

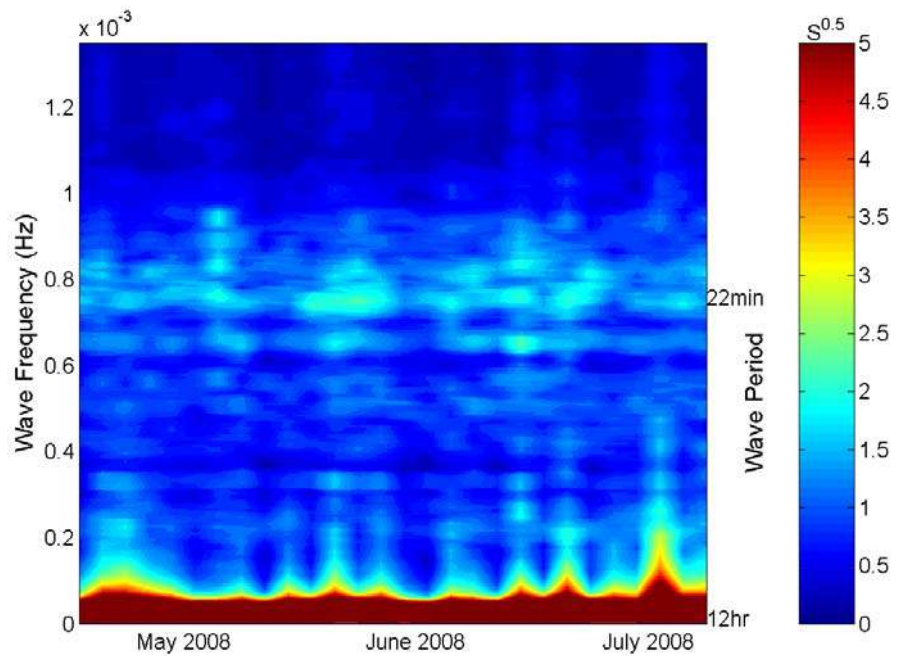


Figure 4.18 Wave Spectrum at the tide gauge station in Los Angeles harbor during May, June and July, 2008

In order to further illustrate the wave energy distribution, the water level time series and the corresponding spectral analysis on a normal day July 21, 2008 in each of the tide gauge were shown in Figure 4.19 and 4.20 respectively. Those figures reveal the fact that as long as there exists a wave in the incident wave group which has a period within the first resonant mode range, it will be amplified and contain more energy as revealed from the spectrum analysis.

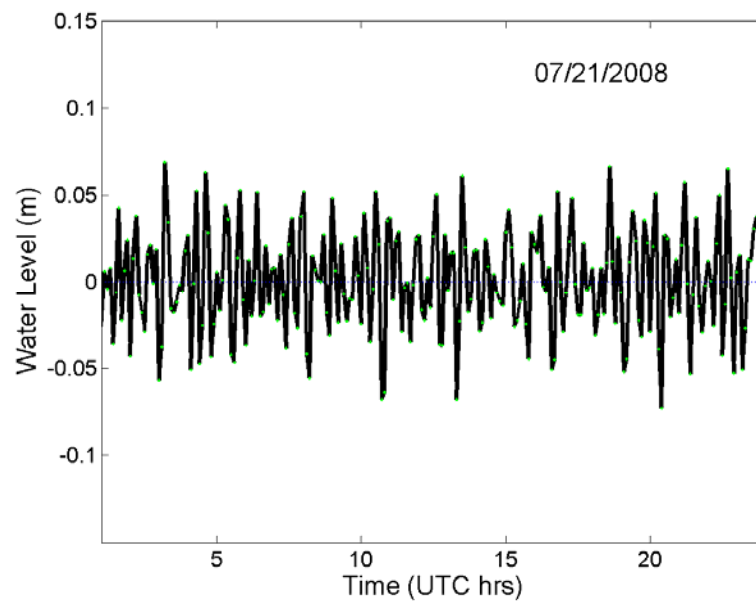


Figure 4.19 (a) Water level time series at the tide gauge station in Crescent City Harbor on July 21, 2008

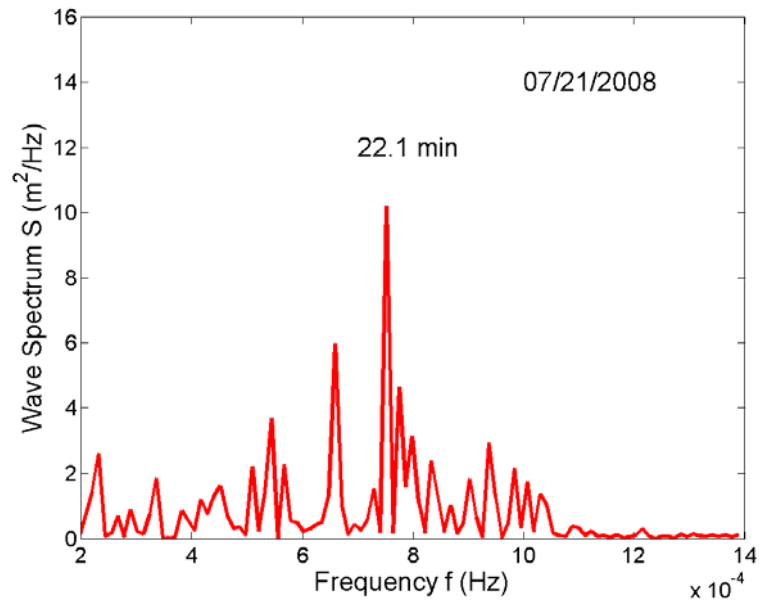


Figure 4.19 (b) Wave spectrum at the tide gauge station in Crescent City Harbor on July 21, 2008

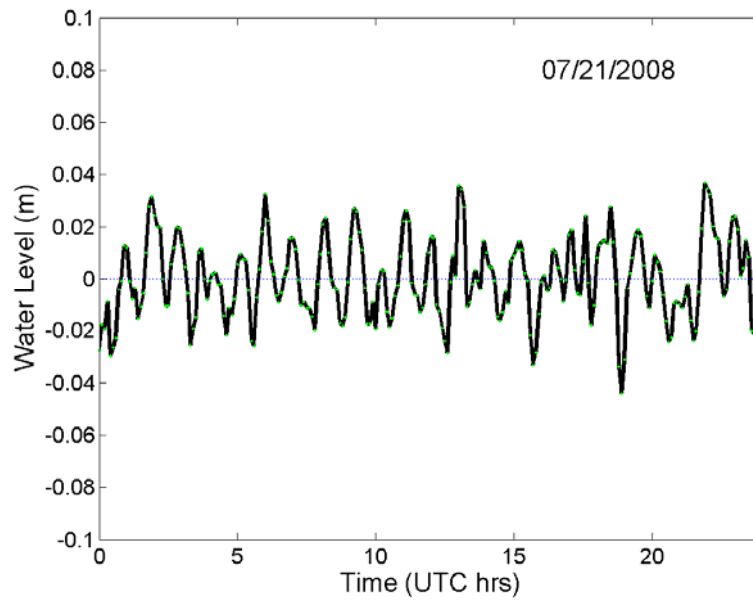


Figure 4.20 (a) Water level time series at the tide gauge station LA Berth60 on July 21, 2008

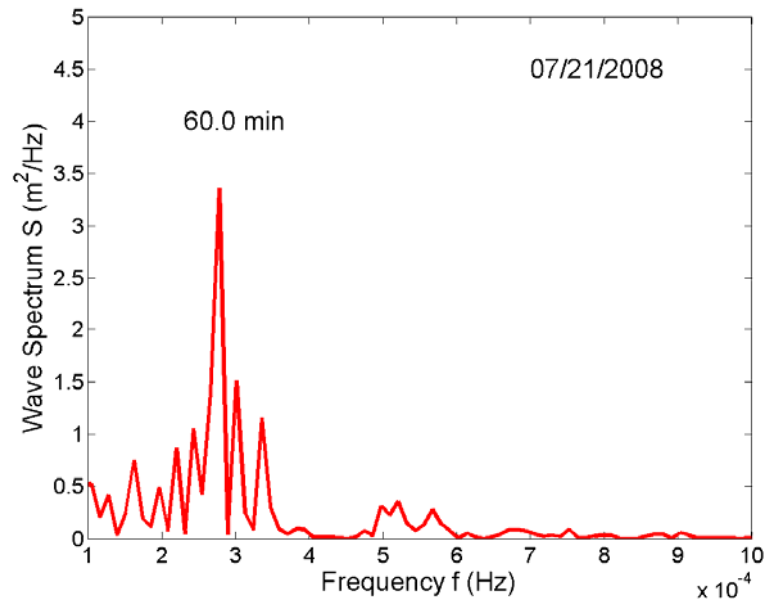


Figure 4.20 (b) Wave spectrum at the tide gauge station LA Berth60 on July 21, 2008

4.4 Discussion on Local Response

As discussed in the previous section, the wave oscillation condition inside a harbor or bay is determined by the harbor or bay itself. However there are still two questions which need to be answered: Is the oscillation condition determined by the harbor layout or/and the bathymetry and how large the simulations domain should be in order to fairly represent the local characteristics?

To answer the first question, several scenarios are examined. The first one is to assume uniform depth for the entire simulation domain, the uniform depth used here is 40 ft, which is approximately the average depth of the entire domain. The hypothesis is that the response will be the same for both real bathymetry and uniform depth condition if only

the plan form determines the response characteristics. The resulted response curves at point A, B, C and D indicated in Figure 4.21 are plotted in Figure 4.22 (a), (b), (c) and (d) respectively for comparison. It can be seen that the uniform depth model captures some of the resonance modes but not all of them. The amplification factor obtained from the uniform depth model is much lower than the one resulted from the real bathymetry model. Which means that the plan form of the harbor as well as the bathymetry are important in determining the wave oscillation characteristics.



Figure 4.21 Air photo of Los Angeles/Long Beach harbor with location ABCD noted

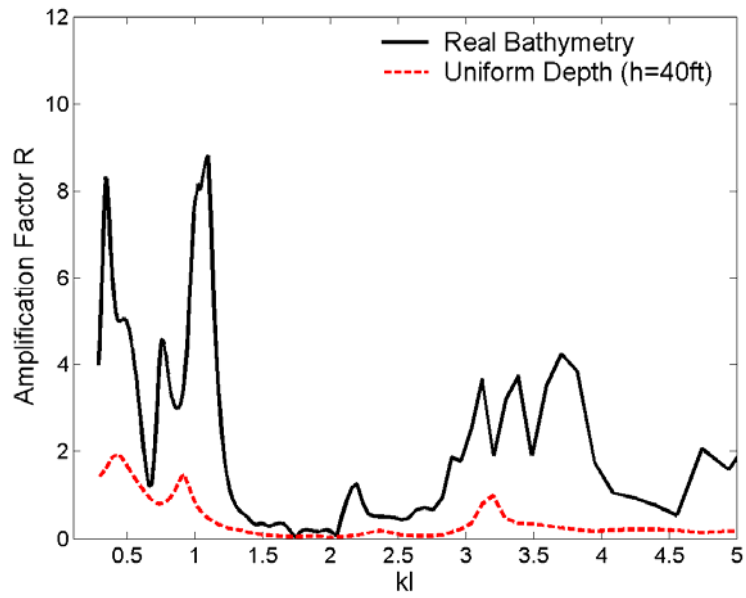


Figure 4.22 (a) Simulated response curves at location A for real bathymetry and uniform depth conditions

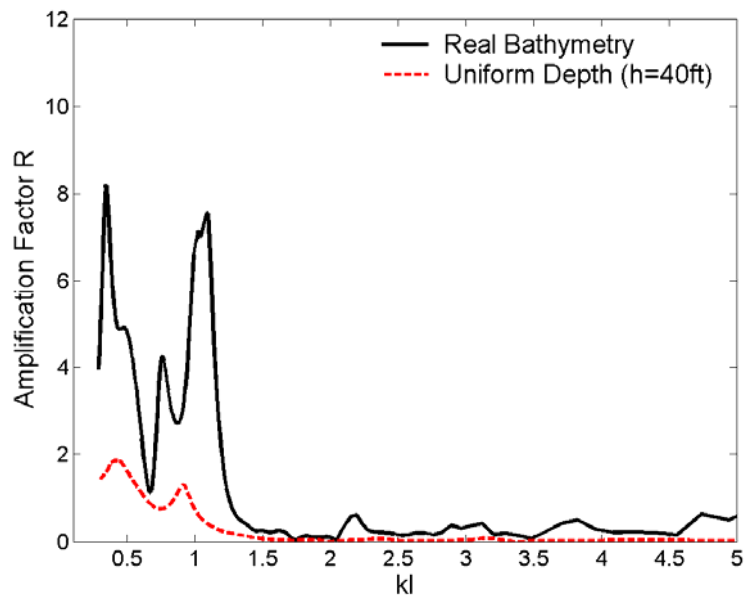


Figure 4.22 (b) Simulated response curves at location B for real bathymetry and uniform depth conditions

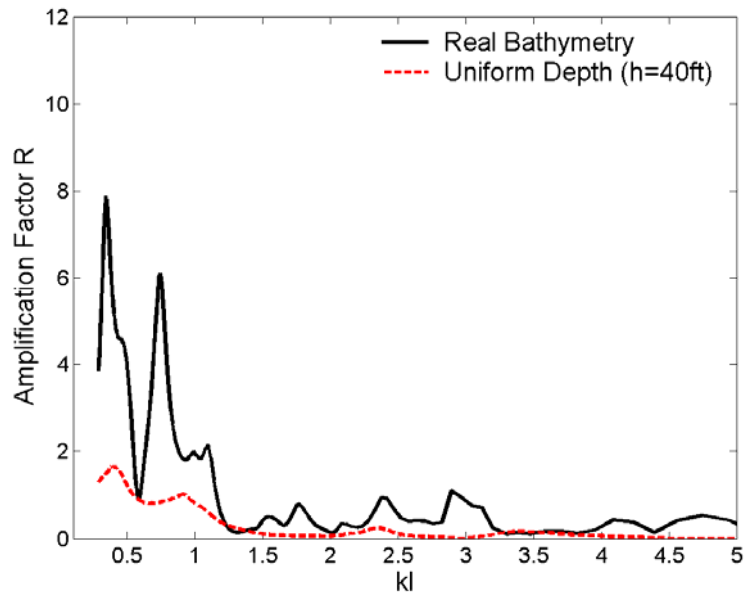


Figure 4.22 (c) Simulated response curves at location C for real bathymetry and uniform depth conditions

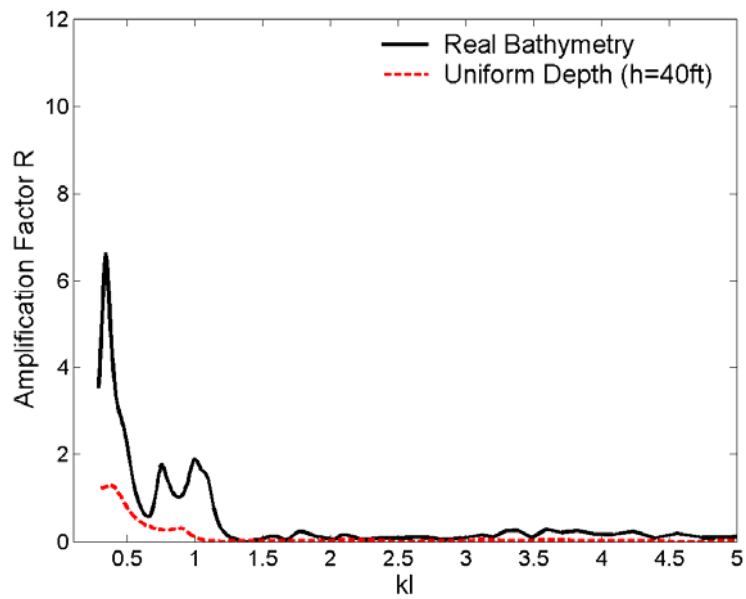


Figure 4.22 (d) Simulated response curves at location D for real bathymetry and uniform depth conditions

The second scenario is assuming the region outside the breakwaters has a uniform depth (54 ft) and the inside region has the real bathymetry. This will further prove the conclusion that the wave oscillation is induced by the local layout and bathymetry but not the outside continental shelf if the result is comparable between the real and assumed conditions. The computed response curves at the four locations A, B, C and D for the two conditions are plotted in Figure 4.23 (a) – (d) respectively. It's seen that the assumption of uniform depth outside the breakwaters gives more comparable results than the one from the uniform depth for the entire domain. The assumed condition captured most of the modes, but the amplification factor is similarly lower than the real bathymetry condition. This further proves the local response theory and further confirms the importance of correct bathymetry input in the wave oscillation simulation.

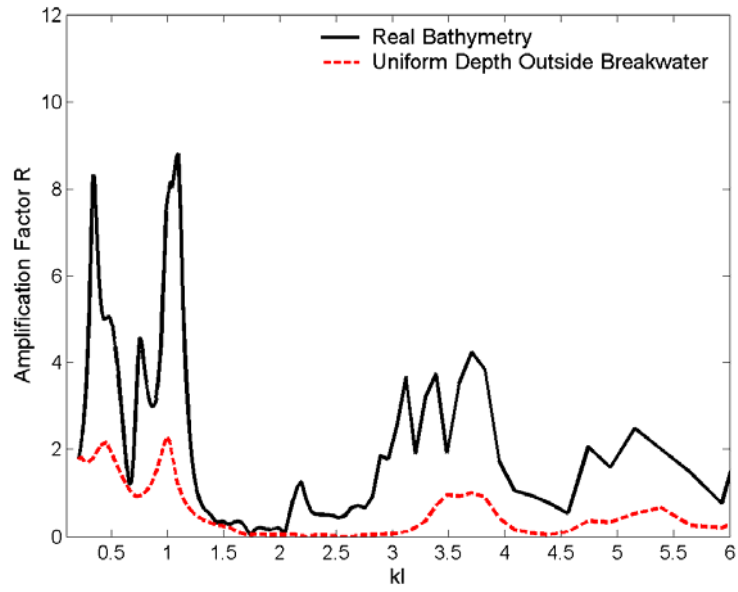


Figure 4.23 (a) Simulated response curves at location A for conditions of real bathymetry and uniform depth for the outside breakwater region

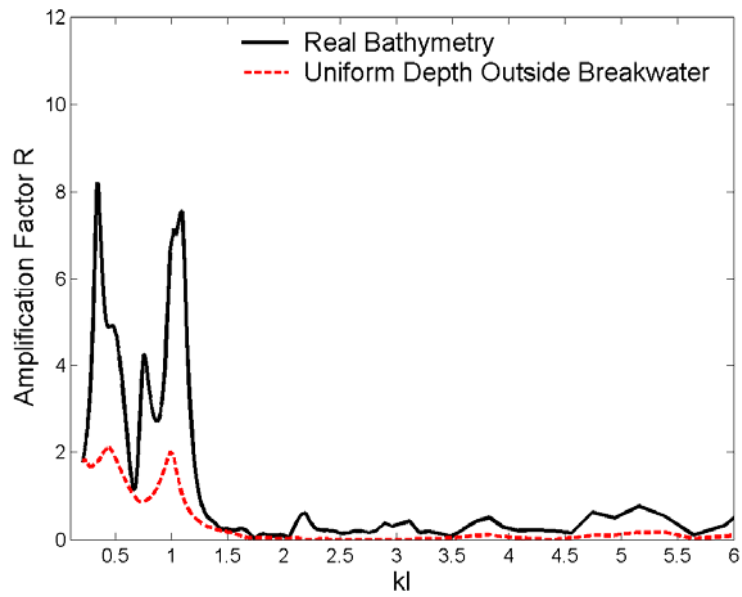


Figure 4.23 (b) Simulated response curves at location B for conditions of real bathymetry and uniform depth for the outside breakwater region

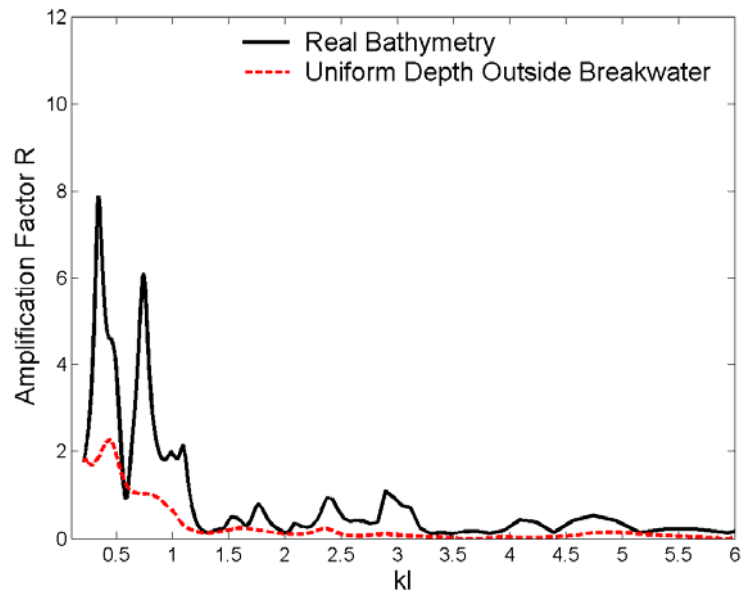


Figure 4.23 (c) Simulated response curves at location C for conditions of real bathymetry and uniform depth for the outside breakwater region

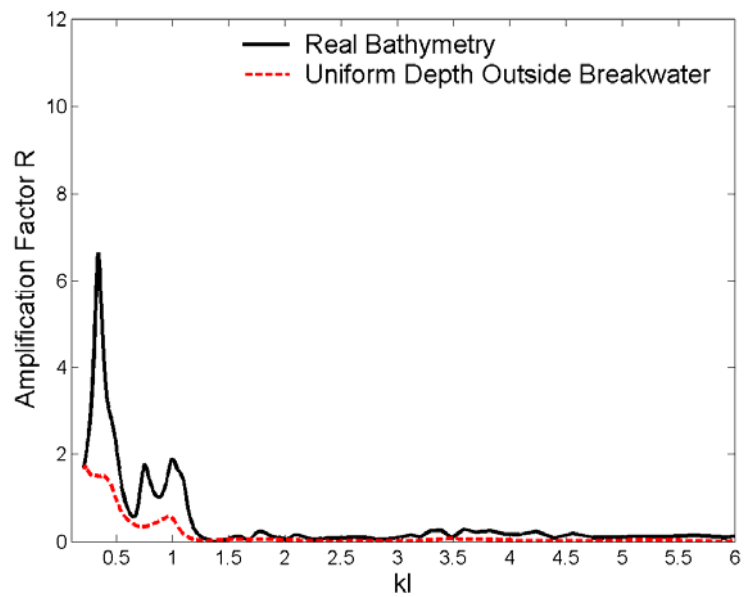


Figure 4.23 (d) Simulated response curves at location D for conditions of real bathymetry and uniform depth for the outside breakwater region

To answer the second question on how large the simulation domain should be to include the local characteristics in order to obtain the reliable simulation results, three different sizes of simulation domains were generated and compared. The bathymetry condition for the entire San Pedro Bay is illustrated in Figure 4.24. The region near the ports of Los Angeles and Long Beach is relatively flat with a sloping shelf connected to the outside region. The bathymetry becomes flat again outside the sloping shelf. The three simulation domains were selected in the way that the small one covers the inside flat area (the semi circle has a radius of 8.6 miles), the medium one covers half of the sloping shelf (the semi circle has a radius of 12 miles), and the large one covers the entire sloping shelf (the semi circle has a radius of 14.8 miles), as shown in Figure 4.25.

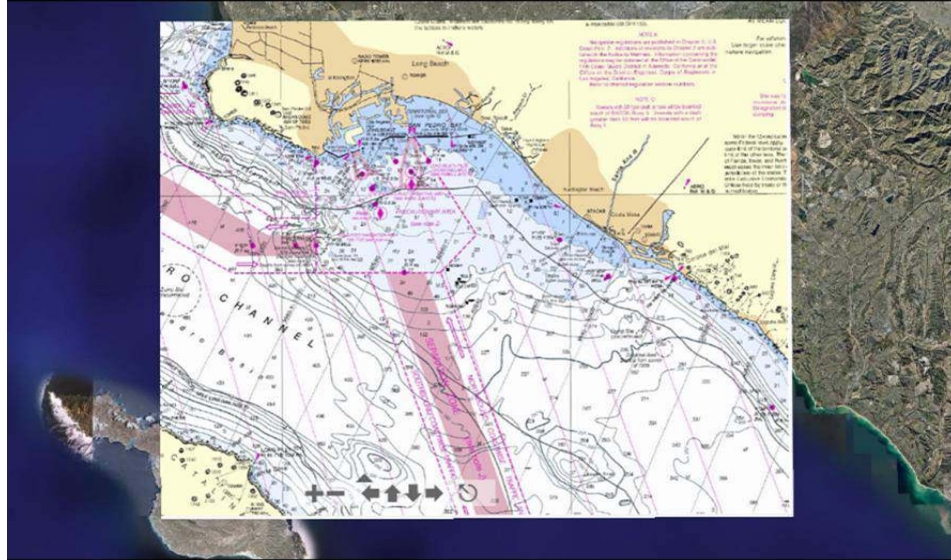


Figure 4.24 Bathymetry map of San Pedro Bay

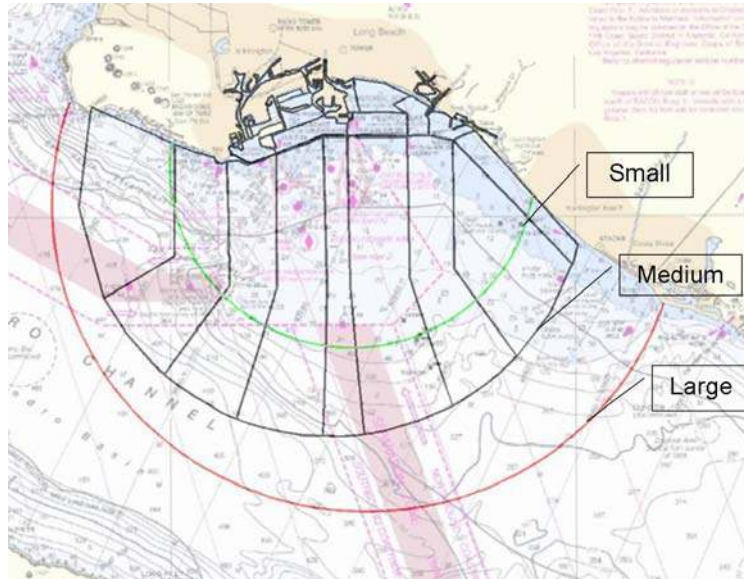


Figure 4.25 Three simulation domains noted by small, medium and large

The location A B C and D noted in Figure 4.21 are selected for the result comparison. The computed response curves from the three simulation domains at A, B, C and D are plotted in Figure 4.26 (a) – (d) respectively. The incoming wave direction used in the calculation is direction 2 indicated in Figure 4.12. It's seen that the results from different domains agree very well. They all captured the same simulation modes although there is a slight difference at the amplitudes of amplification factors. The result sufficiently draws the conclusion that the simulation domain does not need to be very large to capture the local characteristics for the wave oscillation study inside a harbor or bay, which may save a lot of computation cost.

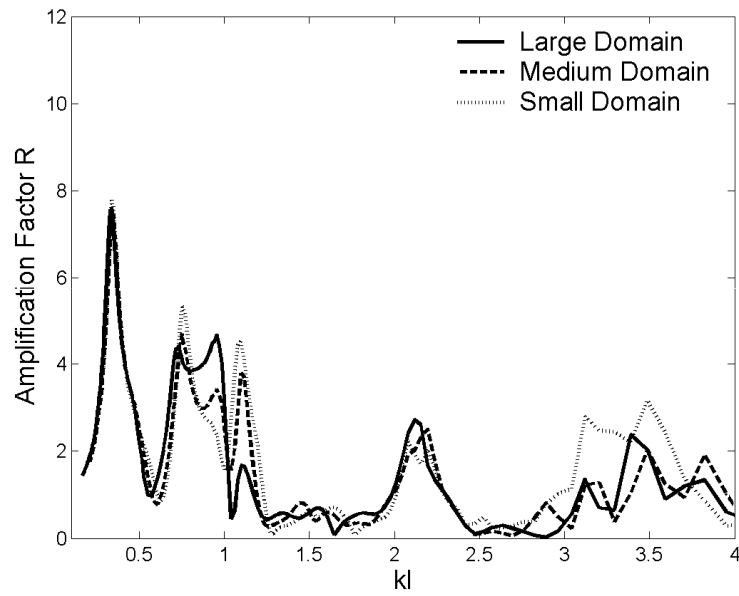


Figure 4.26 (a) Simulated response curves form three simulation domains at location A noted in Figure 4.21

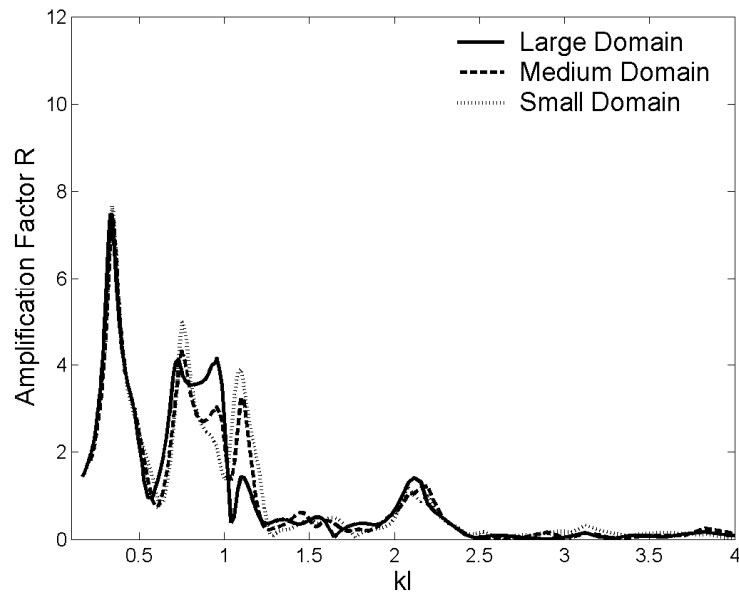


Figure 4.26 (b) Simulated response curves form three simulation domains at location B noted in Figure 4.21

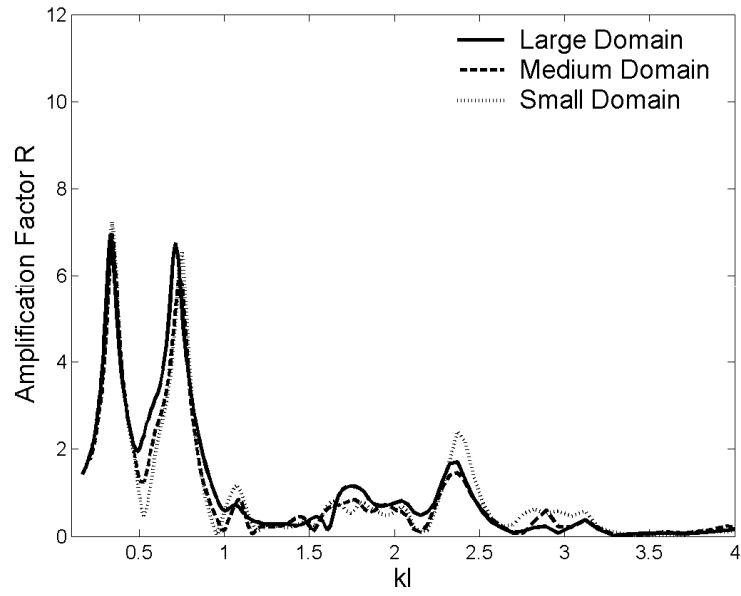


Figure 4.26 (c) Simulated response curves form three simulation domains at location C noted in Figure 4.21

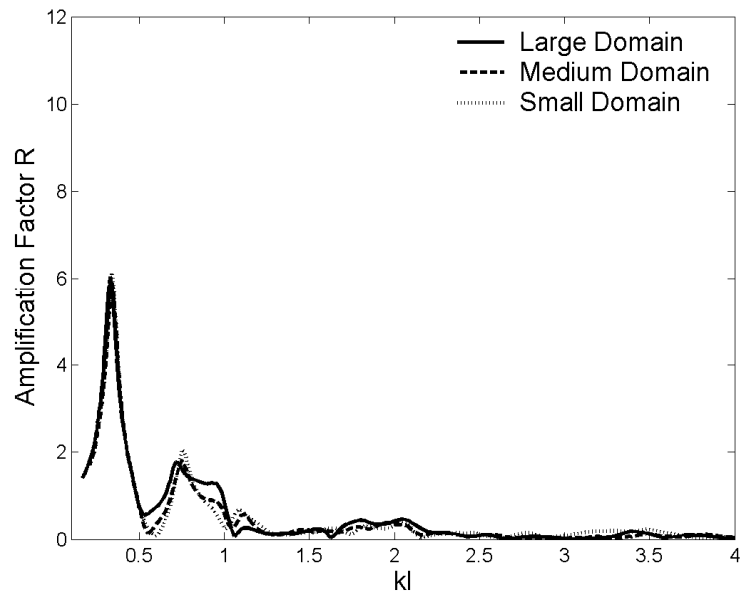


Figure 4.26 (d) Simulated response curves form three simulation domains at location D noted in Figure 4.21

4.5 Modeling of Bay of Fundy, Canada

As discussed in earlier sections, the layout and bathymetry of a harbor basin determines the wave oscillation characteristics inside the harbor basin. The wave length associated with the resonant modes is related to the characteristic length of the harbor basin. The characteristic length of the ports of Los Angeles and Long Beach is larger than that of the Crescent City Harbor, thus the resonant wave periods are longer for San Pedro Bay than that of Crescent City Harbor. It is interesting to note that if the size of a bay is large enough, the first resonant mode might coincide with the daily action of the flooding and ebbing tide. In the following, it will be shown that the observed large tidal range in Bay of Fundy is actually the result of resonant oscillation due to the tidal action.

Bay of Fundy, located between the Provinces Nova Scotia and New Brunswick in Canada as shown in Figure 4.27 is well known for having the largest tidal range in the world. Approximately 100 billion tons of water flushes in and out the bay twice a day. The dominant tide is the Principal lunar M2 tide, with a period of 12 hr and 25 min or 12.42hr. When the moon is full or new, the tide may be as high as 53 feet (16 m) at the head of the bay. The highest tide level occurs in the south branch Cobequid Bay.



Figure 4.27 Map of Bay of Fundy and Gulf of Main

Why is there such a large tide range in this region? It was first explained as because of the funnel shape of the bay (contraction in width) and the continuously upward slope from the mouth to the head (reduction in water depth), the tide is forced to rise. However it was pointed by Marmer as early as in 1922 that even the combination of those two are not enough to produce tides with such enormous ranges. Marmer used the theory of standing waves in a tank to explain the natural resonance in the Bay of Fundy. Several approaches of scales of the bay were used to estimate the natural resonance period of the bay, and the consequent periods obtained ranged from 11.6 hr to 13.0 hr. It was concluded that the 12.42 hr tide (M2 tide) is very close to the natural period of oscillation in the Bay of Fundy, which is the primary factor to the tidal phenomena in this area. Later on researchers had continuously worked on this problem to find the natural oscillation

period of the bay. Proudman got period of 11.06 hrs with a constant depth approach in 1953 and Rao (1968) found the period to be about 9hr which only considered the Bay of Fundy alone. With the integration of the Bay of Fundy and Gulf of Maine, the natural period obtained by Garrett (1972) was 13.3 hrs. And he modified it to be 12.38 to 12.98 hr in 1974 with a numerical model. The period estimated by Greenberg in 1979 was about 13 hrs. The oscillation periods of Bay of Fundy together with the Gulf of Maine are studied in present research.

As shown in the Figure 4.28, the simulation domain includes the Bay of Fundy and the Gulf of Maine. The main blocks of the mesh are superimposed. The model grid contains 77,247 nodes and 18,924 elements. The outside semicircle has a radius of 126.8 miles. The incoming wave direction used in the simulation is illustrated by the arrow outside the semicircle, which is perpendicular to the diameter of the semicircle. Tides are long waves, they will be mostly reflected by the vertical boundary. However considering the natural beach, the reflection coefficient used here for the beach is 0.96. For the river inlets at the head of the bay, the reflection coefficient is 0.67 with the assumption that some energy will propagate into the rivers.

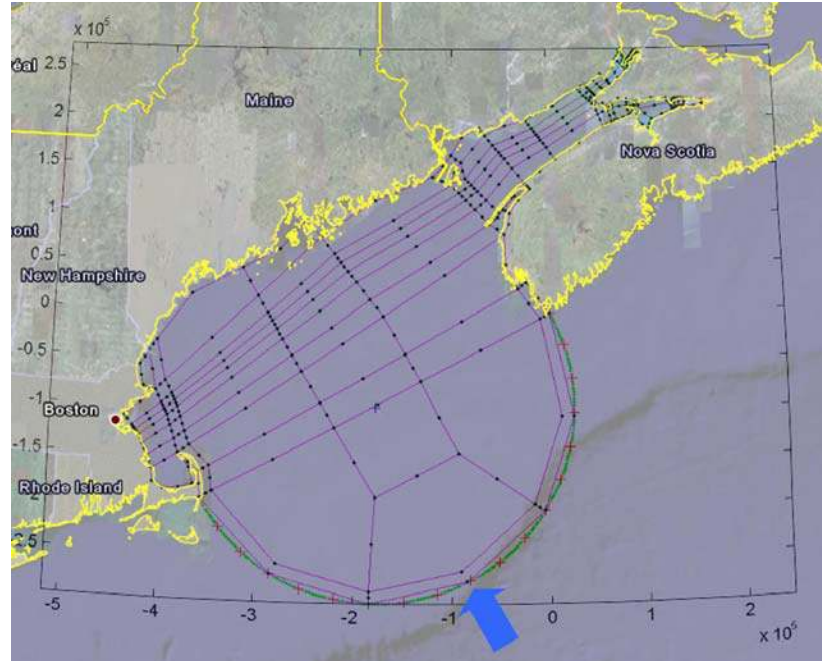


Figure 4.28 Simulation domain for Bay of Fundy with mesh and incoming wave direction superimposed

The present FEM model was used to simulate the response curves at locations inside the Bay of Fundy. Ten locations were chosen for the demonstration, which are noted in Figure 4.29 as 1 to 10. Gauge 1, 2 and 3 are located in the bay, and 4, 5 and 6 are located in the south branch and the other four are located in the north branch.



Figure 4.29 Locations of gauge 1 to 10 selected for the result demonstration

For a clear comparison, the response curves at gauge 1,2,3,4,5 and 6 are plotted together in Figure 4.30 and 1,2,3,7,8,9 and 10 are plotted together in Figure 4.31.

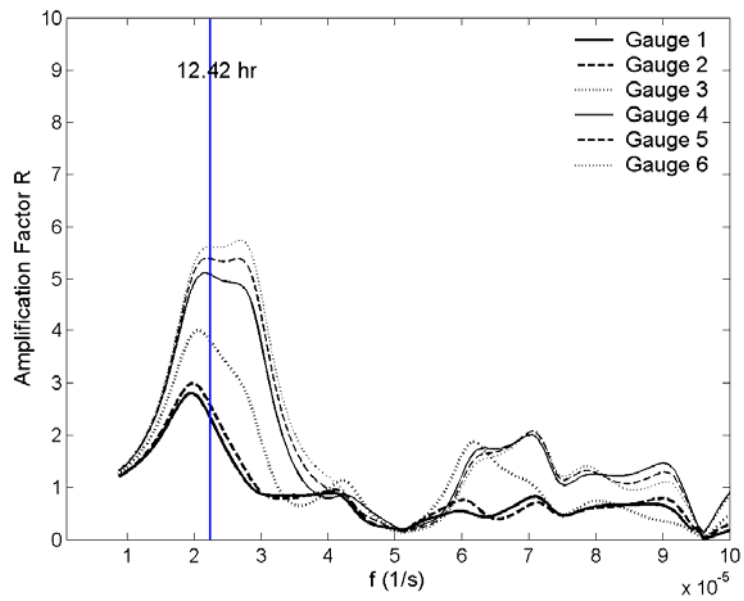


Figure 4.30 Response curves at gauge 1,2,3,4,5 and 6

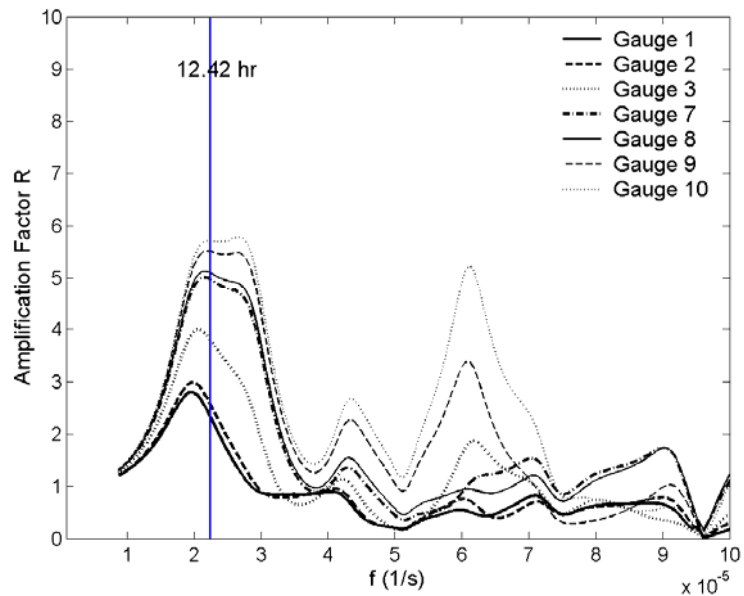


Figure 4.31 Response curves at gauge 1,2,3,7,8,9 and 10

The response curves are plotted as amplification factor R (ratio of wave height H_r at the indicated location to the incident wave height H_i , $R = H_r/H_i$) versus wave frequency f . From Figure 4.30 and 4.31, it's seen that the tidal range increase toward the inner region. That is because the 12.42 hr tide is within the first mode of the bay (also called the pumping mode), in which the amplification of wave heights increase toward the inner location in the harbor basin. The tide is significantly amplified at the head of the bay area, exactly as found in the field data.

There's another interested thing shown in the two figures that it seems the peak of the first mode shifts to the right (higher wave frequency or shorter wave period) when the gauges move more inside, roughly from 14 hr to 10 hr. But the amplification factor for 12.42 hr tide increases when the gauge moves more inside of the bay.

In order to show how the tide is amplified inside the simulation domain, the modes for the 12.42 hr wave are plotted in Figure 4.32 and 4.33. In Figure 4.32, the distribution of amplification factor is plotted. It's seen that the amplification factor in the Cobequid Bay, located in the south brunch of the bay head, is as high as 8. In fact, the south brunch was observed to have higher tide than the north brunch (Chignetco Bay) as simulated. It was observed that the tide has a height about 4 to 8 ft in the nearshore region outside the Gulf of Maine. The distribution of tide height is plotted in the Figure 4.33 with the assumption that the outside tide is 7.5 ft. The corresponding tide in the Cobequid Bay is more than 50 ft with the assumption of 7.5 ft tide outside the Gulf of Maine. The tremendous tidal phenomena inside Bay of Fundy are well presented in Figure 4.33.

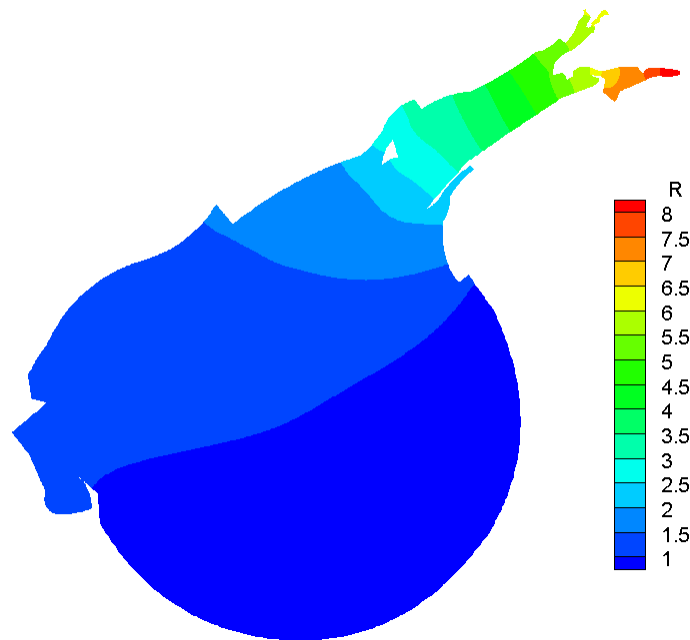


Figure 4.32 Distribution of amplification factor in the simulation domain

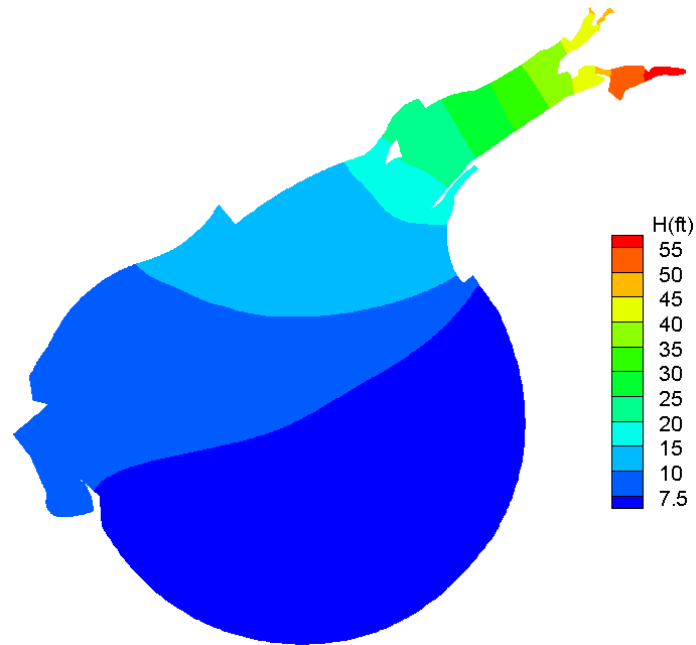


Figure 4.33 Distribution of tidal range in the simulation domain (assuming that the tidal range outside of Gulf of Maine to be 7.5 ft)

Within Bay of Fundy, there exists several tide gauge stations. Some of them have tide records available since the beginning of 2007 (<http://www.waterlevels.gc.ca>). In order to test the simulation results, 13 tide stations were selected for comparison, as illustrated in Figure 4.34. The station Out Wood Island is located approximately at the entrance of the bay, the stations Dipper Harbour West and St. Martins are inside the bay. Stations Baxters Harbour, Scots Bay, Diligent River, Five Islands and Burntcoat Head are in the south branch Cobequid Bay, and the stations Herring Cove, Cape Enrage, Joggins and Hopewell Cape are in the north branch Chignecto Bay.



Figure 4.34 Locations of 13 tide stations in Bay of Fundy

Since the station Outer Wood Island is very close to the inlet of the bay, it was chosen as the reference point to compute the amplification factor. The tidal ranges at the 13 stations for the four weeks (the first 7 days of August and November in 2007 and February and May in 2008) are normalized by the corresponding tidal ranges at the station Outer Wood island to get the amplification factors. The averages of the amplification factors in the four weeks, as well as the normalized amplification factor with the same reference point from the simulation, are obtained and listed in Table 4.2. The last column lists the differences between the observed and computed amplification factors. It can be seen that the largest difference is 8.81% at the station Dipper Harbour west. For other stations the errors are normally less than 5%, which means the modeling is quite reasonable. The

simulated amplification factor is generally less than the observed ones. This may be improved by increasing the reflection coefficients at the beach boundary.

Table 4.2 Comparison between the observed and simulated amplification factor

	Name of the Gauge	Observed Amplification Factor (Normalized by Outer Wood Island)	Simulated Amplification Factor (Normalized by Outer Wood Island)	Difference (%)
1	Outer Wood Island	1.0000	1.0000	
2	St. Martins	1.8747	1.7436	-6.99
3	Dipper Harbour West	1.4499	1.3221	-8.81
4	Baxters Harbour	2.3371	2.3070	-1.29
5	Scots Bay	2.3728	2.3550	-0.75
6	Diligent River	2.5288	2.4609	-2.68
7	Five Islands	2.8405	2.8628	0.78
8	Burntcoat Head	3.0393	3.0679	0.94
9	Herring Cove	2.1710	2.1031	-3.13
10	Cape Capston	2.1116	2.1138	0.10
11	Cape Enrage	2.2197	2.2097	-0.45
12	Joggins	2.4974	2.3700	-5.10
13	Hopewell Cape	2.5198	2.4212	-3.91

As expected, the simulation for Bay of Fundy reveals the fact that the tremendous tidal ranges in this area are not purely caused by the contraction of bay width and the decreasing of water depth, but also because of the coincidence between the periods of semi-diurnal tides and the natural oscillation period of the first resonant mode of the bay. The tides are amplified as much as 8 times at the head of the bay. The 2-D figures clearly

show the distribution of amplification factors as well as the distribution of the tidal ranges. The simulated results are also compared with the available tide station records. The agreement between the simulated and observed amplification factors normalized by the data at Outer Wood Island (at the inlet of the bay) proves the accuracy and reliability of the present numerical model.

4.6 Summary

From the wave oscillation study in San Pedro Bay, Crescent City Harbor and Bay of Fundy, several conclusions can be drawn as follows:

1. The good agreements between the simulated results and the field observations in these harbor resonance studies prove that the present numerical model is a very useful tool to investigate the resonance mechanism for long waves.
2. The differences of the amplification factor caused by various incident wave directions are the results of wave reflection from the coast or outside jetties, as well as wave diffraction due to the natural obstacles or manmade breakwaters, both of which weaken the wave field inside the harbors or bays.
3. The resonant response characteristics inside a harbor or bay are determined by the local topographical characteristics: the plan form and the bathymetry of the harbor

basin. Thus even for the same incoming waves, the oscillated waves inside different harbors are different.

4. Since the wave induced oscillation is a local response, the simulation domain does not need to be too large, which can save some computation cost for future studies.
5. The characteristic length of the bay and harbor should be on the order of the wave length associated with the oscillation modes in order to create large resonant motion. Therefore, the larger bay or harbor will have longer wave length thus the greater wave periods for the oscillation modes. The large tidal ranges observed in Bay of Fundy are the results of tide induced resonant motion with the wave period at 12.42 hours.

CHAPTER 5 APPLICATION FOR HARBOR IMPROVEMENTS

As shown in the previous chapter that resonant response in a bay or harbor is mainly induced by the local geometrical layout and the bathymetry and less dependent on the origin of the incident waves. The question now is what we can do to alter the resonant response characteristic to minimize the negative effect of long period oscillations. The present computer model has been applied in the evaluation of modification strategies of two harbors: Pohang Harbor in Korea and Hualien Harbor in Taiwan. This chapter will present and discuss the results obtained from modifications of harbor configuration on the wave oscillation condition in these two harbors.

5.1 Modeling of Pohang Harbor, Korea

5.1.1 Introduction

Pohang new harbor situated in the Yongil bay in the southeast of Korea, is the largest industrial harbor in Korea and is one of the largest industrial harbors in the world. The harbor handles cargos of steel company POSCO and other industrial complex in the region. The pier structure and the loading and unloading facilities are capable of handling 36 ships concurrently which handle 47 million tons yearly including 250,000 DWT size ship. The left map in Figure 5.1 shows the location of Yongil bay and the right photo

presents an air photo of the harbor region with the model grid layout superimposed. The Pohang Harbor is highlighted by the circle.

Since Pohang Harbor is located in a natural bay, they together compose a larger harbor. It's not reasonable to just focus on a small region, the harbor and the bay were studied together to catch all the possible resonant modes within the harbor basin.

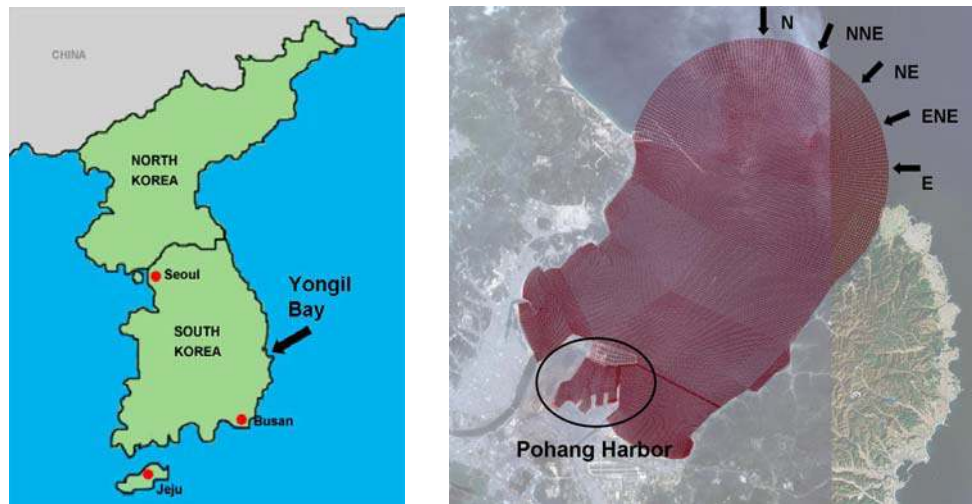


Figure 5.1 Location of Yongil Bay (left) and the layout of simulation domain with mesh and incoming wave directions superimposed (right)

Due to its location and the coastline orientation, Pohang new harbor has been found to provide fairly good protection against typhoons coming from the south. However, seiche motions due to long period waves have occurred frequently. This has produced undesirable wave and ship oscillations in the harbor, especially during the season with waves coming from the northeast direction. Such long period oscillations affect negatively the loading and unloading activities of the ship. Field measurement programs,

such as the one by Ministry of Construction in 1987 and 1999, have shown the existence of the long period wave oscillation within the harbor.

In an effort to reduce the long period wave oscillations inside the harbor, the harbor was modified at the beginning of 1990s. Figure 5.2 shows the layouts of the harbor before and after the modification. The outside jetty was enclosed in 1996 and the second breakwater closer to the entrance was built in 1992.



Figure 5.2 Layouts of Pohang Harbor before and after the modifications

5.1.2 Study of the Previous Condition of Pohang Harbor

The present finite element model has been applied to the greater Pohang new harbor region for the seiche study. Since the expansion plan may call for breakwater construction in the outer harbor area a very large region has been included in the model. The grid layout shown in Figure 5.1 (right photo) contains 5,950 elements and 24,853 nodes. The modeling results were compared with the field measurements for the

conditions both before and after the modifications. More strategies for future modification and expansion of harbor facilities have been proposed. The pros and cons of those plans will be discussed after the simulation results have been presented.

Field measurement data conducted by Ministry of Construction in 1987 were used to compare with the simulation results for the layout condition before the modifications.

The two stations T1 and T2 indicated in Figure 5.2 (left) were selected for the comparison. Figure 5.3 (a) presents the response curve at Station T1 in Pohang new harbor at various wave frequencies for the harbor configuration before modification. It covers the wave periods from 100 minutes to 60 sec. The ordinate is the amplification factor defined as the wave height at Station T1 divided by the incident wave height. The abscissa is the wave frequency with unit at 10 cycles per minute (the right hand limit corresponds to 60 sec wave). Several resonant modes are clearly seen from Figure 5.3.

Figure 5.3 (b) presents the spectral density curve for Station T1 covering the same frequency range based on the data obtained in the field measurement program (Ministry of Construction, 1987). The first four resonant periods indicated by the four vertical lines in Figure 5.3 (a) are the resonant periods obtained from the field data shown in Figure 5.3 (b) i.e. 4,800 sec, 1,650 sec, 490 sec, and 260 sec. It is seen that the present computer results compare very well with the field data, especially for the first few resonant modes.

It is also noted that several resonant modes also exist for wave coming from the north direction for wave period between 60 sec and 120 sec.

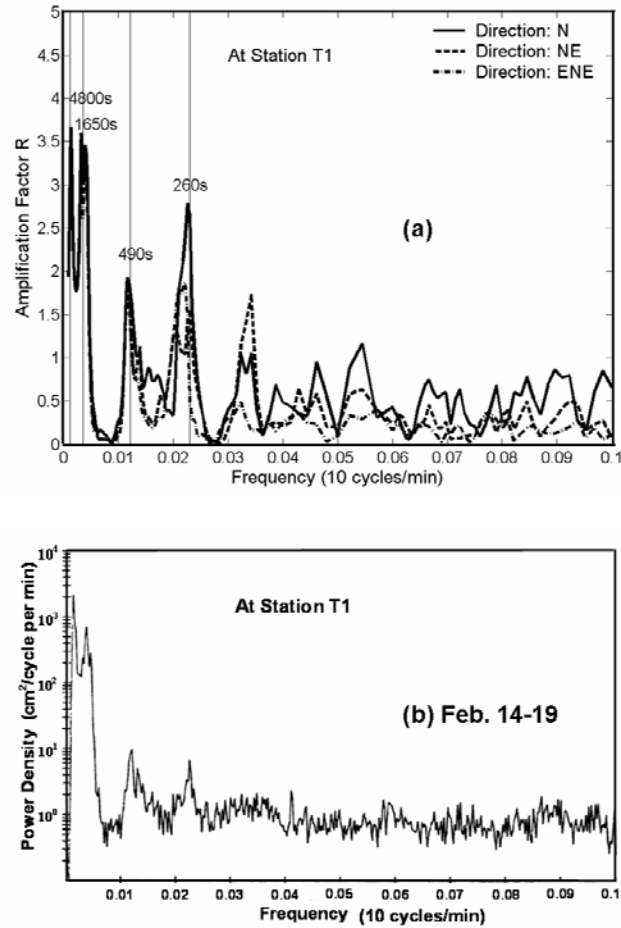


Figure 5.3 Results of numerical simulation (a) and field data (b) at Station T1

Similar results for Station T2 are shown in Figure 5.4 (a) and 5.4 (b) for computer simulation results and field measurements. The vertical lines plotted in Figure 5.4 (a) are obtained from the field data shown in Figure 5.4 (b). The simulation results agree very well again with the field observation. The computer model appears to capture the major resonant response of the harbor region.

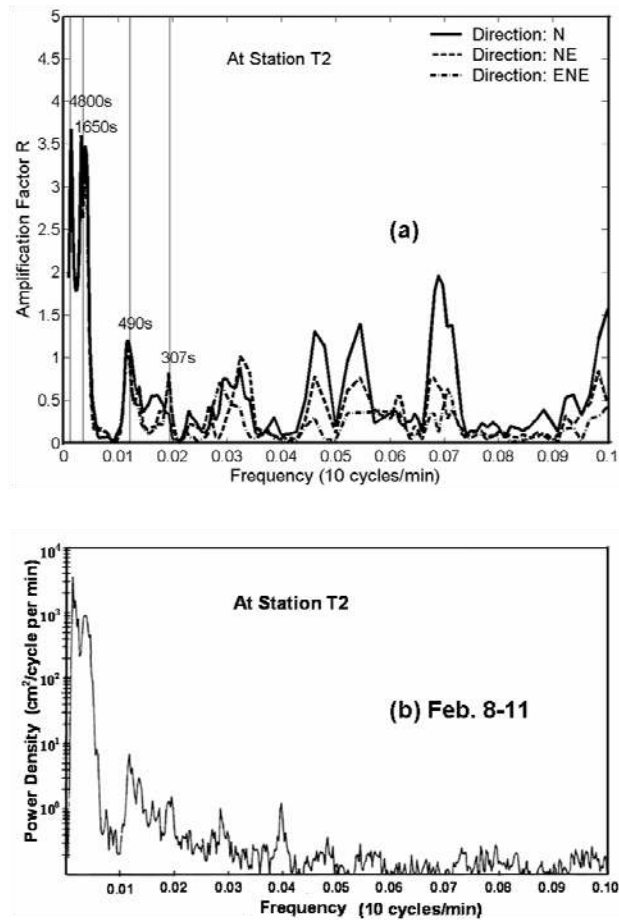


Figure 5.4 Results of numerical simulation (a) and field data (b) at Station T2

5.1.3 Study of the Present Condition at Pohang Harbor

As shown in Figure 5.2 (right), the harbor was modified by enclosing the outside jetty and building another inside breakwater, which is the present harbor layout. Wave measurements were conducted continuously at the four inside locations as indicated by P1, P2, P3 and P4 from Sep. 14 to Oct. 17, 1999. The present numerical model was applied to obtain the response characteristics under this modified harbor layout.

Simulation results at those four locations were compared with the field data and they are presented in Figure 5.5 (a) to (d) respectively.

In Figure 5.5, the left panels are the simulated response curves at the four locations for incoming wave direction from northeast (NE), which is the wave direction that usually results in large oscillations. The ordinate shows the wave frequency and the abscissa shows the amplification factor at the noted location. The right panels are the wave spectrums obtained from field measurements. The abscissa shows time, and the ordinate shows wave frequency (on the left) and wave period (on the right). The square root of the wave spectrum, which is proportional to wave amplitude, was presented with color contours. The wave spectra show the wave energy distribution along wave frequency at the four locations during the whole month.

The dark red lines at the bottom of those spectral plots indicate the high energy of the tides. The red lines shown at about 5000 sec (frequency 0.0002) indicate the first mode of resonance within the harbor, corresponding to the red line in the spectra on the left panels. Around 2000 sec (frequency 0.0005), there is a distinct green line in each spectrum. Which is the second mode corresponding to the green lines in the response curves on the left panels. The third mode indicated by the yellow line in each left panel covers wave period from 1300 to 1700 sec (frequency 0.00059 to 0.00077). It can be seen from the spectra that there is always some energy exists within this frequency band. The mode at about 520 sec (frequency 0.00192) only exists at P1, P3 and P4, but not P2. There is

some energy illustrated by lighter color shown in the spectra at the corresponding wave frequency accordingly. For location P2, the simulated amplification factor is small after the third mode, which is verified by the spectrum that there is no significant energy focusing in that frequency band. For Location P3, there exists a mode at about 350 sec (frequency 0.00283), emphasized by the purple line in the left panel of Figure 5.5 (c). The spectrum in Figure 5.5 (c) clearly shows the energy band.

Generally, the simulated response curves correlate very well with the wave spectra from field data. This is shown by the concurrent wave frequency between the simulation and observation, as well as the similar ratios between the simulated amplification factors and the observed wave amplitudes. It can be explained that because of the resonance, the waves within the resonance frequency bands were accordingly amplified, making the energy significant to be revealed by the spectral analysis.

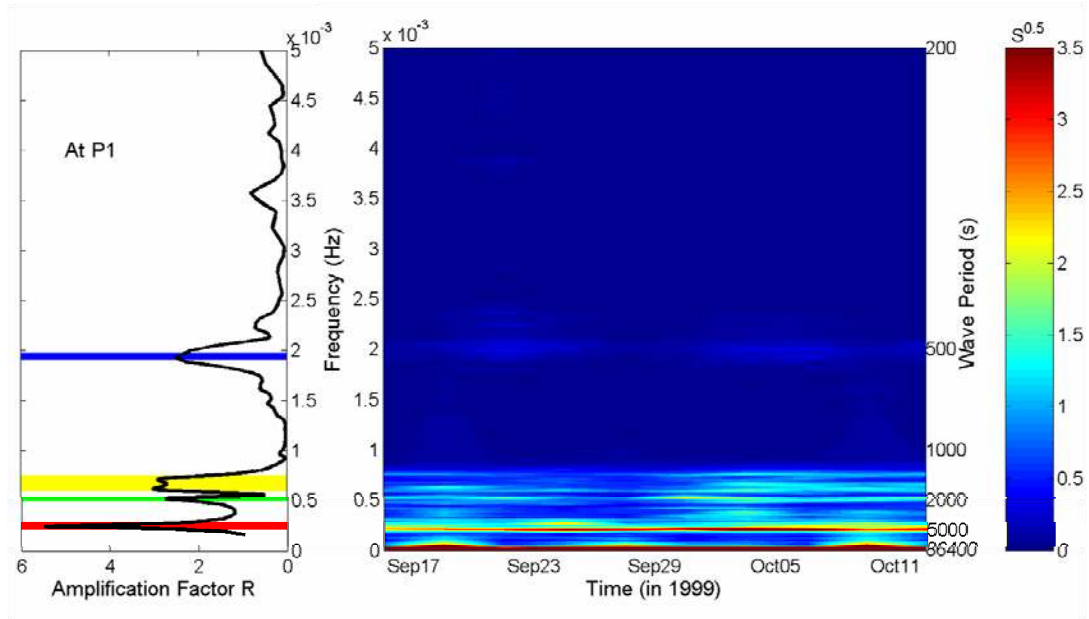


Figure 5.5 (a) Comparison between the simulated response curve for NE wave direction and the wave spectrum obtained from field data (1999) at Location P1

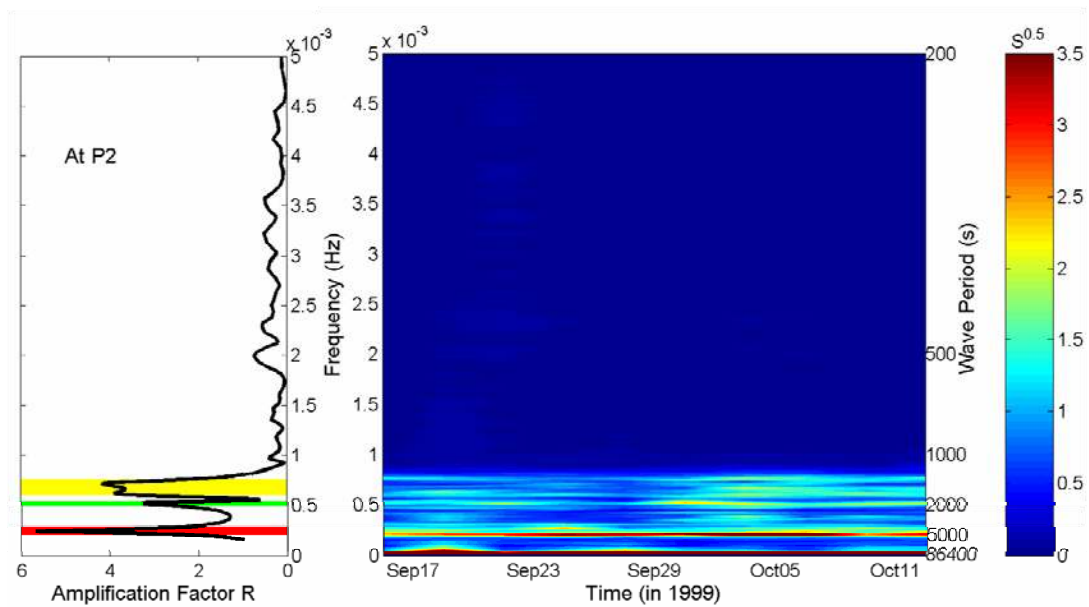


Figure 5.5 (b) Comparison between the simulated response curve for NE wave direction and the wave spectrum obtained from field data (1999) at Location P2

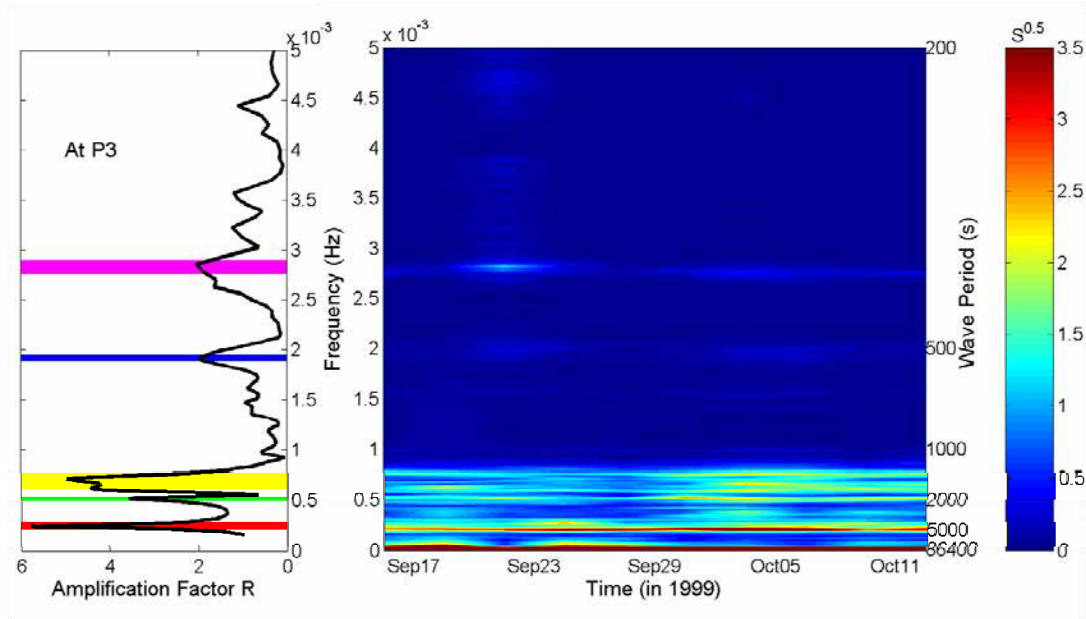


Figure 5.5 (c) Comparison between the simulated response curve for NE wave direction and the wave spectrum obtained from field data (1999) at Location P3

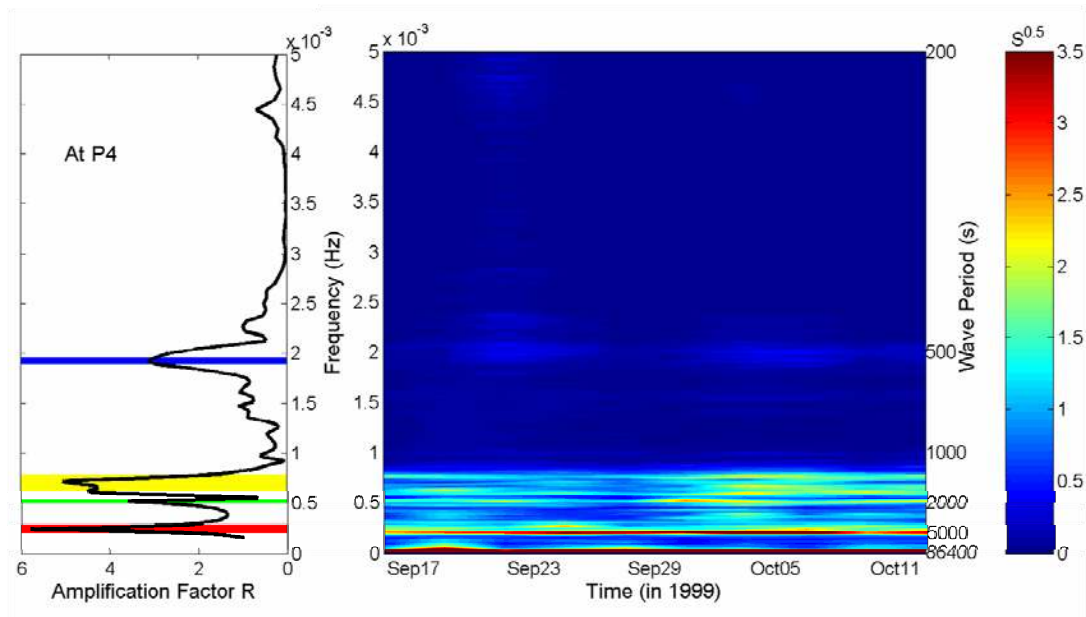


Figure 5.5 (d) Comparison between the simulated response curve for NE wave direction and the wave spectrum obtained from field data (1999) at Location P4

To check the effects caused by the modification, the computer model generated response curves before and after the modification at station T1, T2 and T9 indicated in Figure 5.2

are plotted in Figure 5.6, 5.7 and 5.8. It can be seen that the amplification factor is significantly diminished for the wave period range from 100 sec to 200 sec, a region in which severe ship motions were found to occur. Thus, the modification of harbor layout will be helpful in reducing the seiche problem in Pohang Harbor.

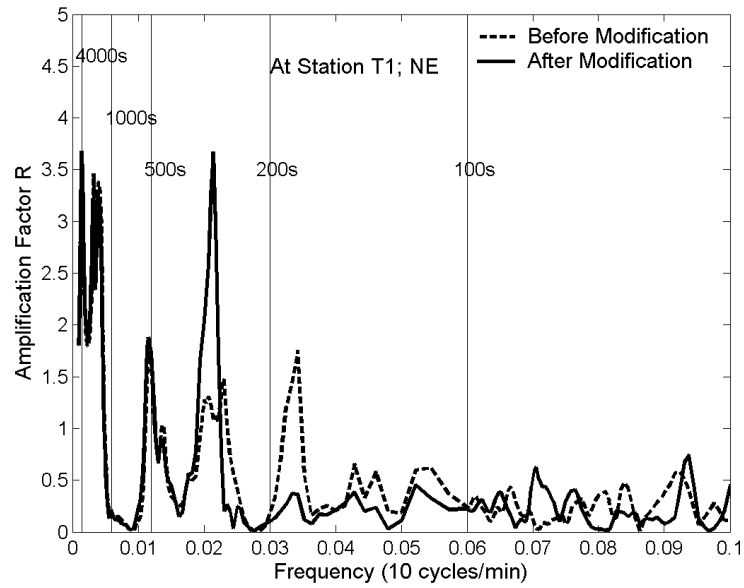


Figure 5.6 Response curves before and after the modification at Station T1 in Pohang Harbor

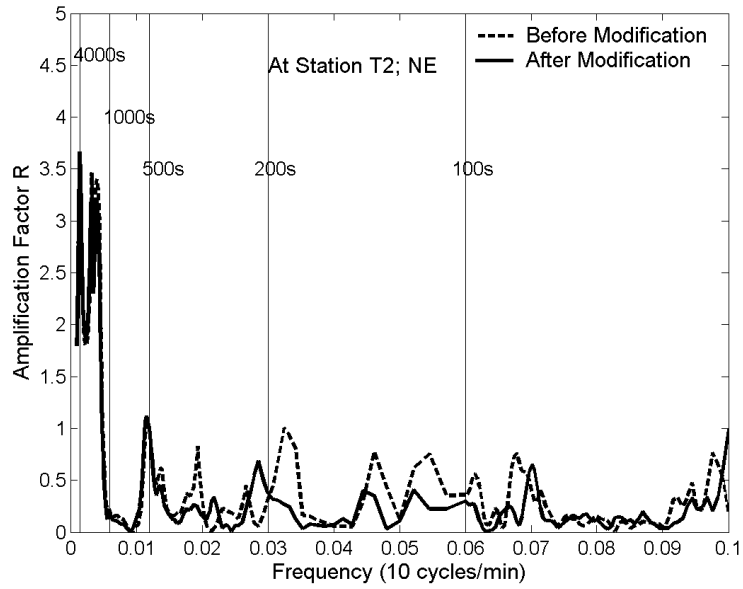


Figure 5.7 Response curves before and after the modification at Station T2 in Pohang Harbor

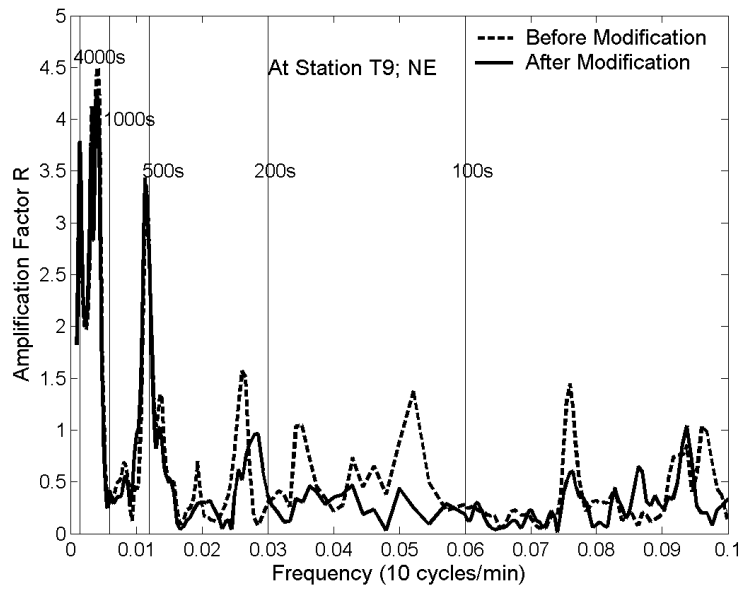


Figure 5.8 Response curves before and after the modification at Station T9 in Pohang Harbor

5.1.4 Modeling of Additional Modification Strategy for Pohang Harbor

As discussed earlier, the modification appears to help reducing the seiche motion, however the seiche problem was not totally eliminated. Pohang new harbor was still experiencing about 2 months of downtime on average each year (Jeong, et al., 1997). There were as high as 20 cm long period waves recorded. In order to reduce the oscillation due to long period waves, several modification strategies are proposed in this present study. The strategies include the elongation of the jetties and breakwaters, installing energy dissipaters, and the combination of them.

The first Modification strategy (so called Case A) is to expand the enclosed outside jetty 300 meters toward east, as shown in Figure 5.9. The points P1, P2, P3 and P4 are those locations selected for the result comparison.



Figure 5.9 Layout of Pohang new harbor with the modification Case A

The computed response curves at location P1, P2, P3 and P4 for present condition and after strategy A are plotted in Figure 5.10 (wave direction is NE). It can be seen that the amplification factors at those points are slightly reduced for waves less than 180 sec (frequency larger than 0.0055), but increased for waves between 180 sec to 220 sec (frequency ranges from 0.0046 to 0.0055). The improvement is not significant. Which is expected because modification scale is very small compared with the whole size of the harbor. And the entrance is still the same size even the outside jetty is elongated. The long waves can still propagate into the harbor.

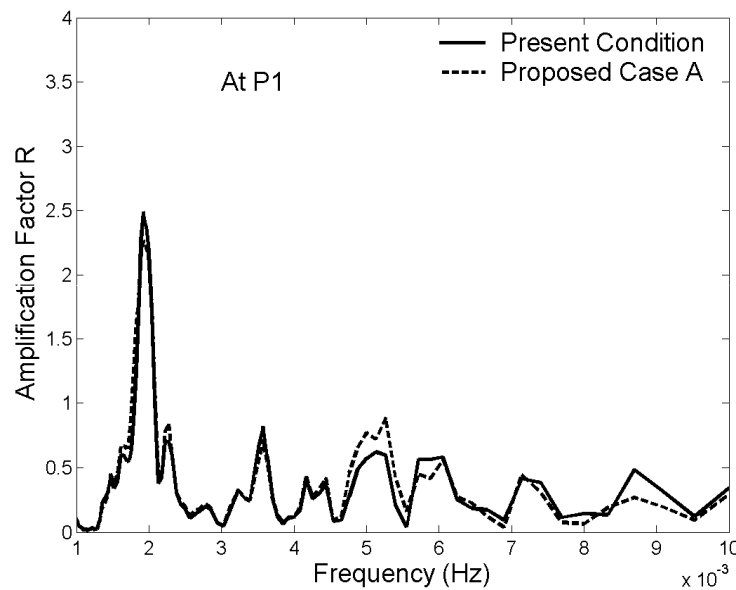


Figure 5.10 (a) Response curves at location P1 for present condition and after proposed Case A

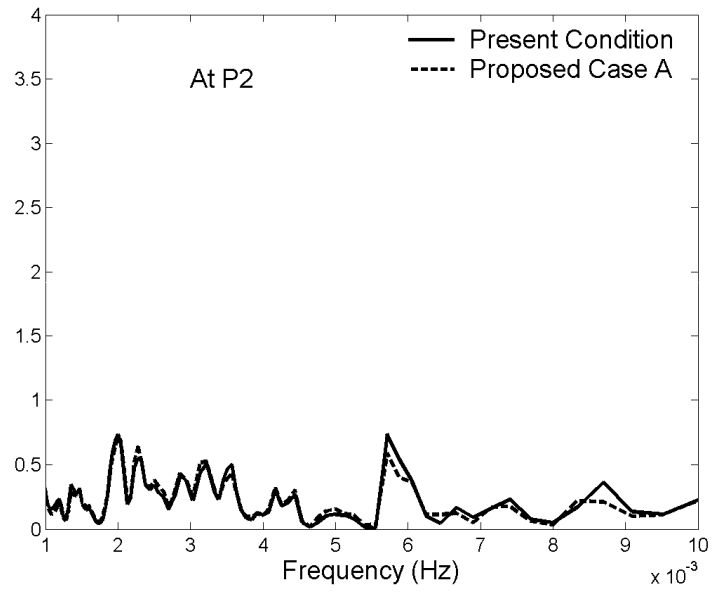


Figure 5.10 (b) Response curves at location P2 for present condition and after proposed Case A

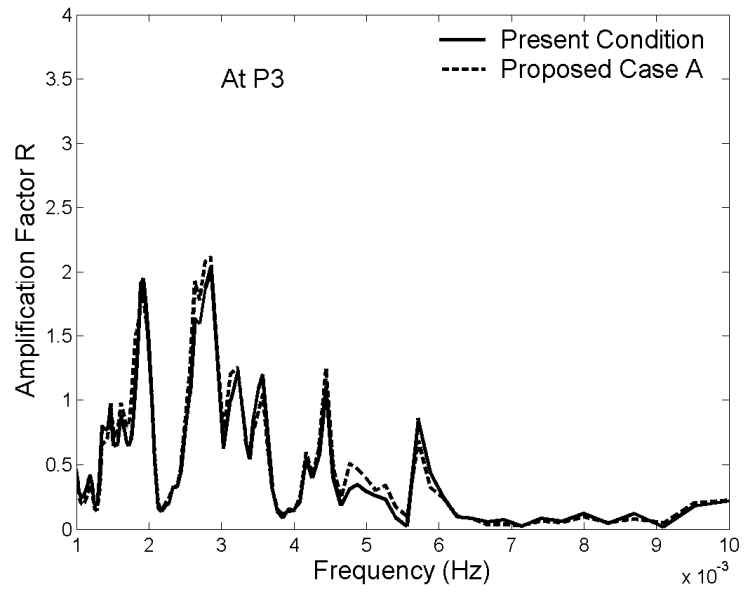


Figure 5.10 (c) Response curves at location P3 for present condition and after proposed Case A

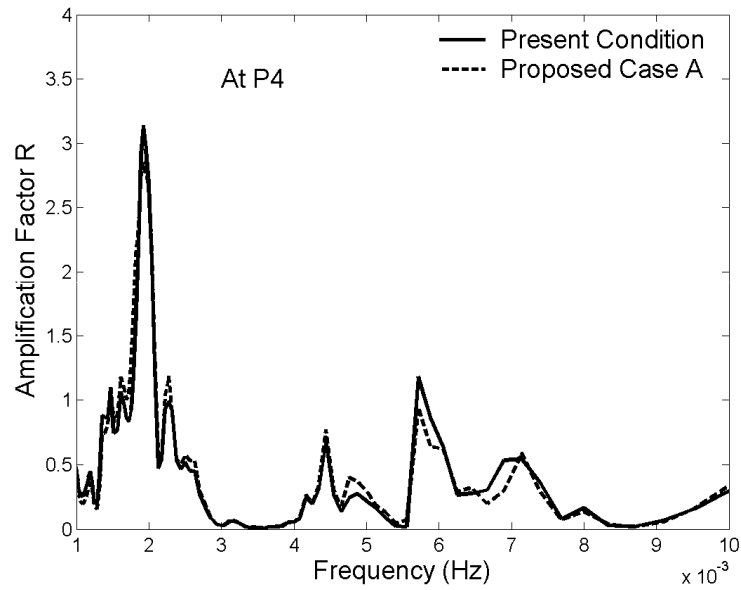


Figure 5.10 (d) Response curves at location P4 for present condition and after proposed Case A. The proposed modification strategies B and C (Case B and Case C) are going to elongate the breakwater which is closer to the harbor inlet with 100 meters but with different angles, as shown in Figure 5.11. Case B extends the breakwater along the original direction while Case C extends it with a 125° angle.



Figure 5.11 Layouts of Pohang new harbor with the modification Case B (left) and C (right)

The simulated response curves after the modification at those four locations are plotted in Figure 5.12. It can be seen that there is no significant difference produced by the two modification strategies. The reason is that the scale of the modification is too small compared with the whole harbor. The modification slightly increased the amplification factor at P1 because of the increased reflection from the elongated breakwater. The amplification factor at the mode with wave period of 170 sec (with frequency of 0.0058) at P2, P3 and P4 are slightly reduced. That is because the waves can more easily reach inside where P2, P3 and P4 located without the elongation of the breakwater. Overall the improvement in response characteristics is quite insignificant.

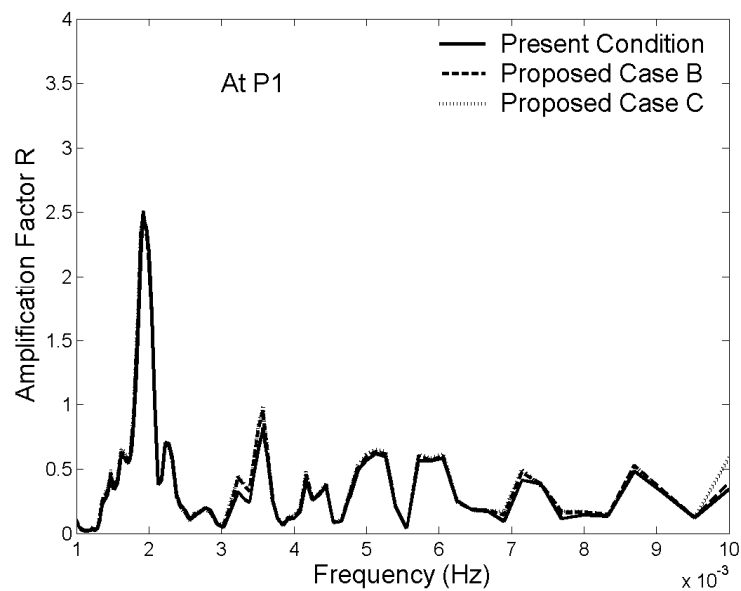


Figure 5.12 (a) Response curves at location P1 for present condition and after proposed Case B and C

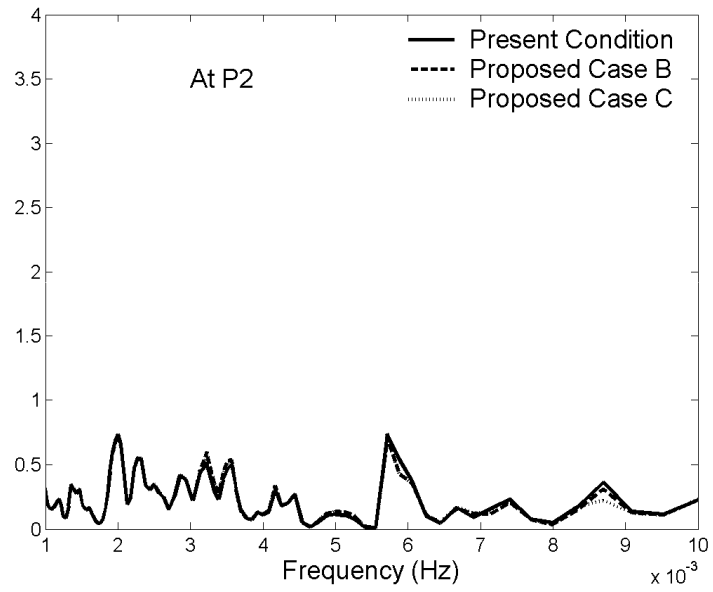


Figure 5.12 (b) Response curves at location P2 for present condition and after proposed Case B and C

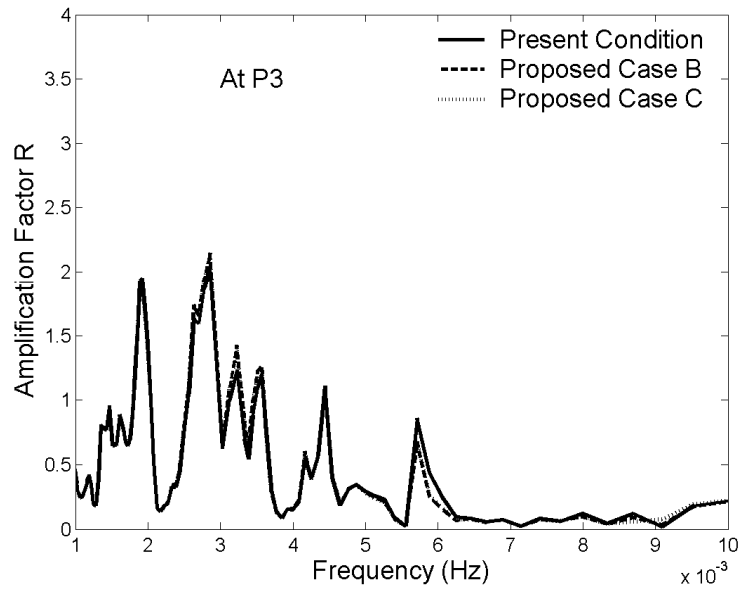


Figure 5.12 (c) Response curves at location P3 for present condition and after proposed Case B and C

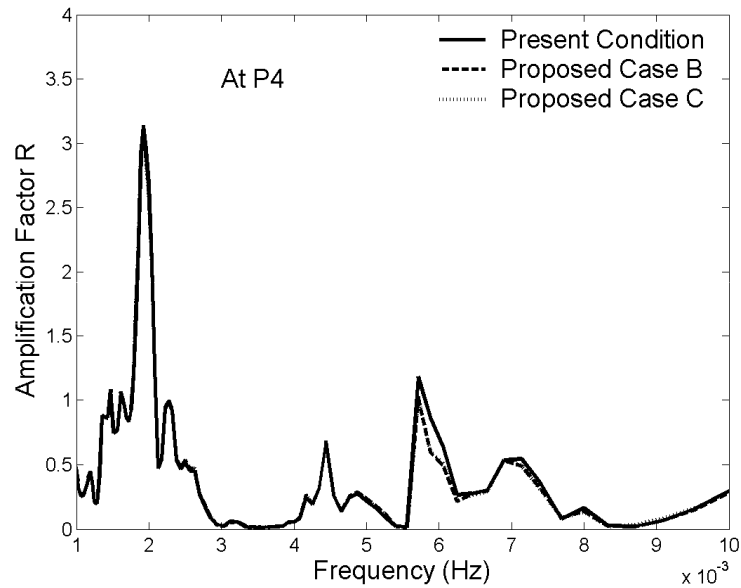


Figure 5.12 (d) Response curves at location P4 for present condition and after proposed Case B and C. Instead of expanding the outside enclosed jetty, the next strategy (so called Case D) is to build a 300 meter jetty attached to the original one as shown in Figure 5.13. The simulated results are plotted in Figure 5.14, in which strategy A is also included for comparison. It's seen that the simulated amplification factor for Case D is slightly smaller than Case A. Case D is more preferable since it needs much less construction compared with Case A.

However the construction of breakwater at the entrance might block the navigation channel, which is closely located to the existing enclosed jetty.

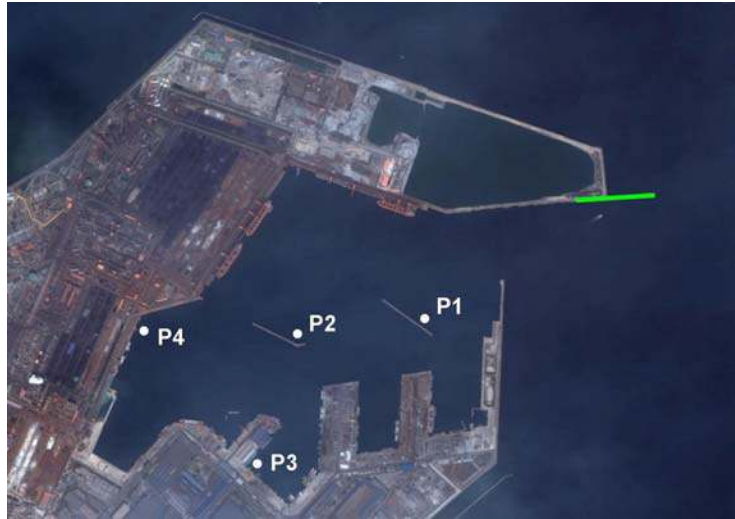


Figure 5.13 Layouts of Pohang new harbor with the modification Case D

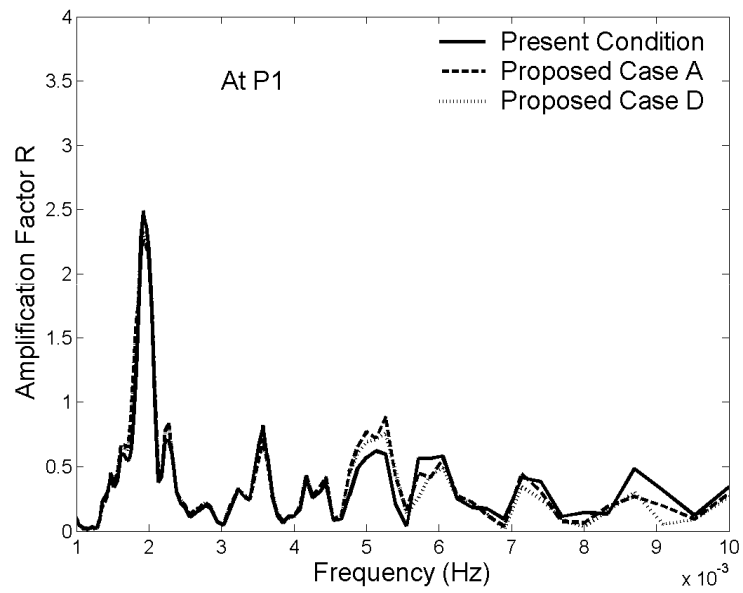


Figure 5.14 (a) Response curve at location P1 for present condition and after proposed Case A and D

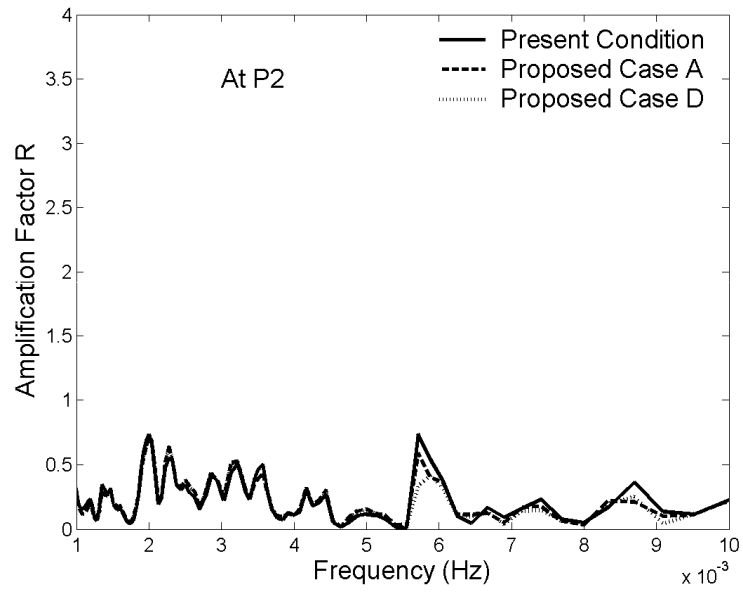


Figure 5.14 (b) Response curve at location P2 for present condition and after proposed Case A and D

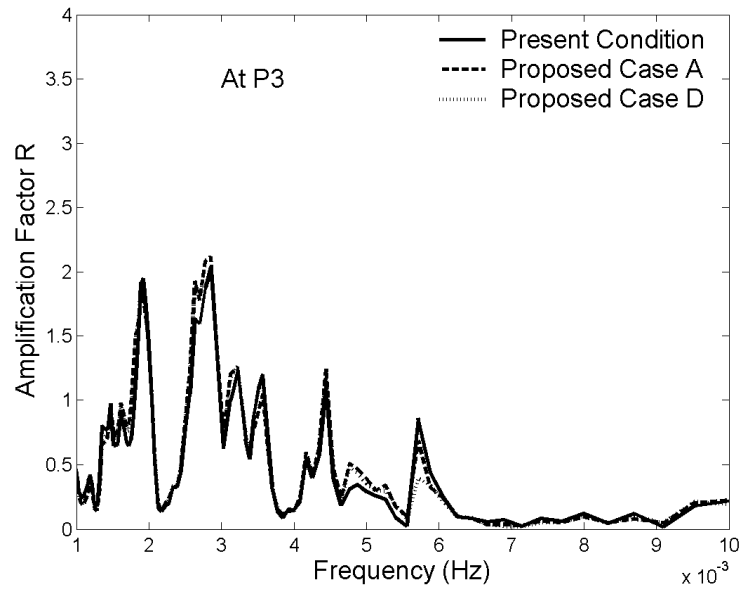


Figure 5.14 (c) Response curve at location P3 for present condition and after proposed Case A and D

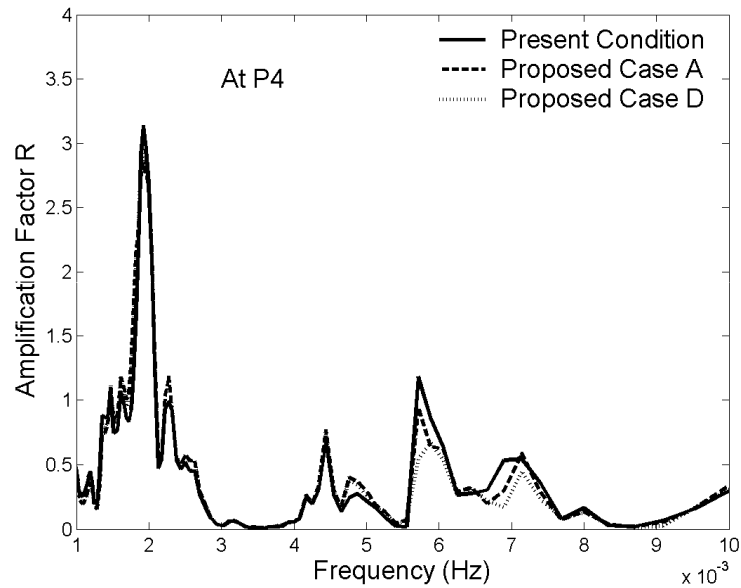


Figure 5.14 (d) Response curves at location P4 for present condition and after proposed Case A and D. The results of several proposed modifications have not shown significant improvement in response characteristics, since they have only slightly reduced the amplification factor. The combinations of Case A and B, A and C, D and B, D and C all have been studied and without exception the results are not shown significant improvement. It appears that simply elongating the jetty or breakwater is not the best way to solve the oscillation problem, especially when the length scale associated with the proposed modifications is still quite small.

Energy dissipater is another approach for reducing the resonant response. Considering the loading and unloading activities, the energy dissipaters were proposed to be constructed a little further away from those locations where big ships are moored (Case E), as shown in Figure 5.15. Two reflection coefficients for the energy dissipater are assumed, 0.8 and 0.5

respectively. The simulation response curves for present condition and Case E are plotted in Figure 5.16 for comparison. Additionally, the result for Case D is also included in Figure 5.16 for comparison.

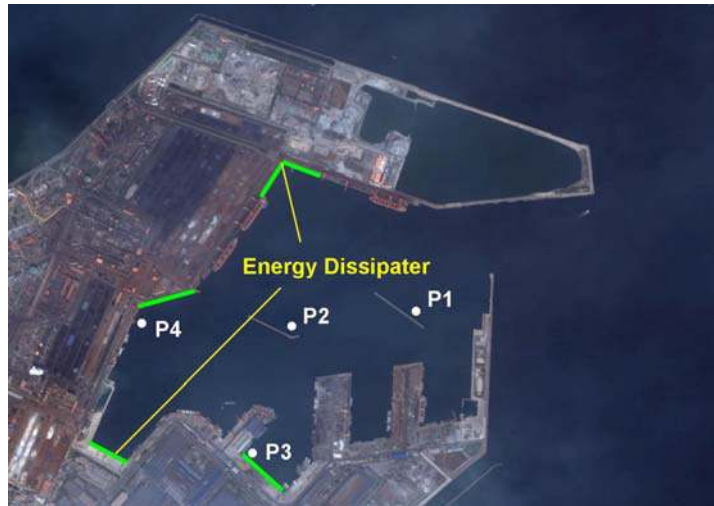


Figure 5.15 Layouts of Pohang new harbor with the modification Case E

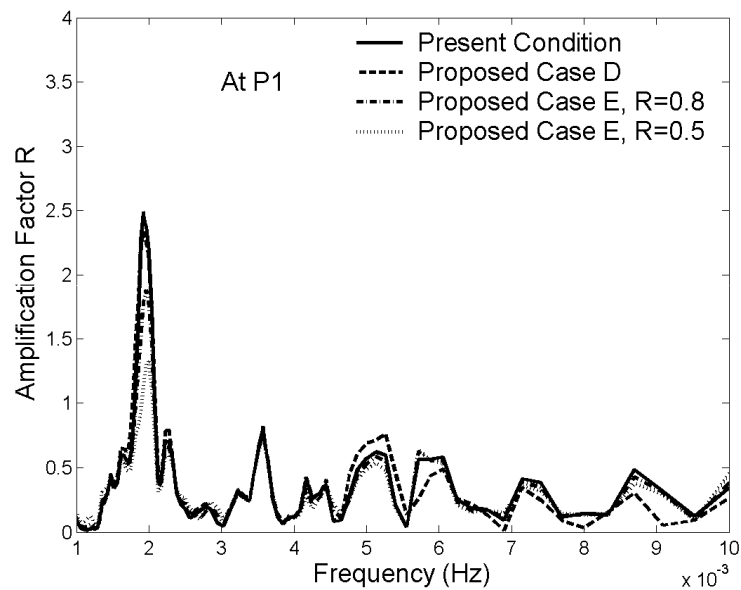


Figure 5.16 (a) Response curves at location P1 for present condition and after proposed Case D and E

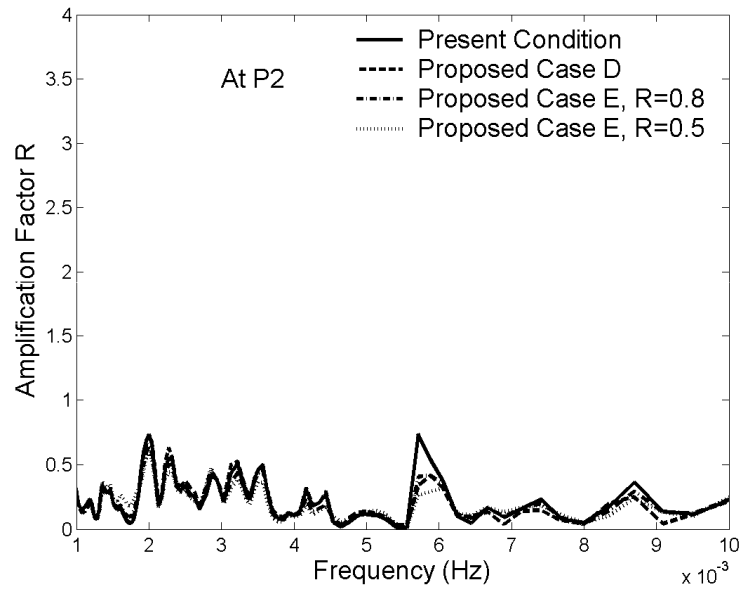


Figure 5.16 (b) Response curves at location P2 for present condition and after proposed Case D and E

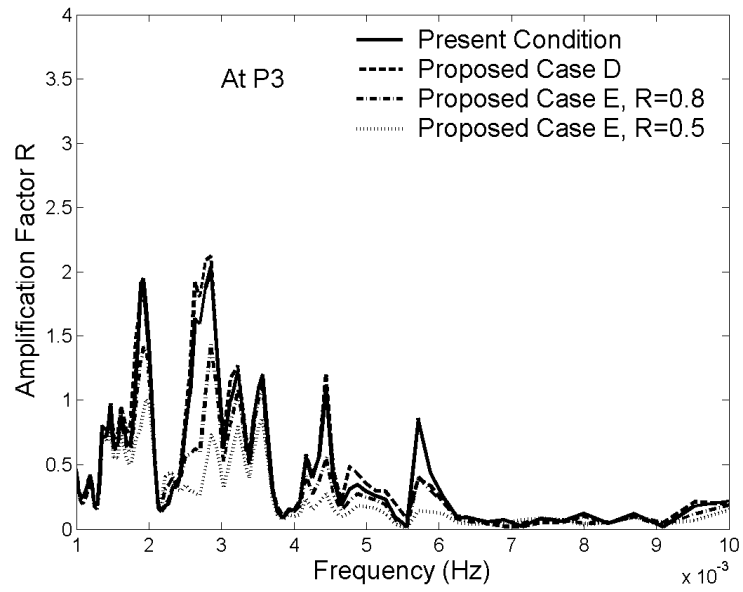


Figure 5.16 (c) Response curves at location P3 for present condition and after proposed Case D and E

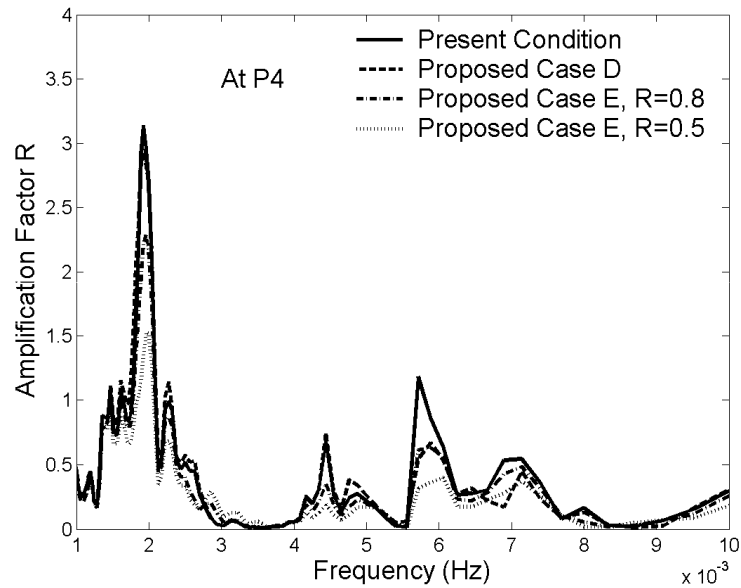


Figure 5.16 (d) Response curves at location P4 for present condition and after proposed Case D and E. The results shown in Figure 5.16 show that Case E with energy dissipaters gives slightly better by similar results with Case D when the reflection coefficient is 0.8. But the computation with reflection coefficient 0.5 significantly reduces the amplification factors for the important wave periods range from 100 sec to 200 sec, much better than that of Case D. Although to build and design energy dissipaters to achieve a reflection coefficient of 0.5 for long waves is not an easy task, the result is still very promising since it points the direction engineers must pursue to solve the oscillation problems. The energy dissipaters will be very effective to reduce the swell caused by relatively shorter waves, which might be the reason causing the downtime in Pohang New Harbor (Jeong, et al., 1997). Among the five strategies, the construction of energy dissipaters (Case E) is the most effective compared with all other proposed strategies.

5.2 Modeling of Hualien Harbor, Taiwan

5.2.1 Introduction

Hualien Harbor is located in the eastern coast of Taiwan and facing the Pacific Ocean (shown in Figure 5.17). It has a long history of harbor resonance problem induced by typhoons during the typhoon seasons. Excessive water surface oscillations in the harbor induce large ship motion, delay cargo loading or unloading activities, and damage ships and marine structures. In the last twenty years, on several occasions, harbor resonances have resulted in mooring lines being snapped, ships and dock facilities being severely damaged. To avoid damages as typhoons approached, the ships have been ordered to move out of the harbor!



Figure 5.17 Location of Hualien Harbor, Taiwan

5.2.2 Simulation of Present Condition at Hualien Harbor

The grid layout for the simulation of the present condition is shown in Figure 5.18 (left). The radius of the outside semicircle of the domain is about 4 kilometers. To provide clarity only the major grid blocks are shown. The present grid system contains 72,955 nodes and 17,823 elements. The bathymetry was obtained from the field survey data conducted by Harbor and Marine Technology Center (HMTC) and other organization commissioned for this region.



Figure 5.18 Air photos of Hualien Harbor, Taiwan with simulation domain imposed (left) and stations #8, #10, #17 and #22 indicated (right)

The model for the present condition is simulated and compared with the field data measured by HMTC during typhoon Tim in July 1994 (Su and Tsay, 2002). The model results and field data at key stations #22, #17, #8 and #10 are presented in Figure 5.19. It shows the amplification factor as a function of the incident wave period. It is seen that the comparison is quite good with respect to the resonant periods, the resonant bandwidth

and the peak amplification factors. The results clearly indicate that there exists a broadband of resonant response for wave periods between 100 sec and 160 sec and the computer model results appear to have captured the resonant modes correctly.

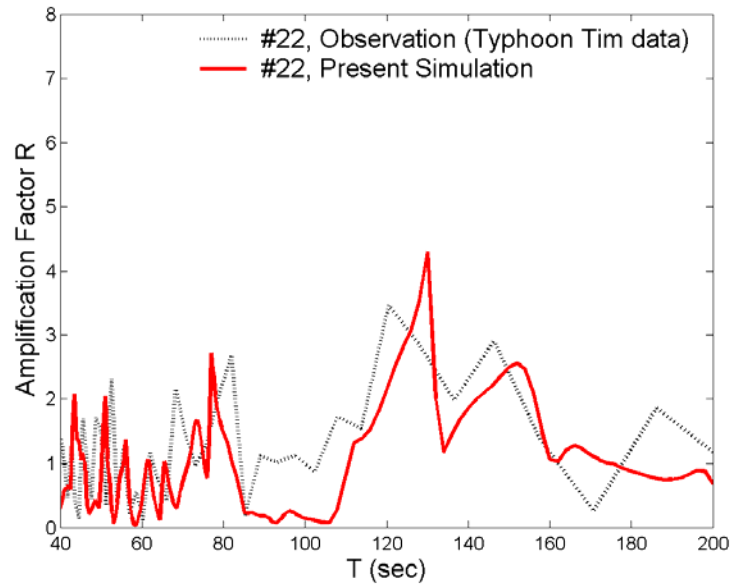


Figure 5.19 (a) Simulated response curve and the observed field data at stations #22

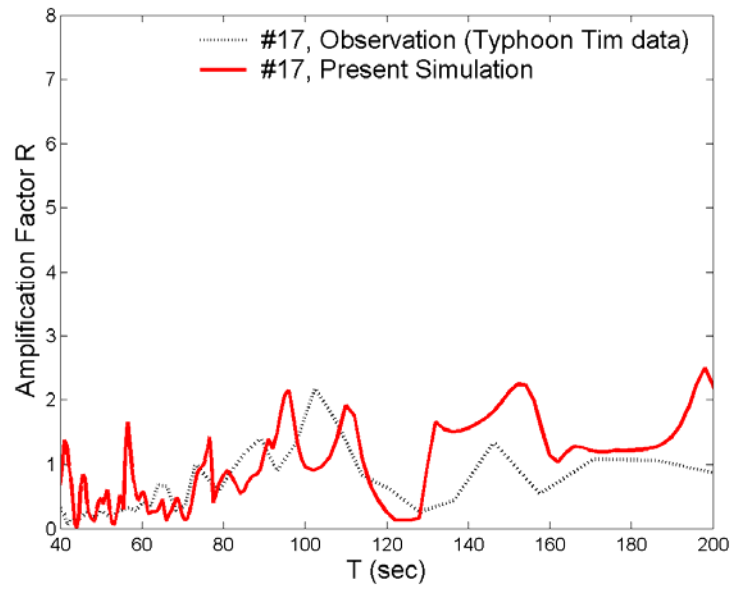


Figure 5.19 (b) Simulated response curve and the observed field data at stations #17

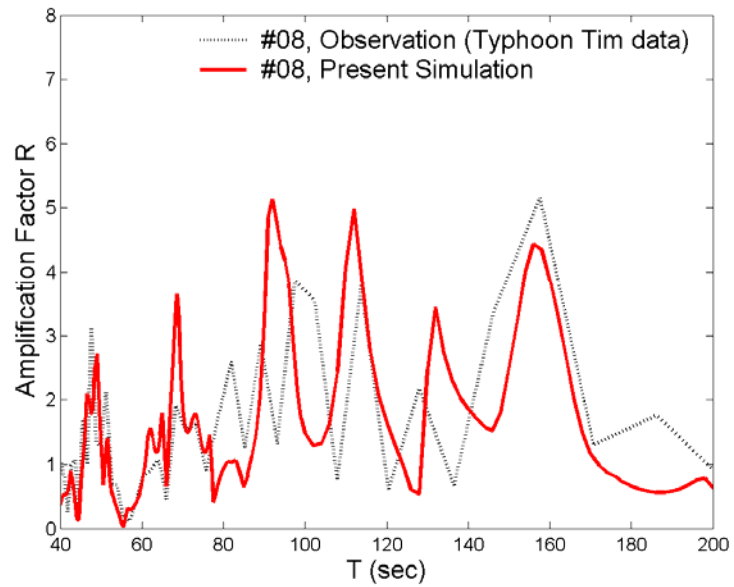


Figure 5.19 (c) Simulated response curve and the observed field data at stations #08

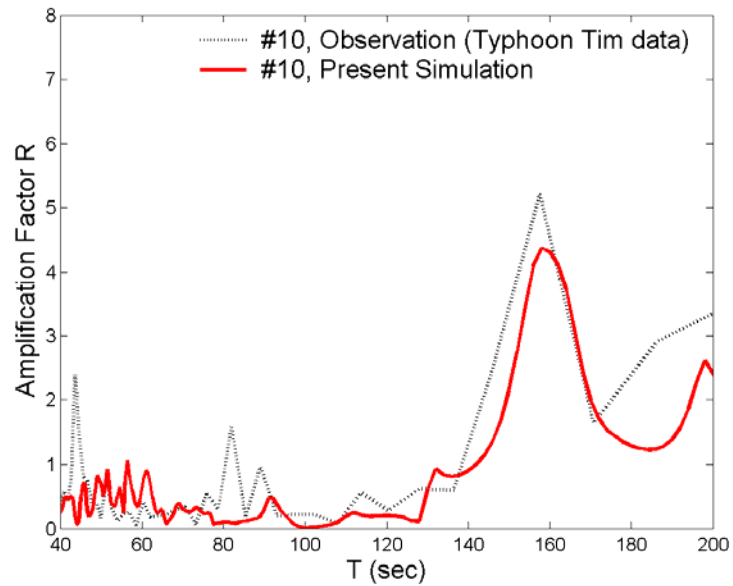


Figure 5.19 (d) Simulated response curve and the observed field data at stations #10

To minimize the harbor resonance problem in Hualien Harbor, several modification strategies were studied. The modification strategies and their effects will be discussed one by one in the following sections.

5.2.3 Modification Strategy 1: A Second Opening

The first modification strategy is to make a second opening at the east bank of inner harbor with a width of 150 m, as shown in Figure 5.20. The purpose of the second opening is to release some energy of the oscillation waves during the typhoon seasons, thus hopefully decrease the ship motions. The reflection coefficients used in the simulation are also indicated in Figure 5.20. The reflection coefficient is assigned to be

0.82 for the beach and 0.98 for the vertical wall boundaries inside and outside of the harbor.



Figure 5.20 Layout of the second opening modification strategy with reflection coefficients indicated. The simulated response curves for the second opening strategy at the four stations are shown in Figure 5.21. The observed data as well as the simulated results for the present condition are also included for the comparison. For station #17, the second opening results in lower amplification factors for wave periods from 140 sec to 160 sec, but higher amplifications for other wave periods. For station #22, the amplification factors increase significantly for the periods from 60 sec to 80 sec and from 120 to 160 sec. It's seen that the oscillation condition in the outer harbor basin becomes worse instead of getting better. For the inner harbor area at station #8, the oscillation condition gets worse for the wave period range from 120 sec to 140 sec and from 170 sec to 200 sec. There is also no significant improvement at station #10. The results show that the second opening does not help much in reducing the harbor resonance problem. It appears that for second opening, instead of releasing out the energy, more energy can propagate into the harbor

basin from the second opening, and the waves could be trapped at the outer harbor area, making the oscillation condition at station #22 worse than the present condition.

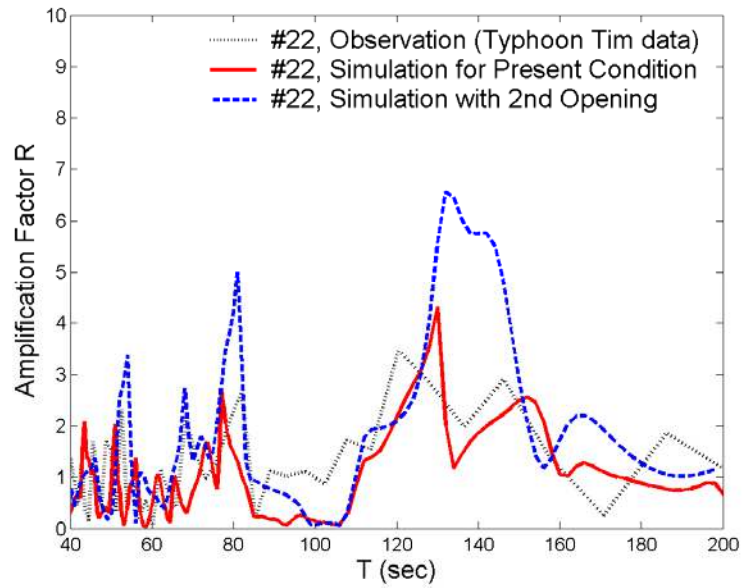


Figure 5.21 (a) Simulated response curves for the second opening modification strategy at stations #22

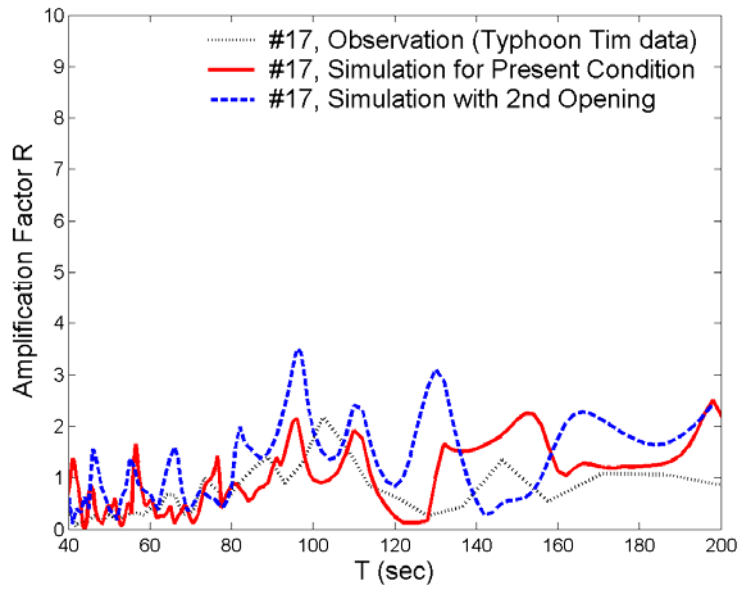


Figure 5.21 (b) Simulated response curves for the second opening modification strategy at stations #17

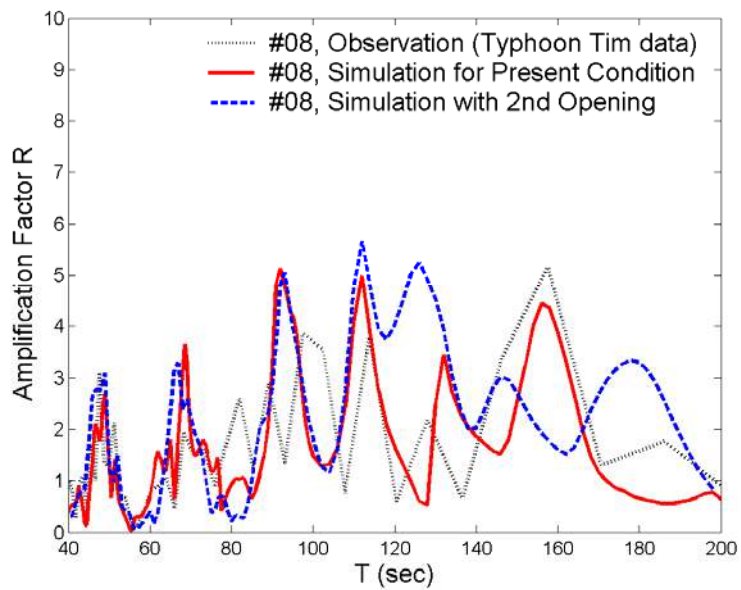


Figure 5.21 (c) Simulated response curves for the second opening modification strategy at stations #08

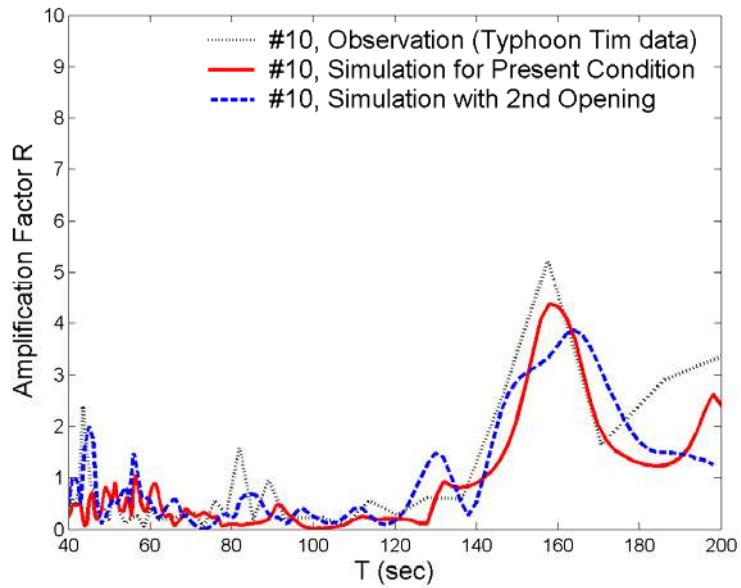


Figure 5.21 (d) Simulated response curves for the second opening modification strategy at stations #10

5.2.4 Modification Strategy 2: An Interior Gate

The second modification strategy is to build an interior gage in the navigation channel as shown in Figure 5.22. It was observed that normally before a typhoon arrives, the pre-generated waves already get in and generate large seiche motions inside the harbor. The purpose of the interior gate is to prevent the waves from propagating inside the inner harbor after all boats move inside before the forecasted typhoon approaches. The circled area with a diameter of 500 m is proposed to be dredged to 25 m deep for ship turning purpose. The reflection coefficients used in the simulation are also indicated in Figure 5.22.

The simulation result for the modification strategy of an interior gate is plotted in Figure 5.23. The inner harbor area is not included in the simulation domain because of the assumption that the inner area is much more protected because of the interior gate. It should be mentioned that there might be wind induced oscillation for the inner harbor area, but it's not the same mechanism as addressed in this study. From simulated response curves shown Figure 5.23, it's seen that the amplification factors decrease at both station #22 and #17 for wave period from 140 sec to 200 sec, but not for other wave periods. Since the wave periods that cause the large ship motions are not clearly studied, it's still hard to say that the modification strategy of an interior gate would work for the outer harbor. However, introduction of the interior gate will surely protect the inner harbor to some extent.

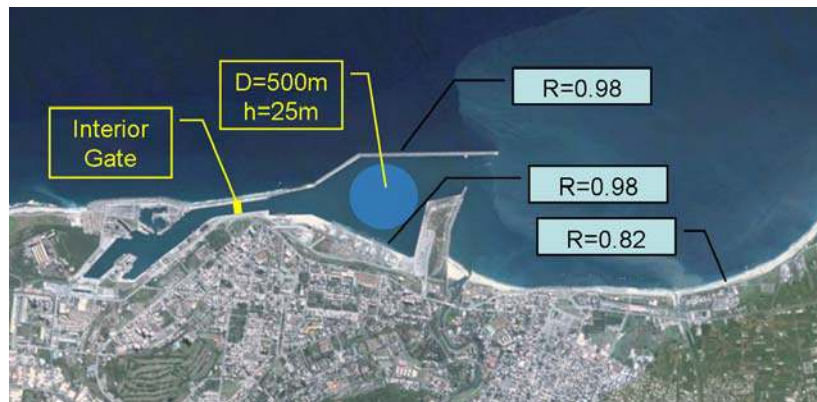


Figure 5.22 Layout of the interior gate modification strategy with reflection coefficients indicated

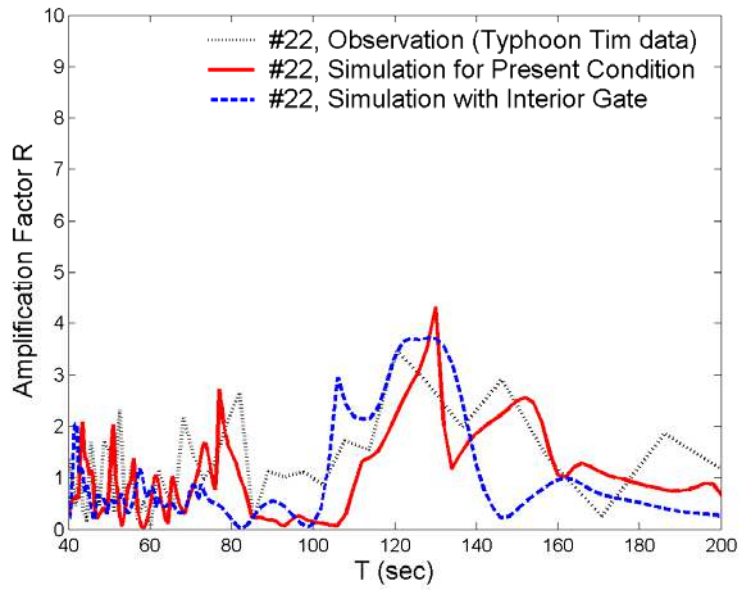


Figure 5.23 (a) Simulated response curves for the interior gate modification strategy at stations #22

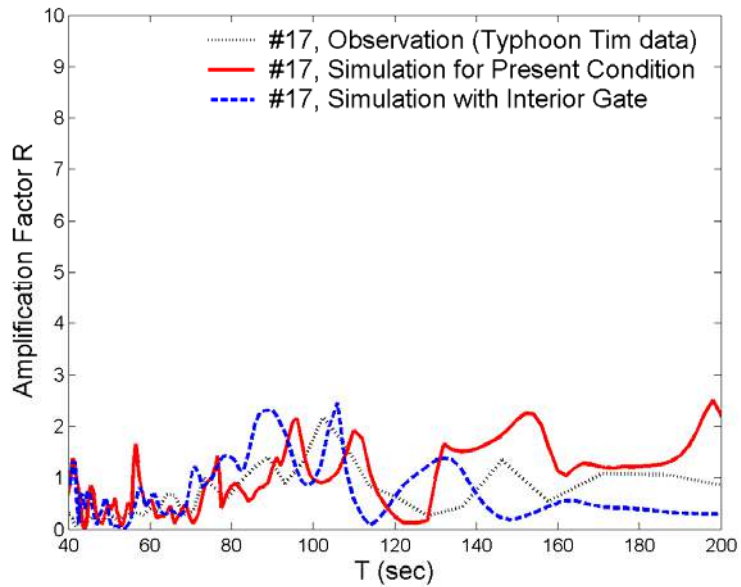


Figure 5.23 (b) Simulated response curves for the interior gate modification strategy at stations #17

5.2.5 Modification Strategy 3: Energy Dissipaters

The third modification strategy is to install energy dissipaters at the wharfs region in the outer harbor and at the head of the inner harbor as shown in Figure 5.24. The circular area with a 25 m depth for the ship turning is still proposed. The reflection coefficient of the energy dissipaters is assigned to be 0.8 in the computation.

The simulated response curves at the four stations are plotted in Figure 5.25. It is demonstrated by the response curves that the energy dissipaters effectively reduce the amplification factors in all the four stations presented. It seems that the energy dissipaters would work well if they can be properly designed and installed.



Figure 5.24 Layout of the energy dissipater modification strategy with reflection coefficients indicated

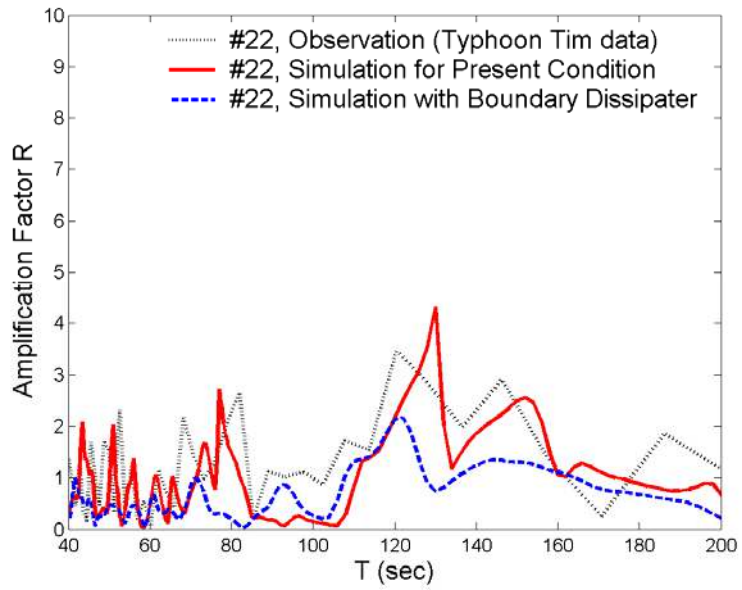


Figure 5.25 (a) Simulated response curves for energy dissipater modification strategy at station #22

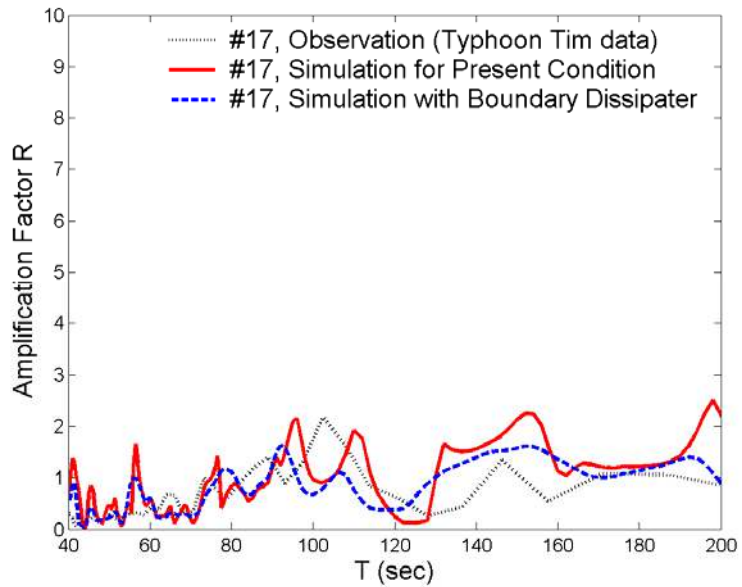


Figure 5.25 (b) Simulated response curves for energy dissipater modification strategy at station #17

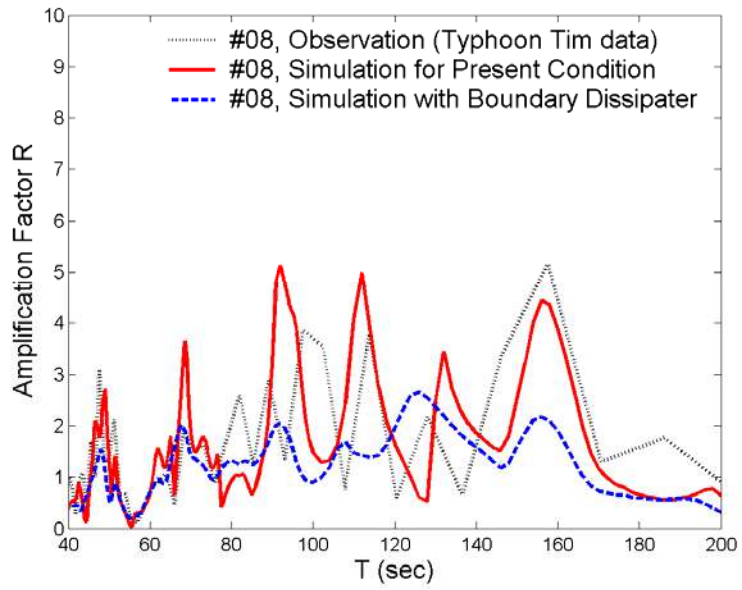


Figure 5.25 (c) Simulated response curves for energy dissipater modification strategy at station #08

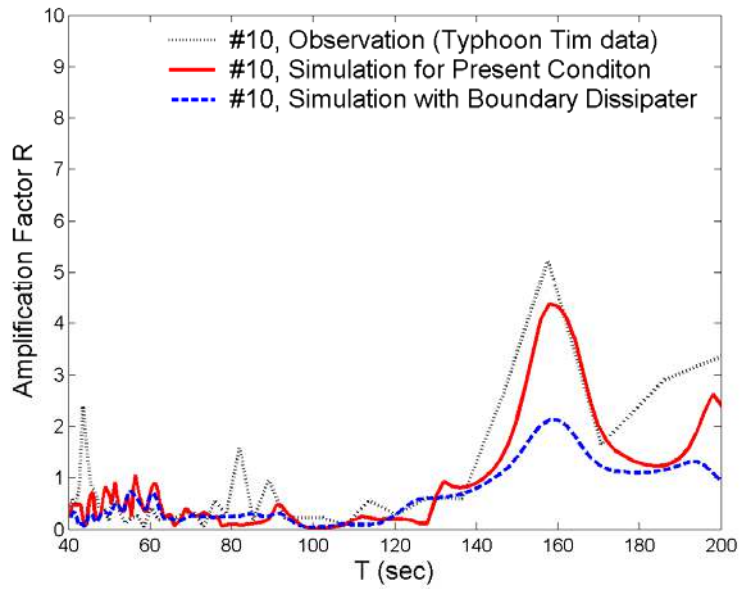


Figure 5.25 (d) Simulated response curves for energy dissipater modification strategy at station #10

5.2.6 Modification Strategy 4: Energy Dissipaters with A Jetty Added

The fourth modification strategy is to add a jetty at the entrance of the harbor based on the layout of previous modification strategy. The added jetty is proposed to act as a local resonator to dissipate the wave energy before it enters inside. The layout of this modification strategy is shown in Figure 5.26 with the reflection coefficients used in the simulation noted. The reflection coefficient is assigned to be 0.8 at the added jetty boundary.

The response curves at the four reference locations for this modification strategy are plotted in Figure 5.27. In order to clarify the effect of the added jetty, the simulation result for the modification strategy of energy dissipaters discussed in the previous section is also plotted for comparison. It's seen that the added jetty moderates the oscillation condition for wave period from 100 sec to 130 sec, but slightly increase the amplification factor for waves ranges from 140 sec to 200 sec. As a resonator, the added jetty only can help solving the problem for certain wave periods, but the troublesome wave periods have not been eliminated.

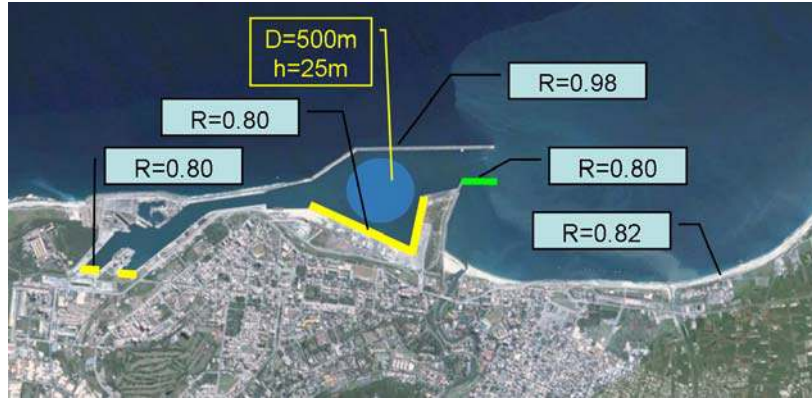


Figure 5.26 Layout of the added jetty modification strategy with reflection coefficients indicated

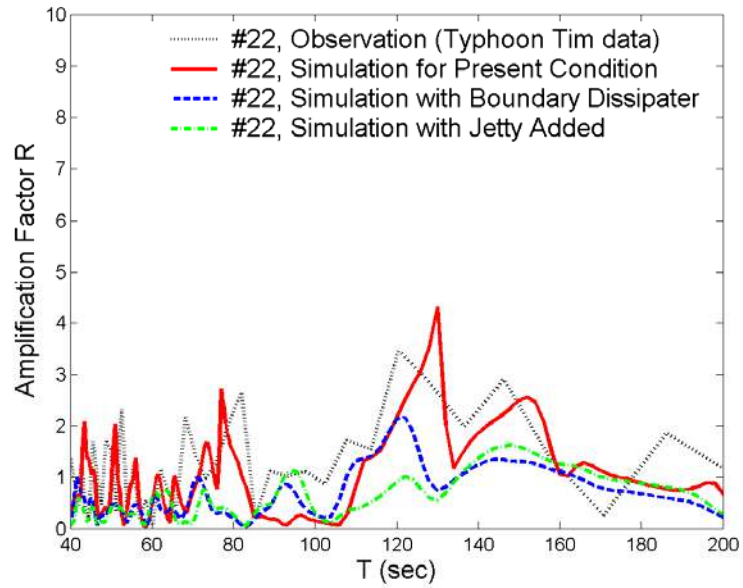


Figure 5.27 (a) Simulated response curves for the added jetty modification strategy at station #22

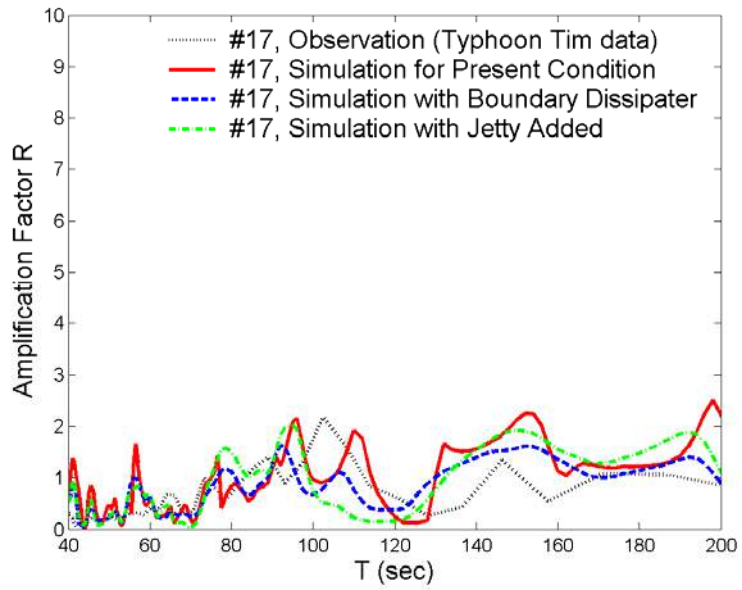


Figure 5.27 (b) Simulated response curves for the added jetty modification strategy at station #17

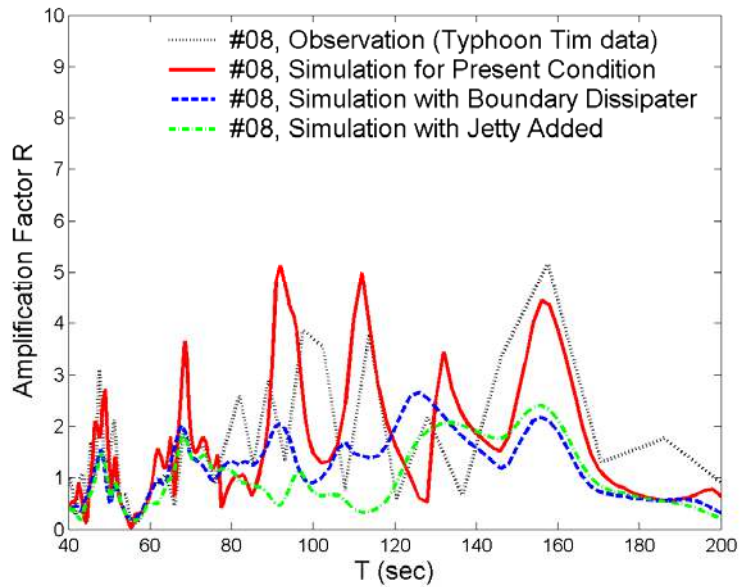


Figure 5.27 (c) Simulated response curves for the added jetty modification strategy at station #08

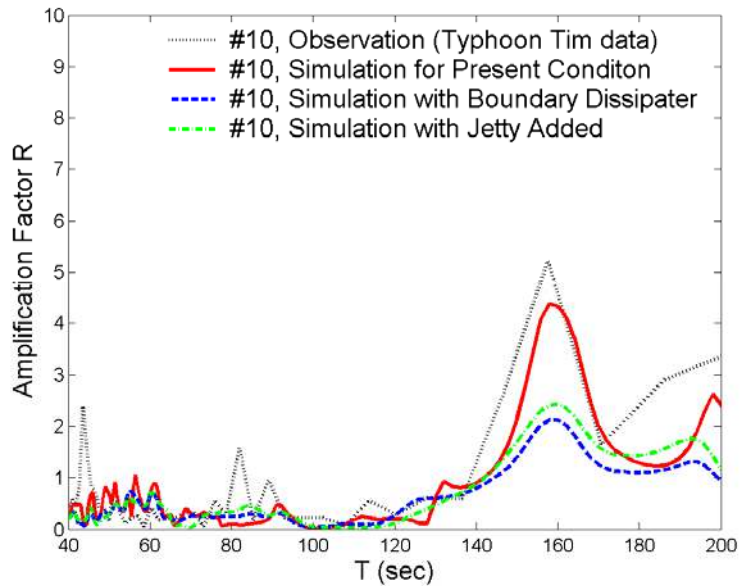


Figure 5.27 (d) Simulated response curves for the added jetty modification strategy at station #10. The energy dissipater and the added jetty appear to mitigate the oscillation problem to some degree. However the feasibility of those constructions needs to be evaluated. The energy dissipater at the wharfs in the outer harbor is not easy to construct since the platform was already filled with concrete and the energy dissipater would occupy a reasonable large space. The river located at south of the harbor contains the sewage outfall from Hualien city, which makes the jetty not that feasible since the circulation of the current would be blocked due to the jetty.

5.2.7 Modification Strategy 5: Combination of Energy Dissipaters

It seems the most possible location for energy dissipater is at the end of the harbor. There is enough space for constructing sloping boundary that permits wave overtopping. At the

eastern caisson breakwater, rubble mound energy dissipater can be constructed, and along the beach seawalls they were partly constructed and can be remedied more effectively in the future. The new modifications strategy is to try to combine the energy dissipaters at strategic boundaries, as shown in Figure 5.28.

The reflection coefficient for the concrete wall inside the harbor remains 0.98 in the simulation. But the reflection coefficient at the caisson breakwater boundary is assigned to be 0.8 and the one for the beach is 0.5. For the overtopping slope boundary at the end of the harbor, the amplification were tried to be 0.5 and 0.0 respectively in the simulation. The simulated results are illustrated in Figure 5.29. It can be seen that the combined energy dissipaters at the boundary significantly lower the amplification factors, no matter whether the reflection coefficient for the overtopping slope boundary is 0.5 or 0.0. Most of the amplification factors are lower than 1.0 except those at station #22 and #08 for wave periods about 120 sec, which are only slightly higher than 1.0. It can be expected that if the dissipaters are well constructed and can have reflection coefficients similar to those assigned in the computation, the oscillation problem in Hualien Harbor can be significantly reduced.

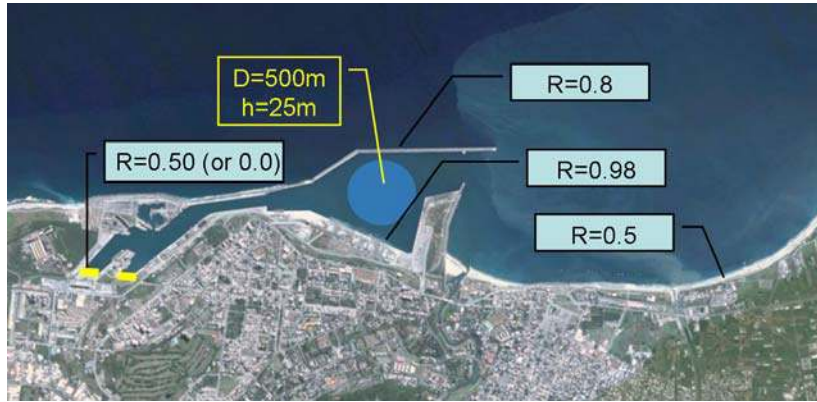


Figure 5.28 Layout of the combined energy dissipater modification strategy with reflection coefficients indicated

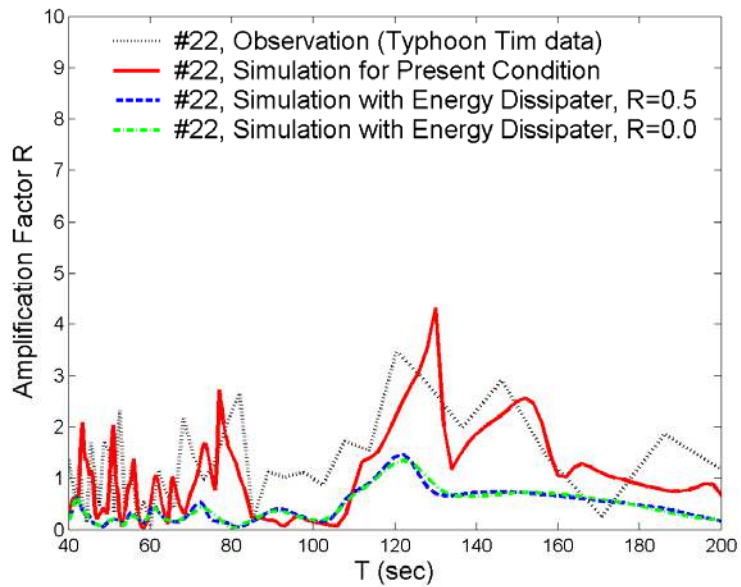


Figure 5.29 (a) Simulated response curves for the combined energy dissipater modification strategy at station #22

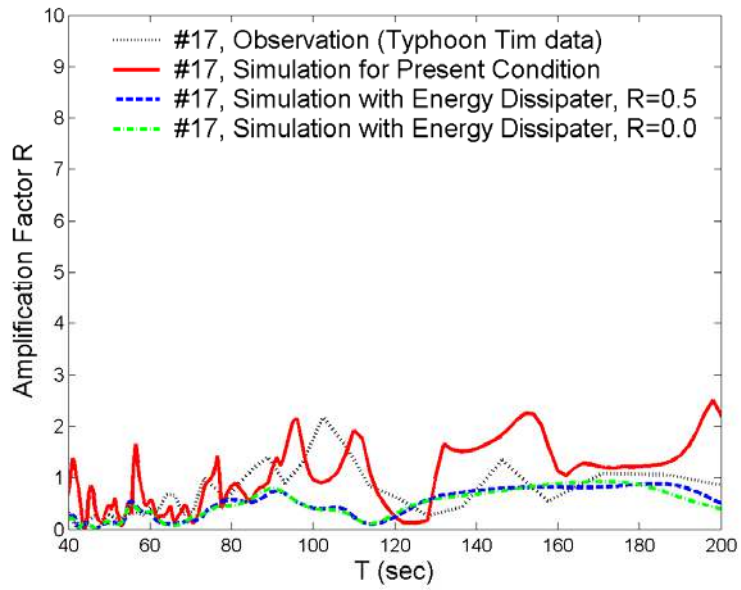


Figure 5.29 (b) Simulated response curves for the combined energy dissipater modification strategy at station #17

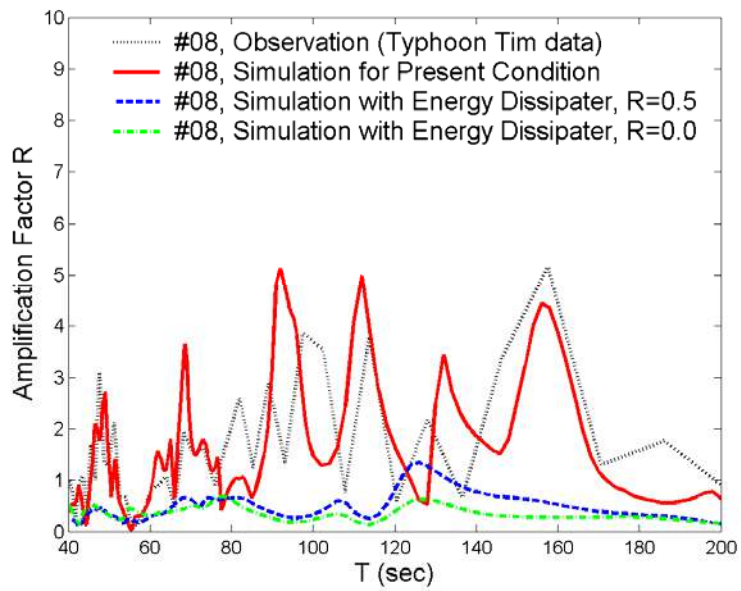


Figure 5.29 (c) Simulated response curves for the combined energy dissipater modification strategy at station #08

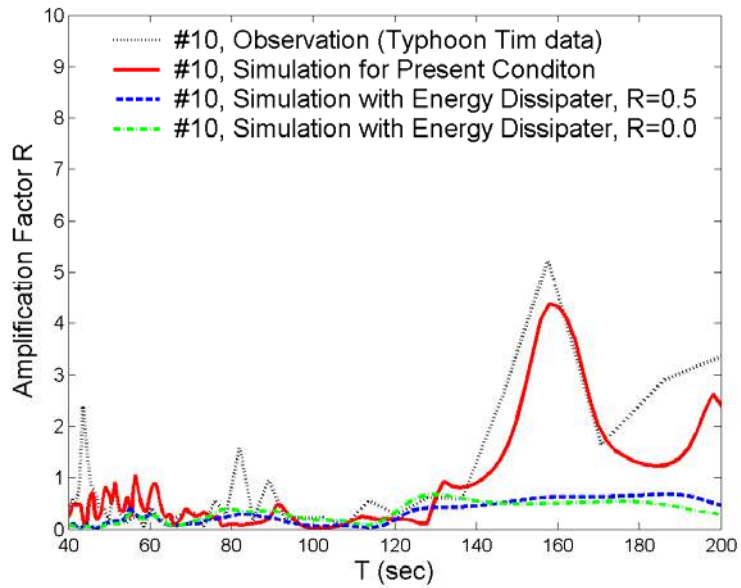


Figure 5.29 (d) Simulated response curves for the combined energy dissipater modification strategy at station #10

5.3 Summary

In this chapter the present FEM model were applied in the simulation for Pohang Harbor and Hualien Harbor to investigate the effectiveness of various modification strategies. The model was further proved to be a very effective engineering tool for harbor planning and design by the good agreement between the simulated results and the available field data.

For the modification strategy study, several conclusions can be drawn:

1. Without drastic changes in the harbor layout, the resonant modes could not be changed significantly. That's why the wave oscillation study is very important in the

harbor layout planning and design. Once the harbor is constructed, the resonant modes cannot be easily altered.

2. More openings for a harbor may not be a reasonable modification strategy since more energy could propagate inside instead of releasing them away from the harbor region.
3. Wave resonators only work for certain wave periods, and might result in a more severe condition for other wave periods.
4. An interior gage can partly solve the wave oscillation problem if the harbor has a narrow navigation channel such as the one in Hualien Harbor since it could block the wave coming from outside. But it is not feasible for a large harbor and it could cause inconvenience for ship moving if the seiche problem is induced by regular winter storms.
5. The boundary dissipaters could help reduce the amplification factor if they can be effectively designed and constructed. This could provide solutions for both Pohang Harbor and Hualien Harbor.

CHAPTER 6 CONCLUSION

As shown in previous chapters, wave induced oscillation in complicated harbor basins can be investigated effectively using the computer model. The good agreements, which are shown, between the prototype measurement and the computer simulation results further reinforce the validity of the computer modeling technique. To investigate wave oscillation problem in a harbor, using physical models will be very costly and time consuming. However, modifications in a numerical simulation can be done easily especially when the original grid is already generated. The computer model can serve as a very powerful and cost-effective engineering tool for harbor planning and design to provide a sheltered environment for moored ships and vessels.

This thesis study reveals several important conclusions. The first one is that the wave oscillation condition inside a harbor or bay is determined by the local plan form and the local bathymetry. Even for the same incoming waves generated in the same events, different harbors will respond to different resonant periods. Even in normal days, the oscillation exists in every harbor, but with relatively lower amplitude. When extreme events such as typhoons, tsunamis, winter storms, or other outer forces happen, the incoming wave energy from outside will significantly increase. This would invoke extreme wave oscillation as well as the induced strong currents inside a bay or harbor, resulting in horrible disasters.

The second point is that the wave oscillation condition inside a harbor won't be significantly changed without dramatically changing of the harbor layout. Once the harbor is constructed, the resonant modes are very difficult to eliminate. That's why the wave oscillation study is very important for harbor planning and design and should be performed before any construction or modification. Once the "troublesome wave periods" to the boats and facilities are determined either by the observation or by computer simulation, the harbor should be modified or designed to "avoid" them.

The third point is that wave oscillation can be diminished or shifted in some extent by modifying the harbor configuration although the oscillation modes are hard to be completely eliminated. As discussed in Chapter 5, different harbors might need different remedy strategies suitable to the local condition. Generally speaking, energy dissipaters should always be considered in harbor design and planning as long as they can be properly constructed. The total reflection condition at a vertical concrete wall could result in a worse oscillation condition.

The fourth point is that this study has a potential to help plan for the emergency response system. Since the wave oscillation characteristics are local response, they will amplify the incident waves in a predictable manner. As long as there exists an observation station somewhere outside, the unusual wave motions can be detected and sent back to the control center. Then the amplification of oscillation waves and the correspondingly induced currents can be predicted.

REFERENCES

- Aida, I., Hatori, T., Koyama, M. (1972). "Long-period waves in the vicinity of Onagawa Bay (I) – field measurements in Onagawa and Okachi Bays." *Journal of the Oceanographical Society of Japan*, Vol. 28, 207-219.
- Aida, I. (1974). "Long-period waves in the vicinity of Onagawa Bay (II) – two-dimensional pattern of bay oscillations." *Journal of the Oceanographical Society of Japan*, Vol. 30, 34-41.
- Aida, I., Koyama, M., Date, D., Sakashita, S. (1975). "Long-period waves in the vicinity of Onagawa Bay (III) – time change of the seiche characteristics in the bay." *Journal of the Oceanographical Society of Japan*, Vol. 31, 61-70.
- Athanassoulis, G.A. and Belibassakis, K.A. (1999). "A consistent coupled-mode theory for the propagation of small amplitude water waves over variable bathymetry regions." *J. Fluid Mech.*, 389, 275-301.
- Balas, L. and Inan, A. (2002). "A numerical model of wave propagation on mild slopes." *Journal of Coastal Research*, Special Issue 36, 16-21.
- Belibassakis, K.A., Athanassoulis, G.A., Gerostathis, T.P. (2001). "A couple-mode model for the refraction-diffraction of linear waves over steep three-dimensional bathymetry." *Appl. Ocean Res.*, 23, 319-336.
- Bendat, J.S. and Piersol, A.G. (2000). *Random data analysis and measurement procedures*, Third Edition. A Wiley-Interscience Publication, JOHN WILEY & SONS, INC.
- Berkhoff, J.C.W. (1972). "Computation of combined refraction-diffraction." *Proc. 13th Coast. Eng. Conf.*, ASCE, New York, N.Y., 471-490.
- Booji, N. (1983). "A note on the accuracy of the mild slope equation." *Coastal Engineering*, 7, 191-203.
- Bowers, E.C. (1977). "Harbor resonance due to set-down beneath wave groups." *J. Fluid Mech.*, Vol. 79, 71-92.

- Chamberlain, P.G. and Porter, D. (1995). "The modified mild slope equation." *J. Fluid Mech.*, 291, 393-407.
- Chandrasekera, C.N., and Cheung, K.F. (1997). "Extended linear refraction-diffraction model." *J. Waterw. Port Coastal Ocean Eng.*, 123, 280-286.
- Chandrasekera, C.N., and Cheung, K.F. (2001). "Linear refraction-diffraction model for steep bathymetry." *J. Waterw. Port Coastal Ocean Eng.*, 127, 161-170.
- Chen, H.S. (1986). "Effects of bottom friction and boundary absorption on water wave scattering." *Applied Ocean Research*, Vol. 8, No. 2, 99-104.
- Chen, H.S. and Mei, C.C. (1974). "Oscillations and waves forces in an offshore harbor." *Report No. 190*, Parsons Laboratory, MIT.
- Chiang, W.L. and Lee, J.J. (1982). "Simulation of large scale circulation in harbors." *J. of Waterw., Port, Coastal and Ocean Division*, ASCE, Vol. 108, No. 1, pp. 17-31.
- Demirbilek, Z. and Panchang, V. (1998). "CGWAVE: a coastal surface water wave model of the Mild Slope Equation." *Technical Report CHL-98-xx*, Prepared for Headquarters, U.S. Army Corps of Engineers.
- Ehrenmark, U.T. and Williams, P.S. (2001). "Wave parameter tuning for the application of the Mild-Slope Equation on steep beaches and in shallow water." *Coastal Engineering*, Vol. 42, 17-34.
- Ganaba, M., Wellford, L.C., Lee, J.J. (1984). "Finite element methods for boundary layer modeling with application to dissipative harbor resonance problem." Chapter 15 of *Finite Elements in Fluid* – Vol 5, pp. 325-346, John Wiley & Sons.
- Garcies, M., Gomis, D., Monserrat, S. (1996). "Pressure-forced seiches of large amplitude in inlets of the Balearic Islands." *Journal of Geophysical Research*, Vol. 101. No. C3, pp. 6,453-6,467.
- Garrett, C. (1972). "Tidal resonance in the Bay of Fundy and Gulf of Maine." *Nature*, 238, pp. 441-443.
- Garrett, C. (1974). "Normal resonance in the Bay of Fundy and Gulf of Maine." *Can. J. Earth Sci.*, Vol. 4, pp. 549-556.

- Giese, G.S., Chapman, D.C., Black, P.G., Fornshell, J.A. (1990). "Causation of large-amplitude coastal seiches on the Caribbean coast of Puerto Rico." *Journal of Physical Oceanography*, Vol. 20, pp. 1449-1458.
- Giese, G.S. and Hollander, R.B. (1987). "The relationship between coastal seiches at Palawan Island and tide-generated internal waves in the Sulu Sea." *Journal of Geophysical Research*, Vol. 92, No. C5, pp. 5151-5156.
- Giese, G.S., Hollander, R.B., Fancher, J.E., Giese, B.S. (1982). "Evidence of coastal seiche excitation by tide-generated internal solitary waves." *Geophysical Research Letter*, Vol. 9, No. 12, pp. 1305-1308.
- Gilmour, A.E. (1990). "Response of Wellington Harbor to the tsunamis of 1960 and 1964." *New Zealand Journal of Marine and Freshwater Research*, Vol. 24, 229-231.
- Girolamo, P.D. (1996). "An experiment on harbour resonance induced by incident regular waves and irregular short waves." *Coastal Engineering*, Vol. 27, pp. 47-66.
- Gomis, D., Monserrat, S., Tintoré, J. (1993). "Pressure-forced seiches of large amplitude in inlets of Balearic Islands." *Journal of Geophysical Research*, Vol. 98, No. C8, pp. 11,437-14,445.
- Greenberg, D.A. (1979). "A numerical model investigation of tidal phenomena in the Bay of Fundy and Gulf of Maine." *Marine Geodesy*, Vol. 2, No. 2, pp. 161-187.
- Grilli, S.T., Skourup, J., Svendsen, I.A. (1989). "An efficient boundary element method for nonlinear water waves." *Eng. Analysis with Boundary Elements*, 6(2), 97-107.
- Heath, R.A. (1982). "Generation of 2-3-hour oscillations on the east coast of New Zealand." *New Zealand Journal of Marine and Freshwater Research*, Vol. 16, 111-117.
- Horikawa, K. and Nishimura, H. (1970). "On the function of tsunami breakwaters." *Coastal Eng. J.* 13, 103-112.
- Houston, J.R. (1978). "Interaction of tsunamis with the Hawaiian Islands calculated by a finite element numerical model." *Journal of Physical Oceanography*, Vol.8, No.4, 93-102.
- Houston, J.R. (1980). "Combined refraction and diffraction of short wave using the finite element method." *Applied Ocean Research*, Vol. 3, No. 4, 163-170.

- Huang, N.E., Shih, H.H., Shen, Z., Long, S.R., Fan, K.L. (2000). "The ages of large amplitude coastal seiches on the Caribbean coast of Puerto Rico." *Journal of Physical Oceanography*, Vol. 20, pp. 2001-2012.
- Hwang, L.S. and Tuck, E.O. (1970). "On the oscillations of harbors of arbitrary shape." *Journal of Fluid Mechanics*, Vol. 42, 447-464.
- Ippen, A.T. and Goda, Y. (1963). "Wave induced oscillations in harbors: the solution for a rectangular harbor connected to the open-sea." *Report No. 59*, Hydrodynamics Laboratory, M.I.T.
- Ito, Y. (1970). "Head loss at tsunami-breakwater opening." *Proceedings of the 12th ASCE Conference on Coastal Engineering*, 2,123-2,131.
- Jeong, W.M., Oh, S.B., Chae, J.W., Kim, S.I. (1997). "Analysis of the wave induced downtime at Pohang new harbor." *J. of Korean Society of Coastal and Ocean Engineers*, Vol. 9, No. 1, pp.24-34.
- Jonsson, I.G. and Carlsen, N.A. (1976). "Experimental and theoretical investigations in an oscillatory turbulent boundary layer." *Journal of Hydraulic Research*, 14, 45-60.
- Kim, J.W., and Bai, K.J. (2004). "A new complementary Mild Slope Equation." *J. Fluid Mech.*, 511, 25-40.
- Kravtchenko, J. and McNown, J.S. (1955). "Seiche in rectangular ports." *Quarterly of Applied Mathematics*, Vol. 13, 19-26.
- Kulikov, E.A. and Rabinovich, A.B. (1996). "The landslide tsunami of November 3, 1994, Skagway Harbor, Alaska." *J. Geophys. Res.*, Vol. 101, 6,609-6,615.
- Kwak, M., Jeong, W., Pyun, C., Xing, X.Y., Lee, J.J. (2008). "Computer simulation of Pohang New Harbor for seiche reduction." *Proceedings of ICCE 2008*.
- Lee, C. and Yoon, S.B. (2004). "Effect of higher-order bottom variation terms on the refraction of water waves in the extended mild slope equation." *Ocean Engineering*, 31, 865-882.
- Lee, J.J. (1969). "Wave induced oscillations in harbors of arbitrary shape." *Report No. KH-R-20*, W.M. Keck Laboratory, Caltech (266 pages).

- Lee, J.J. (1971). "Wave-induced oscillations in harbors of arbitrary geometry." *J. Fluid Mech.* Vol. 45, Part 2, 375-394.
- Lee, J.J., Chang, C., Zhuang, F. (1992). "Interactions of transient nonlinear waves with coastal structures." *23rd Conference on Coastal Engineering.*
- Lee, J.J., and Lai, C.P. (2006). "Assessing impacts of tsunamis on Taiwan's and China's southeast coastlines." *Proceedings of ICCE 2006*, Sept 2-8, 2006, San Diego.
- Lee, J.J., Lai, C.P., Li, Y. (1998). "Application of computer modeling for harbor resonance studies of Long Beach & Los Angeles harbor basins." *Proceedings of 26th International Conference on Coastal Engineering*, ASCE, 1,196-1,209.
- Lee, J.J. and Raichlen, F. (1972). "Oscillations in harbors with connected basins." *Journal of Waterways, Ports, Coastal and Ocean Engineering Division*, ASCE, Vol. 98, No. WW3, 311-332.
- Lee, J.J. and Xing, X.Y. (2008). "Chapter 25: Computer modeling for harbor planning and design." *Handbook of Coastal and Ocean Engineering*. Edited by Young C. Kim, World Scientific Publishing Company.
- Lee, J.J., Xing, X.Y., Magoon, T. (2008). "Uncovering the basin resonance at Crescent City Harbor region." *Proceedings of ICCE 2008.*
- Lejeune, A., Lejeune, M., Sahloul, M. (1989). "Wave plan computation method in study of the Calvi Bay erosion in Corsica, France." *International Journal for Numerical Methods in Engineering*, Vol. 27, 71-85.
- Leendertse, J.J. (1967). "Aspects of a computational model for long-period wave propagation." *Memo KM-5294-PR RAND Corp.*, Santa Monica, CA.
- Lepelletier, T.G. (1980). "Tsunamis - harbor oscillations induced by nonlinear transient long waves." *Report No. KH-R-41*, California Institute of Technology.
- Lepelletier, T.G. and Raichlen, F. (1987). "Harbor oscillations induced by non-linear transient long waves." *J. of Waterw., Port, Coast. And Ocean Engineering*, ASCE, 113(4), 381-400.

- Magne, R., Belibassakis, K.A., Herbers, T.H.C., Ardhuin, F., O'Reilly, W.C., Rey, V. (2007). "Evolution of surface gravity waves over a submarine canyon." *J. Geophys. Res.*, Vol. 112, C01002.
- Magoon, O.T. (1965). "Structural damage by tsunamis." *Coastal Engineering, Santa Barbara Specialty Conference*, ASCE, pp.35-68.
- Marmer, H.A. (1922). "Tides in the Bay of Fundy." *Geographical Review*, Vol. 12, No. 2, pp. 195-205.
- Massel, S.R. (1993). "Expanded refraction-diffraction equation for surface waves." *Coastal Engineering*, 19, 97-126.
- Massel, S.R. (1995). *Ocean Surface Waves: Their Physics and Prediction*. World Scientific Publication, Singapore.
- McNown, J.S. (1952). "Waves and seiche in idealized ports." *Gravity Wave Symposium, National Bureau of Standards Circular 521*.
- Mei, C.C. (1999). "Mild-slope approximation for long waves generated by short waves." *Journal of Engineering Mathematics*, Vol. 35, 43-57.
- Mei, C.C. and Agnon, Y. (1989). "Long-period oscillations in a harbor induced by incident short waves." *J. Fluid Mech.*, Vol. 208, 595-608.
- Mei, C.C., Stiassnie, M., Yue, D.K. (2005). *Theory and applications of ocean surface waves*. World Scientific Publishing Company.
- Metzner, M., Gade, M., Hennings, I., Rabinovich, A.B. (2000). "The observation of seiches in the Baltic Sea using a multi data set of water levels." *Journal of Marine Systems*, 24, 67-84.
- Miles, J.W. and Munk W. (1961). "Harbor paradox." *Journal of the Waterways and Harbor Division*, ASCE, Vol. 87, 111-130.
- Miles, J.W. and Lee, Y.K. (1975). "Helmholtz resonance of harbors." *J. Fluid Mech.*, Vol. 67, Part 3, 445-464.
- Ministry of Construction (1987). *The report of wave measurement and numerical experiment in Pohang new harbor*, 108-116.

- Morison, M.L. and Imberger, J. (1992). "Water-level oscillations in Esperance Harbor." *Journal of Waterway, Port, Coastal, and Ocean Engineering*, Vol. 118, No. 4, pp. 352-367.
- Okihiro, M. and Guza, R.T. (1996). "Observations of seiche forcing and amplification in three small harbors." *Journal of Waterway, Port, Coastal, and Ocean Engineering*, Vol. 122, No. 5, pp. 232-238.
- Okihiro, M., Guza, R.T., Seymour, R.J. (1993). "Excitation of seiche observed in a small harbor." *J. Geophys. Res.*, Vol. 98, No. C10, 18201-18211.
- O'Hare, T.J. and Davies, A.G. (1992). "A new model for surface wave propagation over undulating topography." *Coastal Engineering*, 18, 251-266.
- Powers, D.M. (2005). *The Raging Sea: The Powerful Account of the Worst Tsunami in U.S. History*. Kensington Publishing Corporation.
- Proudman, J. (1953). *Dynamical oceanography*, Methuen-Wiley, London 409 pp.
- Raichlen, F. (1965). "Long period oscillations in basins of arbitrary shapes". Chapter 7, *Coastal Engineering, Santa Barbara Speciality Conference*, 115-145.
- Raichlen, F. (1966). "Harbor resonance". *Estuary and Coastline Hydrodynamics*. Edited by A.T. Ippen, McGraw Hill Book Company, New York, 218-340.
- Raichlen, F. and Lee, J.J. (1992). "Oscillation of Bays, Harbors, and Lakes". Chapter 13, *Handbook of Coastal and Ocean Engineering*. Gulf Publishing Company. Edited by Herbich, J.B.
- Rao, D.B. (1968). "Natural oscillations of the Bay of Fundy." *J. Fish. Res. Bd. Can.*, Vol. 25, pp. 1097-1114.
- Su, C.H. and Tsay, T.K. (2002). "Numerical simulation on harbor oscillations in Haw-Lien harbor." *Report NO. MOTC-IOT-IHMT-NB9001-1*. Institute of Harbor & Marine Technology Institute of Transportation, Tai-Chung, Taiwan.
- Synolakis, C.S. and Bernard, E.N. (2006). "Tsunami science before and beyond Boxing day 2004." *Phil. Trans R. Soc.* A364, 2231-2265.

- Tada, T., Tsuji, Y., Tsukamoto, M., Ueno, Y., Kawashima, M., Egawa, T., Yamazaki, Y. (1992). "Comparison of observed and theoretically calculated seiches of Heda Bay, Japan." *Pageoph*, Vol. 138, No. 2, pp. 309-322.
- Terra, G.M., Berg, W.J., Maas, L.R.M. (2005). "Experimental verification of Lorentz' linearization procedure for quadratic friction." *Fluid Dynamics Research*, Vol. 36, 175-188.
- Tintoré, J., Gomis, D., Alonso, S. (1988). "A theoretical study of large sea level oscillations in the Western Mediterranean." *Journal of Geophysical Research*, Vol. 93, No. C9, pp. 10,797-10,803.
- Titov, V.V., Rabinovich, A.B., Mofjeld, H.O., Thomson, R.E., González, F.I. (2005). "The global reach of the 26 December 2004 Tsumatra tsunami." *Science*, Vol. 309, No. 5743, pp. 2045-2-48.
- Titov, V.V. and Synolakis, C.E. (1998). "Numerical modeling of tidal wave runup." *Journal of Waterways, Port, Coastal and Ocean Engineering*, ASCE, 124 (4), 157-171.
- Tsai, L.H., Xing, X.Y., Lee, J.J. (2008). "Improving harbor resonance induced by typhoon waves for Hualien Harbor." *Proceedings of ICCE 2008*.
- Ünlüata, Ü. and Mei, C.C. (1975). "Effects of entrance loss on harbor oscillations." *Journal of the Waterways Harbors and Coastal Engineering Division*, Vol. 101, No. WW2, 161-179.
- Wiegel, R.L. (1964). "Tsunamis, storm surges, and harbor oscillations." Chapter 5 in *Oceanographical Engineering*, Prentice-Hall, Englewood Cliffs, N.J., 95-127.
- Wilson, B. (1972). "Seiches." *Advances in Hydrosociences*, 8, 1-94.
- Wu, J.K. and Liu, P.L. (1990). "Harbor excitations by incident wave groups." *J. Fluid Mech.* Vol. 217, 595-613.
- Xing, X.Y., Lee, J.J., Raichlen, F. (2008). "Comparison of computed basin response at San Pedro Bay with long period wave records." *Proceedings of ICCE 2008*.
- Yu, X. (1996). "Finite analytic method for mild-slope wave equation." *Journal of Engineering Mechanics*, Vol. 122, No. 2, 109-115.

Zelt, J.A. and Raichlen, F. (1990). "A Lagrangian model for wave- induced harbour oscillations." *J. Fluid Mech.*, 213, 203-225.